The Late-Pleistocene sedimentation history in the Eastern Arabian Sea: Climate-Weathering-Productivity linkage

Thesis submitted to the Department of Marine Sciences, Goa University, Taleigao Plateau, Goa, India, for the degree of Doctor of Philosophy in Marine Science

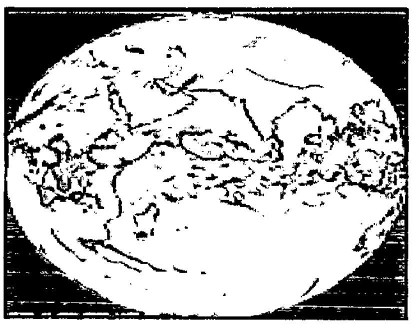

Ms. Anjali R. Chodankar

Research Supervisor
Dr. Virupaxa K. Banakar

2004

National Institute of Oceanography, Donapaula, Goa, India

Goa University, Taleigao Plateau, Goa, India

Contents

Statement

As required under the University Ordinance 0.19.8 (vi), I state that the present thesis entitled "The late Pleistocene sedimentation history in the Eastern Arabian Sea: Climate-Weathering-Productivity linkage", is original contribution and the same has not been submitted on any previous occasion. To the best of my knowledge, the present study is the first comprehensive work of its kind for the area mentioned.

The literature related to the problem investigated has been cited. Due acknowledgements have been made wherever facilities and suggestions have been availed of.

Chodankar

Anjali R. Chodankar
(Alias Anjali Y. Volvaiker)

Certificate

This is to certify that the thesis entitled "The Late Pleistocene sedimentation history in the Eastern Arabian Sea: Climate-Weathering-Productivity linkage", submitted by Mrs. Anjali R. Chodankar (Alias Anjali Y. Volvaiker) for the award of the degree of Doctor of Philosophy in Marine Sciences is based on original studies carried out by her under my supervision. The thesis or any part thereof has not been previously submitted for any other degree or diploma in any universities or institutions.

Dr. Virupaxa K. Banakar
Research Guide
Geological Oceanography Division
National Institute of Oceanography
Donapaula, Goa, India.

31 August 2004.

All the corrections suggested by the referees have been incorporated.

11/05/2005.

R. SHANKAR.

Acknowledgements

First of all I wish to thank the National Institute of Oceanography for providing me an opportunity to work for this thesis while I was working as a Project Trainee. It is indeed a great gesture from this esteemed institution, which supports several young students wishing to improve their qualification while working for various scientific programs on contract. The former director Dr. E. Desa was kind enough to permit me to register for the Ph.D. and to utilize the facilities. The friendly and supporting attitude of several NIO-members has helped me to accomplish this work.

I gratefully thank Dr. Virupaxa Banakar for introducing me to this fascinating field of palaeoclimate. No words would express my deep sense of gratitude to Dr. Banakar, who has been a smiling source of inspiration and a tough taskmaster. He motivated and encouraged me a lot to understand the research problem and address the palaeoclimate issues.

I sincerely thank Drs. N. B. Bhosle, M. V. S. Guptha and A. L. Paropkari for patiently reading the draft thesis and constructive suggestions. The discussions with Dr. Satish Shetye were of great help in writing the coastal currents and monsoon relationships. The help of professors Tadamichi Oba, M. Yamamoto, and Dr. T. Kuramoto of the Hokkaido University, Japan in obtaining the stable isotope and organic component data, and Dr. V. Ramaswami in obtaining grain-size data on laser particle analyzer is sincerely acknowledged.

The encouragement and support by senior colleagues Drs. R. Nigam, G. Parthiban, J. N. Pattan, N. Ramaiah, P. Marathe, P. D. Naidu, A. V. Mudholkar and M. Thamban, and my friends Rajani, Avina, Anjelina, Ranjita, Velina, etc, while on cruise for sampling and in lab for analytical work gave me lot of strength to accept challenges in advanced marine research work. I thank Hilda, Usha, Pratima, Sunithi, Lina, Lucinda and many others at National Institute of Oceanography for all the support and help.

When the part of this work was selected (out of over 1100 papers submitted) for the International Young scientists Global Climate Change Conference-2003 at Trieste, Italy as an invited paper by the START Secretariat (USA), it was a nice feeling and exciting experience to present this work in front of several experts in the field. I sincerely thank the START for that opportunity. I gratefully acknowledge the EMR, CSIR, New Delhi for awarding me with Senior Research Fellowship.

The encouragement and guidance by my co-supervisor Prof. U. M. X. Sangodkar of the Goa University and the FRC members Drs. N. H. Hashimi, and Vishwanath, and time-to-time administrative and scientific guidance by Prof. G. N. Nayak, HOD of Marine Sciences, Goa University were of great help.

Last but not least, the sustained love and support of my husband Ritesh, parents, uncles, aunts, brothers, sisters, and in-laws gave me energy to complete this work. Although just few months old, my young daughter lovely Isha did not trouble me much while finalizing this thesis and has been additional source of energy for me in pursuing the challenging tasks of oceanographic science.

Anjali R. Chodankar.

Summary

This thesis is aimed to understand the response of the Indian monsoons and associated biogeochemical processes in the Eastern Arabian Sea (EAS) to the past climate change. The EAS bordering the western coast of India is an important region to understand the past climate variation because the region has been shown to contain valuable sedimentary records relating to evidences of regulating glacial-interglacial climate. However, the palaeoclimate studies from this region are very limited unlike the western part of the basin. The role of low-latitude tropical oceans gains importance in global climate change as the southern high-latitude oceans failed to provide unambiguous evidences for regulating the glacial-interglacial climate. Few intriguing observations such as the Indian Monsoons providing important feedback for global climate change, Arabian Sea hosting high productivity and intense denitrification, and the past changes in the Indian Monsoons correlating with the northern high latitude Dansgaard-Oeschger type rapid climate fluctuations render the Arabian Sea as one of the very significant oceanic areas for understanding the feedbacks for the past climate change.

The EAS is a complex and dynamic water body experiencing intense summer monsoons with well-defined precipitation gradient along the west coast of India. The moderate to high productivity, intense oxygen minimum zone, higher accumulation of organic matter and terrigenous input from the Deccan Rivers characterize the EAS. Another peculiar feature of this region is the presence of low-salinity tongue developed due to inflow of the low salinity water from the Bay of Bengal along the western continental margin of India. The structure of the low-salinity tongue is determined by the relative intensity of the Poleward Coastal Currents (PCC) and the northern Arabian Sea high salinity water, which in turn are dependent upon the summer monsoon intensity and evaporation-precipitation balance in the region. In addition, the previous studies related to the monsoon driven productivity changes in the Arabian Sea have yielded contrasting results. In that, the Western Arabian Sea sediments have recorded interglacial high productivity while the eastern region sedimentary records have indicated glacial high productivity. Those studies were relying mostly on individual proxy records. If one has to comprehensively understand the climate forcing on marine regime, it is necessary to look in to the complex interlinks of the multitudes of marine processes. This can be

achieved only by studying strictly paired multiple proxies from the intact sediment repository. Therefore, the objectives of the thesis are centered on a theme of comprehensive understanding of the EAS response to the past climate change utilizing multi-proxy investigations, which are listed in Chapter 2.

Three sediment cores were collected from different water depths (200 m - 2500 m) in the EAS covering northern and southern region. The sediment texture was determined using standard pipette analyses and the sediment grain-size parameters were obtained using the Laser Particle Analyzer. The calcium (for carbonate estimation), scavenged-Al and –Mn were analyzed on Perkin-Elmer ICP-AES. All the above measurements were carried-out at the Geological Oceanography Division of the National Institute of Oceanography, Goa. The upper mixed layer dwelling planktonic foraminifera *G.sacculifer* tests were picked under the microscope from the sub-sections (2 cm intervals) of the >4 m long sediment cores. These *G. sacculifer* tests were utilized to measure the oxygen and carbon isotopes and the sedimentary organic-carbon and nitrogen isotopes were measured on stable isotope Mass-Spectrometry facility of the Hokkaido University, Japan. The *G.sacculifer* $\delta^{18}O$ variation with the core depth was tuned to the SPECMAP to obtain the chronology for the cores.

The thesis is divided into eight chapters, viz., 1) Introduction 2) Objectives 3) Materials 4) Methods 5) Results 6) Discussion 7) Conclusions and 8) References. The Chapter 1 describes the evolution and development of the palaeoclimatology, oceanographic and climatic settings of the study region, previous studies and unresolved climate related controversies existing for the region. The Chapters 3 and 4 are devoted to provide the details of samples and the methods used for obtaining the required data. In the Method section a brief description of the instrumentation and principles also are given. The Chapter 5 lists the results obtained and several age versus data plots. In this chapter the details of age-model and chronology are also included. The discussions and interpretations in light of the previous studies are presented in Chapter 6 with the support of few schematic models and figures. This chapter also contains a brief note on the EAS productivity vis-à-vis the past global climate scenario. The important observations and the interpretations with respect to the climate forced past changes in the Indian monsoons, coastal current intensity, Deccan River strength, marine productivity and denitrification are presented as Conclusions in the Chapter 7. Most of the relevant references available until date are cited in the text at appropriate places and are listed in the Reference Chapter. At the end of the thesis, the raw data is included as an Appendix.

The continental shelf core covers the Holocene-Last Glacial Period, where as, the two deep-water continental slope cores encompass over 100,000 years sedimentation history enabling me to explore the impact of the climate change on the EAS region both on high-resolution (for Holocene-Last Glacial Period) and on low resolution (Glacial-Interglacial). In the present study a first-time attempt is made to reconstruct the past variation in the summer monsoon intensity utilizing the changes in the characteristic salinity structure of the EAS (i.e., the low-salinity tongue). The global ice-volume corrected (residual)-$\delta^{18}O_{G.sacculifer}$ contrast between the northern- and the southern-cores from deep-EAS is used as a tool for reconstructing the past salinity structure of the low-salinity tongue or the variation in the PCC. It is evident from the fluctuations in the time-series record of the residual-$\delta^{18}O_{G.sacculifer}$ contrast that a definite linkage exists between the intensity of the summer monsoons and the changes in the surface salinity gradient in the EAS due to variation in the PCC. Significant weakening of the summer monsoons during the LGM and intensification during the last warm period (Marine Oxygen Isotope Stage 5) compared to the Holocene is evidenced by the respectively increased and decreased north-south salinity gradients within the low-salinity tongue of the EAS. The disappeared low-salinity tongue during the LGM is interpreted as due to the reduced alongshore pressure gradient resulting from the broken communication between the EAS and the Bay of Bengal. The salinity gradient reconstruction also exhibits high amplitude fluctuations within 4 to 5 ky temporal-band suggesting general instability in the Indian summer monsoons.

The present study demonstrates higher productivity during the Last Glacial Period when the summer monsoons were significantly weaker and winter monsoons stronger. This is in contrast to the observation made in the western Arabian Sea in general and Oman upwelling cell in particular. The multi-proxies from a single deep-water core of the study region provide convincing evidences to propose the glacial high-productivity hypothesis. It is proposed that, a) the collapse of the inter-basin communication between the high salinity Arabian Sea and the low salinity Bay of Bengal weakened the mixed layer stratification, b) the weakened mixed layer stratification led to the increased deep-water nutrient injection in to the photic-zone, and c) the glacial intensification of the winter winds provided adequate limiting micro-nutrient 'iron' derived from the lateritic and basaltic soils of the Deccan region. All the above might have culminated in increasing the marine productivity during the coldest climate of the Last Glacial Period. This part of the present study is the salient feature of the thesis and appears to support the newly emerging evidences of glacial high productivity in regulating the global climate.

The intense OMZ in the Arabian Sea is believed to induce significant denitrification, which is the source for nitrous oxide. The record of the past 100 ky water column denitrification is reconstructed utilizing the sedimentary $\delta^{15}N$. Interestingly, the EAS denitrification record superimposes the previously published records from the western, central, and northeastern Arabian Sea both in timing and amplitude of variation. This homogeneity in the past $\delta^{15}N$ across the entire basin having significantly different modern productivity patterns is puzzling. Secondly, reduced denitrification during the last glacial period when the productivity was higher than the Holocene warranted new explanation. An attempt is made in the present thesis to provide reasonable mechanism for the above de-coupling of the productivity and denitrification in the glacial-EAS. The glacial intensification of the winter winds is invoked to have forced effective ventilation of the EAS-thermocline feeding the OMZ due to intensified deep winter mixing, thus satisfying the increased demand of oxygen during elevated productivity period. The deep-winter mixing is evident in the modern times and responsible for the ventilating the Arabian Sea thermocline. The enhanced glacial productivity on one hand and increased supply of the oxygen to the OMZ-depth due to increased ventilation during the coldest winters of the glacial time appear to have forced the observed decoupling of those intimately related processes. The cross-basin homogeneity in the temporal-trends of the denitrification could be explained by intense horizontal mixing of both thermocline and mixed layer due to vigorous seasonally reversing circulations in the basin.

Finally it is concluded that, the studied sediment cores effectively preserve the records of past variation in biogeochemical processes in response to the climate forced changes in the Indian monsoon system. The past changes in the salinity structure of the low-salinity tongue in the EAS could be a faithful proxy for the summer monsoon reconstructions. The glacial-high productivity and low denitrification may provide new insight to understand the global climate change on glacial-interglacial time-scale. Thus the present work brings out the interlink between the climate forcing-monsoon system-weathering-productivity recorded in the sediments of the Eastern Arabian Sea with well-defined clarity thus achieving the objectives of the proposed work.

Although the work presented here provides comprehensive understanding of the linkage between the past-climate, Indian monsoons, continental weathering and marine productivity, but may not answer all the complex questions related to oceanic response to climate change, as the subject in itself is extremely vast. However, the above observations/interpretations may be important to explain the glacial-low and interglacial-high atmospheric pCO_2. In that, if the biological pump was weak in the glacial southern oceans, then the tropical productivity must have to be increased to account for the reduced glacial atmospheric-CO_2. One of such regions may be the Eastern Arabian Sea!

(The thesis contains around 125 pages, is supported by 29 composite figures, two cartoons, four tables, inserted at appropriate places in the text, over 150 references to the previous works, and one appendix)

Abbreviations used in this thesis

ASHSW	Arabian Sea High salinity Water (Forms in northern Arabian Sea)
BOB	Bay of Bengal (The main low-salinity water source to the EAS)
EAS	Eastern Arabian Sea (The study region in western Indian Margin)
E-P	Evaporation minus Precipitation (Indicator of moisture balance)
Ka	Thousand Years Before Present (Unit of time in to the past)
Ky	Thousand Years (Time unit used for Quaternary)
LAD	Last Appearance Datum (Time or depth of disappearance of any species from sedimentary record)
LGM	Last Glacial Maximum (Immediate past coldest earth ~18Ka)
LGP	Last Glacial Period (Immediate past cold event spanning 24Ka-11Ka)
Ma	Million Years Before present (Unit of time in to the past)
MIS	Marine Oxygen Isotope Stage (Defines the climate events)
OM	Organic Matter (Sediment component derived largely from the biological activity in the upper ocean)
PCC	Poleward Coastal Current (BOB low-salinity water tongue in EAS)
SMC	Summer monsoon Currents (Flow towards equator & east or BOB)
WMC	Winter Monsoon Currents (Flow towards Arabian Sea from BOB)
YTT	Youngest Toba Tuff (A mega eruption in Indonesia around 72-74 Ka. Believed to have global impact and used as a key-point in late Quaternary chronology)

List of Tables and Figures

Introduction

1. Introduction

1.1. Palaeoclimatology:

The oceans cover nearly 70% of the Earth's surface, which drive and regulate its total climate system. The climate encompasses complex and multitude interactions between atmosphere, hydrosphere, cryosphere, biosphere, and lithosphere. Such interactions on large scale may induce distinct changes in the global climate. The excess accumulation of greenhouse gases such as carbon dioxide and methane leading to modern climate warming greatly modify the Earth's climate system. The ENSO type of ocean-atmosphere coupled process modifies the global precipitation pattern. These climate features standout as examples of the complex interactions between atmosphere and hydrosphere. In the 18th century James Hutton and Charles Lyell proposed principles of uniformitarianism considering *'present as key to the past'*; whereas the palaeoclimatologists endeavour to *'predict the future climate by looking in to the past-variations'*. Only when the causes of the past climate fluctuations are understood, it will be possible to anticipate or forecast climatic variations in the future (Bradley and Eddy, 1991). Our present knowledge of the past-Earth has indicated several alternating warm and cold periods particularly in the Pleistocene with amazing rhythm. Hence, the Pleistocene Period is rightly coined as the Great Ice Age. The ocean as a major player involved either in generating such climate variations or in feedback mechanism required for climatic oscillations, hence the oceanic response to the Earth's climate change although very complex has been distinct and measurable. Therefore, oceans provide most important and easily accessible repository for tracing the past climate records. Almost all changes in oceanic environment in response to climate variation could be traced within the seafloor itself. In that, the seafloor sediments faithfully record the changes in water column chemistry, biological activity, air-sea interaction, inter-oceanic overturning, land-ocean interaction, deep-water circulation etc.

Both regional- and global-scale climate changes have been attributed to the uneven heating of the planet by the solar radiation. In other words, Earth's radiation budget largely controls the climate. A steady state climate unchanged over a period should ideally represent well-balanced radiation budget of the Earth i.e., incoming solar radiation equals the outgoing radiations. This balance has fluctuated several times in the past resulting in cooling and warming of the climate, which are commonly known as glacial and interglacial periods respectively. Earth has experienced such dramatic climatic conditions during the last 2.7 million years. Within the late Quaternary itself (since ~1 Ma) there have been ten major cold (glacial) events separated by warm (interglacial) events known as climatic cycles. These climatic cycles are further punctuated by shorter time-span, moderately cold and warm events called stadial and interstadial respectively. The main effect of these glacial-interglacial climate cycles was extensive waxing and waning of the continental ice sheets resulting in fall and rise of the global sea level, which have further modified the continental and oceanic climate set-up. For instance, during the last glacial maximum (LGM) the global sea level was lowered by about 120 m as a result of global oceans loosing large amount of freshwater, which was locked on the continents in the form of ice (Fairbank 1982; Shackleton and Opdyke, 1973). In fact, the climate must have been subjected to such changes on global-scale since the time earth has come into existence (~4.5 billions of years ago) as a part of its natural dynamics. The information related to those changes has been stored in different forms (proxies) on continents and in oceans (e.g., ~3.3 billion years old Banded Iron Formations and few thousand years old marine sediments). The time-scale of changes, which one could resolve depends upon the process involved in the genesis of particular proxy and the location of its formation. The shallow water corals, for example, may provide the information on yearly time-scale, but the deep abyssal oceanic sediment on thousands of years time-scale. The resolution also depends upon the sampling and measurement techniques. Recent studies of the Greenland ice sheets have revealed astonishingly abrupt climatic oscillations with significant amplitude variations (Dansgaard et al., 1984; Oeschger et al., 1984), subsequently named after their discoverers as Dansgaard-Oeschger climate oscillations. The modern anthropogenic forcing on the climate change is an additional signal superimposed on the background of natural climate. It is possible to isolate anthropogenic or local effects from a composite record, if we subtract the natural effect with reasonable confidence. Therefore, it is important to learn about the variability in the past-climate to understand or predict the possible future changes. This highly intriguing, fascinating, and complex branch of earth sciences is termed as 'Palaeoclimatology'.

The Quaternary Period is the most important time in the geological history as far as the past climate variability is concerned, because it provides immediate past climate history based on which one can understand the present and anticipate future changes. In particular, the climate contrast between the Last Glacial Period (LGP: 24 Ka - 11 Ka) and the Holocene (11 Ka to Present) provides valuable information for projecting the future natural climate change. Additionally, the Holocene epoch forms the present day warm and humid climate cycle, while the LGP represents the immediate past cold and dry climate. This pattern of climate cycle has repeated in the past with amazing accuracy and resulted in distinct global as well as local responses in hydrosphere and biosphere. As the oceans host the largest volume of water and the organic production, is the most suitable candidate to trace the past climate. Therefore, the marine sediment has been the widely explored effective archive to study the palaeoclimate on different time scales depending upon the location of the study area. The atmosphere-hydrosphere coupled processes such as monsoon intensity, oceanic upwelling, biological productivity, and atmosphere-continent coupled processes such as dust flux, fluvial erosion etc in response to climate forcing could be understood using the marine sediments.

1.2. History of Ice Age:

The recognition and evolution of the Quaternary climate change has a history of more than two centuries. Today about 10% of the Earth's total land area is covered by glacier ice. Whereas, during the Pleistocene at several times as high as ~30 % of the land surface was covered with the ice and oceanic ice-sheets expanded to great extent resulting in overall cooling of the climate. In 1795, James Hutton suggested that the continental glaciers transported the erratic boulders of granite found in limestone of the Jura Mountains. In 1823, William Buckland, while describing the Quaternary Cave deposits, suggested that the northern Britain and several parts of the north Europe were covered by glacier ice in the past. Those thought provoking studies basically recognised the ice age. Geikie brothers in 1870s extensively described the glacial drifts and their work laid the foundation for the Quaternary ice age. Subsequently, alternating cold and warm events with well-defined rhythm were recognised in global marine sedimentary records spanning several thousands of years. Based on these records past climate models were developed and hypothesis were proposed. The most important of them was the *Orbital Theory* propounded by Milankovitch (1941), which recognized that the past glaciations were principally the function of variations in the Earth's orbital parameters resulting in varying distribution of solar radiance on its surface.

The revolution in Quaternary climate study took place in 1946 when Harold Urey demonstrated that the oxygen isotope ratios of planktonic foraminifera indicate the temperature of the seawater in which they lived. With each 1°C fall in ambient water temperature, the $\delta^{18}O$ of planktonic calcite was shown to increase by 0.2 ‰. Fluctuations in the oxygen isotopic ratios and major changes in the global climate were extensively studied by Emiliani (1955). The subsequent detailed investigations of $\delta^{18}O$ variations in the calcite tests of planktic and benthic foraminifera confirmed the temperature dependence of the oxygen isotopic ratio. Later studies by Olausson

(1965), Shackleton (1967), and Shackleton and Opdyke (1973) led to the conclusion that variations in the calcite-$\delta^{18}O$ with time reflected changes in the oceanic oxygen isotope composition caused mainly by the waxing and waning of the continental ice sheets that led to fall and rise of the global sea level. Fairbanks and Mathews (1978) estimated that 0.011 ‰ of $\delta^{18}O$ variation is associated with 1 m of sea-level change. With the evolution of oxygen isotopic studies of marine biogenic calcite, it has become unequivocally clear that, irrespective of the region the temporal records of both the planktic and benthic foraminifera $\delta^{18}O$ exhibited remarkable global similarity comprising major cold (glacial) and warm (interglacial) events repeating at ~100 ky (orbital eccentricity) frequency. At the outset this observation suggested that, a) the past variations in the climate have forced the global oceans' $\delta^{18}O$ to change accordingly, b) the record of such changes are preserved with remarkable fidelity in the calcite fossils on global scale, and c) the changes were the responses to orbital parameters. The first rigorous attempt to assess the orbital parameters forcing the past climate change was made by Hays et al. (1976). They concluded that most of the changes observed in marine sedimentary records were found to concentrate at frequencies closely corresponding to those expected from the orbital changes (e.g., ~100 kyr Eccentricity, ~41 kyr Obliquity, and ~21 kyr Precession periodicities recognised by Milankovitch). The accurate marine oxygen isotopic stages were defined based on the stacked oxygen isotope data of the foraminifer calcite and tuning the down-core isotope profiles to the solar insolation curve (Imbrie et al., 1984). This insolation-tuned sedimentary marine oxygen isotope profile widely known as the SPECMAP became the reference curve for the Quaternary chronology for demarcating the Marine Oxygen Isotope Stages (MIS). These stages were numbered serially from present warm Holocene period in to the past. Thus the odd numbers indicate the warm interglacial periods and the even numbers indicate cold glacial periods. Numerous other studies carried out using the sedimentary records from the world oceans and regional seas subsequently confirmed the orbital theory of Quaternary climate change (see for examples Imbrie et al., 1984, Bassinot et al., 1994, Shackleton, 2000). In the past decade new discoveries were made using the Greenland ice-cores. Those ice-core studies have revealed that the past cyclic climate change was not solely on orbital frequencies but on much more rapid sub-orbital frequencies (Bond et al., 1993; Dansgaard et al., 1984; Heinrich, 1984; Oeschger et al., 1984). That is not the end, still more and more refinements to climate models and age uncertainties are being taking place to help anticipate the future climate trends with utmost accuracy.

1.3. Oceanography and climate of the study region:

The Arabian Sea is a unique basin composed of complex seafloor, seasonally changing hydrography, and isolation from the Arctic. It covers an area of about 3,863,000 km^2 and is located between 7° N and 25° N latitudes and 55° E and 75° E longitudes forming the northwest water body of the Indian Ocean (Figure 1). It is surrounded by landmasses to the west (Arabia), north (Pakistan) and east by coastal highlands (Western Ghats) of the western India. The basin is narrow in north and wide opens to the Indian Ocean in the south. Arabian Sea has one of the world's largest submarine fans viz., Indus Fan, formed by the sediments brought by the Indus River draining the Himalayas. Other major rivers, Narmada and Tapti join the Arabian Sea in the northern part of the west coast of India. Towards the south many small seasonal rivers draining the Deccan Mountains debouch considerable amount of fresh water and erosion products during the southwest (summer) monsoons. The Zuari-Mandovi drainage is one such river system that discharges in to the Eastern Arabian Sea (EAS) near the Goa province.

The Arabian Sea has several seafloor topographic features. Wide western continental shelf off India (a passive continental margin), narrow shelf off Oman, Owen Fracture Zone, Murray Ridge, and several seamounts. The most impressive geomorphologic feature of the Arabian Sea is the broad active Mid-Ocean Ridge system, which starts in Gulf of Aden and trends southeast as Carlsberg-Ridge, into an enechelon pattern of transform faults called Central Indian Ridge. The Carlsberg Ridge separates deep basin of Arabian Sea into two major sedimentary sub-basins: the Arabian Sea Basin and the Somali Basin. The Laxmi Basin in eastern part of the Arabian Sea bordering India has few conspicuous morphological features such as Raman, Panikker and Wadia seamounts (Bhattacharya et al., 1994).

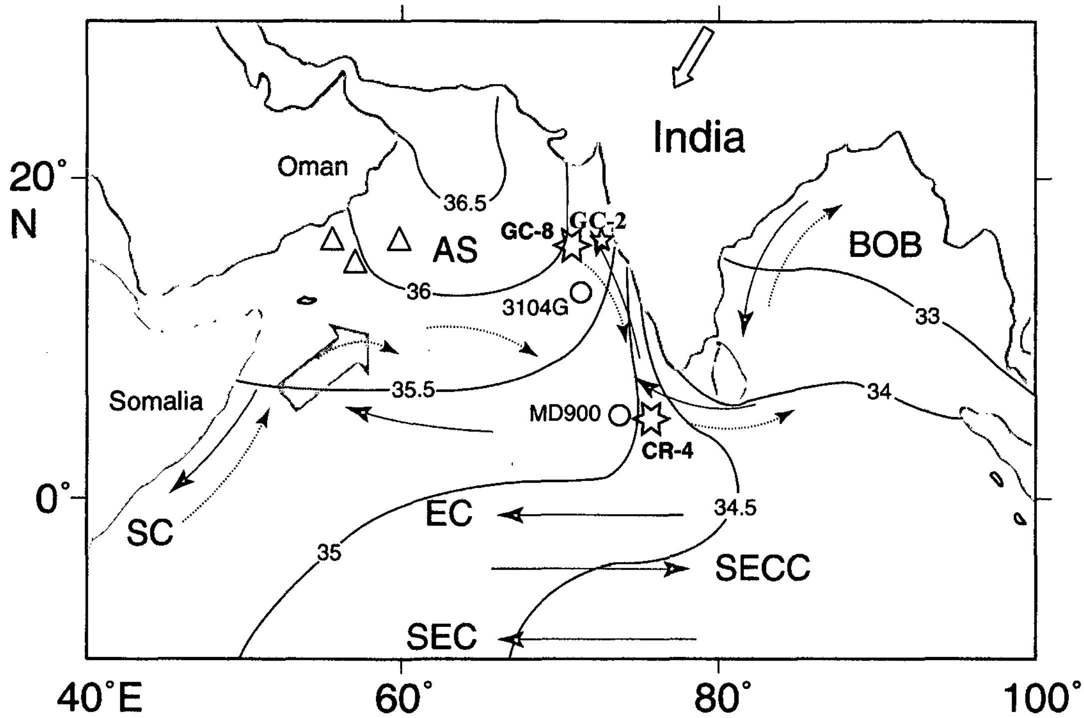

Figure 1: The northern Indian Ocean hydrography, monsoon system, and sediment core locations used in this study. AS is Arabian Sea and the eastern region of this basin (margin of India) is the present study area. BOB is the Bay of Bengal. The grey shaded thick box arrow indicates summer monsoon winds and open box arrow indicates winter monsoon winds. Continuous curved arrows are the winter monsoon surface water circulations and the broken arrows are the summer monsoon circulations. EC, SECC, and SEC are Equatorial Currents, South Equatorial Counter Currents, and the South Equatorial Currents respectively. The stars are the sediment cores used for the present study (SK117/GC02, SK117/GC08, and SK129/CR04: also see Table 1). Open triangles are the sediment cores studied for denitrification in the Oman region (Altabet et al., 1999), open circle with MD900 is the core studied by Rostek et al., (1993 & 1997) for palaeo-salinity and –SST reconstructions and 3104G is the core studied by Sarkar et al. (2000) for E-P reconstruction. The salinity contours are denoted with their salinity value. For details of circulation system and terminology see Shankar et al., (2002). There have been several palaeoclimate studies from the Arabian Sea, particularly in the western region, which are not shown in this figure to avoid crowding of the details.

Based on the depth profiles of salinity and potential temperature, Shetye et al., (1993) have identified three distinct water masses in the Arabian Sea, viz., Arabian Sea High Salinity Water (ASHSW), Red Sea Water (RSW), and Persian Gulf Water (PGW). The high salinity dense ASHSW forms in the northernmost Arabian Sea and spreads southwards within the upper 100 m of the mixed layer (Prasannakumar and Prasad, 1999). This water mass is the result of excess evaporation in the northern Arabian Sea. The PGW is located between ~200 m in the Gulf of Oman and ~400 m water depth further south. The PGW is derived from the overflow of Persian Gulf water into the Gulf of Oman over a sill depth of ~60 m and spreads into the Arabian Sea. The PGW loses its identity due to mixing with RSW as it moves southward. The RSW is the outflow from Red Sea over a sill depth of ~150 m. The high salinity RSW is located between ~500 m and ~800 m water depth (core occurs at ~600 m depth) and its southern extension could be traced up to 10° S latitude. The northern extension of the RSW is limited to ~18° N latitude (the comprehensive description of the Arabian Sea hydrography is available in You and Tomczak, 1993). The isolation and stagnation of the intermediate water and the lack of substantial horizontal advection together with very high productivity causes the development of intense Oxygen Minimum Zone (OMZ), which extends between 200 to 1200 m water depths (Wyrtki, 1973; Olson et al., 1993). The core of the OMZ (< 0.5 ml O_2/L) is located around 600-800 m.

The Arabian Sea experiences extremes in both atmospheric forcing and oceanic circulation due to seasonally reversing monsoon wind system (Wyrtki, 1973). During the northern hemisphere summer (May to August), solar radiations warm the land relatively faster than the ocean. As a result of this differential heating a steep pressure gradient is created between the low-pressure northern India-Tibet and high-pressure Equatorial Ocean. The dense oceanic air carrying moisture evaporated from the ocean move landward and subsequently curl towards the Indian subcontinent causing heavy precipitation over the sea and Indian sub-continent known as the summer monsoon (Figure 1). With the onset of winter in November, both the land and the ocean lose heat by the radiation to space. The differential heat capacity of the land and ocean results in relatively greater cooling of the Indian subcontinent than the ocean resulting in cool dry winds to blow from the continent over the Arabian Sea, known as northeast monsoon during the winter (November-February) (Figure 1). The modern winter winds are significantly weaker than the summer winds (Shankar et al., 2002; Shetye et al., 1991) and hence their influence on the biogeochemistry of the Arabian Sea is believed to be low. The winter monsoon continues in a steady state until solar heating of the spring dissipates the temperature gradient that powers it. The development and evolution of these Indian seasonal monsoons are however much more complex.

The surface circulation in the Arabian Sea is modulated by the seasonal variation of the monsoon wind system. The seasonal reversals of the surface wind field over the tropical Indian Ocean are far more dramatic than in other regions of low latitudes, and these reversals have profound impact on the surface current system (Wyrtki, 1973; Hasternath and Greishar, 1991). During the summer monsoon period the low level southeasterly trade winds of the southern hemisphere extend across the equator to become southerly or southwesterly in the northern hemisphere. The frictional stresses of the southwesterlies in turn drive the Somali current, which is a fastest open ocean current on the earth with a speed up to 7 knots (Smith et al., 1991; Shankar et al., 2002), the westward flowing south equatorial current, and the eastward flowing summer monsoon current (SMC). On the other hand, during the winter monsoon period, the oceanic circulation is relatively weak and is characterized by the north equatorial current (winter monsoon currents: WMC) and eastward flowing equatorial counter current. Thus, the direction of the wind-flow from the continent towards the Arabian Sea (in southwest direction) causes the circulation in the Arabian Sea to reverse (Figure 1).

The peculiar monsoon wind regime produces dramatic seasonal changes in physical and biogeochemical processes in the upper water column. Wind induced upwelling of nutrient rich water and related high primary productivity is one of the characteristics of this basin (Kabanova, 1968; Nair et al., 1989). High productivity and non-availability of well ventilated water to the intermediate depth result in the development of extremely low oxygen mid-depth layer causing intense denitrification (Naqvi, 1987), thus making the basin one of the worlds largest nitrogen sink (Codispoti, 1995). The formation of high salinity water in the northern Arabian Sea (Rochford, 1964; Morrison, 1997) due to excess evaporation-precipitation (E-P) (Cadet and Reverdin, 1981), and its seasonal spreading southward along the eastern region (Prasannakumar and Prasad, 1999) are unique seasonal hydrographic features of this basin. Therefore, the Arabian Sea is a complex but interesting natural laboratory to study the past climate. The western part of the Arabian Sea has attracted most of the attention of the palaeoclimatologists due to summer monsoon induced intense upwelling process in that region and proximity to the major desert land of Arabia. Where as, until recently other parts of the Arabian Sea were rather ignored. One of such areas is the EAS bordering the west coast of India. Hence, the present work aims to explore the responses of the highly dynamic EAS to the past climate change.

1.4. Study area:

The EAS comprises a dynamic water body receiving intense summer monsoon overhead precipitation with well-defined precipitation gradient from ~4000 mm in southern Konkan Coast to ~300 mm in northern Saurashtra Coast, decreasing northward at a rate of ~350 mm per degree latitude (Cadet and Reverdin, 1981; Sarkar et al., 2000). This region supports moderately high productivity due to seasonal upwelling (Haake et al., 1993; Sharma, 1977) and strong OMZ due to which high export production is apparent (Rao and Veerayya, 2000 and references therein). In contrast to the large input of the dust to the western Arabian Sea from Arabia (Sirocko et al., 1991; Shimmield et al, 1990), the EAS receives very low dust input and is dominated by the terrigenous load delivered by the large network of rivers quickly draining the Deccan Mountains during the summer monsoon rains and to certain extent the Indus River input derived from the Himalayas particularly in the abyssal depths.

The surface salinity (hereafter only salinity) structure of the Arabian Sea is peculiar. The north to south decreasing, west to east trending isohalines of the basin are punctuated in the eastern region by the inflow of low salinity Bay of Bengal (BOB) water, which forms a low salinity tongue along the western margin of India (Figure 1). As such the basin-wide high salinity build-up due to excess E-P is largely compensated by the inflow of low salinity BOB water drawn by the WMC and its bifurcated arm known as poleward coastal current (PCC), thus maintaining the salt-balance (Prasad, 2001; Prasannakumar and Prasad, 1999). The summer monsoon dependency of the low-salinity water flow in to the EAS has been demonstrated (Shetye et al., 1991), and the details of the mechanism governing the low-salinity tongue are discussed in Chapter 6.1.

The biogeochemical responses of the Arabian Sea in general and western region in particular to the past climate and their linkage with monsoon variations have been traced in the sediment. Therefore, the sedimentary records from the EAS are well-suited repository to explore the fluctuations in closely interlinked past monsoon strength, salinity structure, productivity, and fluvial erosion in Deccan Mountain region. As the eastern region is the least studied region of the Arabian Sea in regard to palaeoclimate reconstruction, may be holding interesting information with respect to the biogeochemical responses associated with the climate change.

1.5. Previous study:

The Indian monsoon system is one of the major atmospheric components of the tropical climate and is a complex system. Previous studies have suggested that the strength of the summer monsoon, upwelling, and productivity in the Arabian Sea are all coupled together. Those investigations were mainly concentrated in the western Arabian Sea, especially in the summer monsoon driven upwelling cell of the Oman Margin. The oxygen isotopes have been extensively used to understand the past changes in the Indian Monsoons.

The oxygen isotope ratio of the biogenic calcite has been the most reliable tool for the palaeo-climate and monsoon reconstruction. The oxygen isotopic composition of calcareous fossils depends upon the isotopic composition of the contemporary ambient water, which in turn depends upon the local salinity and sea surface temperature (SST). The vital-, size- and dissolution-effects affecting the isotopic composition of the calcite tests (Dogde, et al., 1983; Duplessy et al., 1981) may be ignored because the former can be assumed to have uniform effect through time and the latter two problems can be circumvented by careful selection of the sample site (well above carbonate lysocline) and intact specimen from a narrow size-range. In the EAS the salinity depends largely upon the E-P balance and BOB water influx. Where as, the SST in the region depends upon monsoon wind regime and the coastal upwelling. Therefore, the calcite tests of the planktonic foraminifera from sediment cores have been the ideal proxy for understanding the past changes in complex interaction of the E-P, water mass characters, circulation, and monsoon strength (Prell et al., 1980; 1984a, 1984b; Duplessy, 1982; Sarkar et al., 1990; Sirocko et al., 1993; 1996) specific to this study area.

The planktonic foraminifera oxygen isotope based studies from the Arabian Sea have indicated that the strength of summer monsoons has varied greatly during the late Quaternary (Prell., 1978; Prell et al., 1980; Prell., 1983; Niitsuma et al.,1991; Spaulding and Oba, 1992). The studies using ODP sediment cores have shown significant variations in summer monsoon and its effect on oceanic productivity in the Western Arabian Sea (Shimmield et al., 1990). It is believed that the Indian summer monsoon around 9 Ka were intense than during the LGP (24-11 Ka) based on large scale climate models and the past-upwelling records (Clemens and Prell., 1990; Sirocko et al., 1993; 1996; Naidu., 1995). The Holocene E-P balance reconstruction for the EAS by Sarkar et al., (2000) has indicated a steadily increased summer monsoon precipitation since the ~10 Ka up to ~2 Ka. This Holocene summer monsoon trend however does not agree with the summer monsoon variations in the western region recorded by upwelling indicator species (Naidu and Malmgren, 1995). Based on the $\delta^{18}O$ of *G. ruber* from both the Arabian Sea and BOB, Duplessy (1982) suggested that the basin-wide LGM-SSTs were nearly similar to or even slightly warmer than the Holocene. Hence, he assumed that the Holocene-LGM $\delta^{18}O_{G.ruber}$ contrast was solely due to the variation of the salinity in the region. The global circulation models, taking in to account various climatic parameters for Glacial-Holocene boundary conditions suggested that the Indian summer monsoon intensity variation was largely forced by the E-P accounting for ~23 % of the total forcing factor (Prell and Kutzbach, 1992). In contrast to the Duplessy's (1982) assumption, the alkenone based SST reconstructions indicated 2° - 3° C lowered SST in the LGM-EAS (Cayre and Bard, 1999; Rostek et al., 1997; Sonzogni et al., 1998). Similar drop in SST has been recorded in the LGM sections of the tropical South China Sea sediment cores (Kienast et al., 2001). Thus it appears that the LGM-SSTs in the low latitude regions in fact were lower than the Holocene. However, the magnitude of SST-lowering during the LGM was much smaller than in the high latitude regions (Ikehara et al., 1997).

Presently high surface productivity and subsequent oxidation of settling organic matter consumes large amount of dissolved oxygen at low oxygenated intermediate water leading to an exceptionally broad and stable mid-water OMZ in the region (Olson et al., 1993). High content of organic carbon in surface sediments in the EAS, especially western continental margin of India suggest high export production and better preservation (Calvert et al., 1996; Paropkari et al., 1992; Slater and Kroopnick, 1984; Rao and Veerayya, 2000). The primary cause of carbon enrichment in sediment has been previously debated (Paropkari et al., 1987; 1992 and references therein). The pre-existing deep-water anoxic condition (Calvert et al., 1993; Demaison and Moore, 1980; Paropkari et al., 1992), high productivity and favourable sediment texture (Calvert et al., 1995; Pederson and Calvert, 1990; Pederson et al., 1992; Rao and Veerayya, 2000) have been invoked as the causes for good preservation of the carbon in the EAS sediment. Further details are out of the scope of this study. Recent studies however have suggested that the inherent low oxygen character of the feed-water at intermediate depth not only sustains the OMZ (Olson et al, 1993), but also contributes to the preservation of organic carbon (Schulte et al., 1999 and references therein). Irrespective of the debate on carbon inventory of the Arabian Sea sediment, the sedimentary organic matter has been extensively used to understand the past-productivity variations in the basin.

Interestingly, there have been contrasting views with respect to past productivity in the Arabian Sea, which is dealt in detail in Section 6.3. Here it is worth mentioning that the past productivity changes in the basin have exhibited region specific (western versus eastern) responses to the climate change. On one hand, the western Arabian Sea has been shown to record interglacial high productivity (Emeis et al., 1995; Naidu and Malmgren, 1996; Shimmeild et al., 1990; Spaulding and Oba, 1992), while on the other hand, biomarkers and sedimentary organic carbon have indicated enhanced glacial productivity in the EAS (Cayre and Bard, 1999; Rostek et al., 1997; Schulte et al., 1999; Thamban et al., 2001). The observations indicating stronger winter monsoons during the LGM than the Holocene (see Duplessy, 1982) has been the nodal point for the hypothesis invoking glacial high productivity; where as, the summer monsoon driven intense basin-wide upwelling has been the central cause for interglacial high productivity.

Thus the EAS appears to be an intriguing region with respect to its response to the past climate driven monsoon variations. Hence, it is necessary to explore this region in detail to understand the effects of past climate on relative strength of the monsoons and associated responses such as productivity, fluvial input of detritus, hydrography, denitrification etc. Did these parameters in the EAS responded in concert with each other as a coupled responses to the varying monsoon regime or were they decoupled responses for a given climatic scenario needs to be addressed using multi-proxy approach, and forms the theme of the present investigation.

2. Objectives of the present study

For the present study, it is proposed to investigate the linkage between past variations in the Indian monsoon system and its effect on the photic zone productivity, local hydrography, and fluvial input in the EAS utilizing a multi-proxy approach. The following causal relationships need to be explored to achieve that objective.

a) The past variations in the relative intensity of the Indian monsoons by tracking the relative changes in E-P and coastal circulation using planktonic foraminifera-$\delta^{18}O$ and available alkenone-SST patterns from the region. Both the high-resolution Holocene-Glacial and low-resolution glacial-interglacial time slices would help in reconstruction of the past monsoon variations.

b) The fluvial silicate-detritus distribution in the sediment column deposited on the continental shelf, in the vicinity of any Western Ghat Rivers is expected to produce characteristic signals in concert with the summer monsoon intensity. Because, the Western Ghat Rivers are dependent upon the summer-monsoon and are exclusively seasonal. Therefore, the down-core variations of specific size detrital grain ratios may be able to provide important clues about the variations in summer monsoon rains.

c) There is a large volume of work on record showing strong relationship between upwelling, productivity, and the summer monsoon intensity particularly from the western Arabian Sea. If the summer monsoons were solely responsible for driving the productivity in the Arabian Sea, then the proxies such as biogenic-calcite, organic-matter, and scavenged-Al from the EAS also are expected to produce overlapping signals in concert with the past summer monsoons.

d) The high productivity and low oxygen characteristic intermediate water maintain intense modern-OMZ in the Arabian Sea. The past variation in the OMZ intensity could be evaluated through variation in water column denitrification recorded by the sedimentary nitrogen-isotopes. The past changes in denitrification intensity may be a useful tool to understand the variation in monsoon intensity (vis-à-vis productivity) and intermediate water hydrography.

Three gravity cores representing three different depositional environments in the EAS were selected for the present work from the collection of the National Institute of Oceanography (see Figure 1 & Table 1). Due to certain analytical constraints it was not possible to generate strictly paired data for the studied cores, and hence the interpolation technique was used to evolve common time-scale for different variables wherever required. The chronology for Holocene-LGP sections of the cores may contain certain uncertainty due to the non-availability of AMS-^{14}C dates. I have rigorously assessed the structure of the oxygen isotope profiles while evolving age models; however, refrain from discussing several subtle fluctuations in view of the above chronological limitation particularly for the Holocene-LGM section.

3. Material

Sediment cores selected for the present study were collected using 6 m long cyclindrical gravity corer during ORV. Sagar Kanya cruise-117 (SK-117: October 1996) and -129 (SK-129: December 1997). Two cores were from the central-EAS off Goa (SK-117 collection) and one core was from the southern-EAS (SK-129 collection). For convenience I refer the former core locations as 'northern region' and the latter core location as the 'southern region' of the EAS. The core-tops of the selected sediment cores were assumed to be intact as evident by fluffy upper layer and the cores do not contain any indications of slumping or turbidite. The cores were sub-sampled on board at 2 cm intervals after scraping-off about half a cm outer layer to eliminate any contamination caused due to mixing of younger and older sediment when the corer penetrates into the sediment column. Sub-samples were transferred to clean and labelled polyethylene bags, sealed and stored in labelled plastic bottles.

The relevant details of the samples are given in Table 1 and their locations in Figures 1. The core SK-117/GC-02 is from the continental shelf region (15° 28. 96' N and 72° 50. 72' E, water depth 226 m), ~150 km off from the discharge point of two Deccan Rivers viz., Mandovi and Zuari flowing through the State of Goa. Therefore, this core is expected to record continental detritus-input signals generated by the variation in the intensity of those rivers. The preliminary microscopic observations indicated that a significant portion of the coarse fraction indeed contain abundant detrital grains, thus providing an opportunity to quantify the variations in terrigenous supply. The core SK-117/GC-08 (15° 29. 71′ N and 71° 00. 98′ E, water depth 2500 m) was located on the continental slope region off the GC-02 core. This location falls within the seasonally varying modern-ASHSW front (Prasannakumar and Prasad, 1999; Prasad, 2001) and should be able to provide a record of the past changes in the intensity and spreading of that northern Arabian Sea origin ASHSW high salinity water mass. The core SK-129/CR-04 (6° 29. 67′ N and 75° 58. 68′ E, water depth

2000 m) on the other hand was located below the modern WMC, which advect low BOB water in to the Arabian Sea. Therefore, this core in combination with the GC08 may be able to provide a record of variation in the strength of WMC and EAS-characteristic PCC (Shetye et al., 1991). The two deep-water cores (SK117-GC08 and SK129-CR04) are also expected to provide information on relative changes in the past salinity-balance in the EAS, because, the modern salinity budget of the Arabian Sea is largely governed by the monsoon currents (see Prasannakumar and Prasad, 1999; Shankar et al., 2002). Apart from these specific potentials, the cores must have preserved the past records of climate driven changes in marine productivity. Thus the material selected for the present study has a potential for a comprehensive understanding of the monsoon and biogeochemical response of the EAS to the past climate.

Table 1. Details of samples used in the present work.

Core	Latitude (N)	Longitude (E)	Water-depth (m)	Core length (cm)	Type of the sediment
SK117-GC-02	15° 28. 96′	72° 50. 72′	226	390	Carbonate ooze. Shell fragments and silicate grains occur within the carbonate and silt matrix.
SK117-GC-08	15° 29. 71′	71° 00. 98′	2500	408	Carbonate ooze intermixed with clay and silt material. The YTT* characteristic glass-shards are abundant at ~290 cm depth in core.
SK129-CR-04	06° 29. 67′	75° 58. 68′	2000	504	Carbonate ooze intermixed with clay and silt material. The YTT* characteristic glass-shards are abundant at ~220 cm depth in core.

(*YTT = Youngest Toba Tuff originated from the Indonesian Archipelago volcanism has been dated to be ~72 Ka (Ninkovitch,1978). This tuff has been shown to have transported by winds across the Arabian Sea up to Arabia (Rose and Chesner,1987); across the equator in to the southern hemisphere (Pattan et al., 1999); and even up to the Greenland (Zielinski et al., 1996). The extension of the YTT into Greenland indicates the intensity of the eruption. Several researchers have used this volcanic tuff as an excellent tie-point for oxygen-isotopic chronology of the sediment cores. Similarly the presence of YTT in two cores for present study has provided excellent tie-point for establishing the isotope chronology. ***(Hereafter the above sediment cores are referred as GC02, GC08, and CR04 respectively).***

4. Methods

The optimum numbers of representative samples from different marine setting in the EAS have been used for obtaining the required proxy-data. The data acquisition techniques and working principles of analytical tools utilized for the study are briefly described in this section. The proxies used are:

1. Planktonic foraminifera-calcite oxygen isotopes for chronological framework and to understand E-P changes in response to monsoon fluctuation and past variation in the salinity adjustment in the region.
2. Planktonic foraminifera-calcite carbon-isotopes, organic carbon and its carbon-isotopes, sedimentary-nitrogen and its isotopes, and carbonate fluxes for reconstructing the past variation in productivity and OMZ intensity in the region.
3. Sediment texture and grain-size variation to understand the changes in the intensity of fluvial erosion in the Deccan Mountain region.
4. Alkenone unsaturation index to confirm the previously reported SST-shift from the LGM to Holocene.
5. Particle scavenged-Al and –Mn for independently testing the productivity changes.

It is worthwhile to note that the above parameters in modern climate setting are related directly or indirectly to the Indian monsoon intensity. My effort therefore would be to understand interlink between those oceanic responses and the past climate fluctuation in general during the late Quaternary, and in particular from the immediate past Glacial to the present Holocene period. The previous studies have also indicated that the Indian monsoon system and the Arabian Sea responses to the monsoons provide important feedback for the global carbon dioxide cycling (Overpeck et al., 1996; Schulz et al., 1998). Even though the present study is not aimed at carbon dioxide issue, but may provide at least partly explanations for its glacial-interglacial changes.

4.1. Sediment texture analysis:

The proportion of sand, silt, and clay fractions in the sediment was quantified using standard sedimentological techniques such as wet sieving and pipette analysis. The pipette analysis is based on the Stoke's law of settling velocity (Folk, 1968). The Stoke's Law is defined as '$V=CD^2$', where V is the settling velocity (cm/sec) of a particle, C is the constant defined by the viscosity of settling medium and the density of the settling particles, and D is the particle diameter (cm) assuming settling particle as a sphere. The weight percent contents of the fractions were used to define the sediment texture following Pettijohn et al., (1972) classification.

The raw sediment was rinsed twice with RO-water (reverse osmosis treated) to remove the salts and dried at ~50°C. The dried salt-free sediment was weighed accurately (10-15 grams) and transferred to clean beaker. The weighed sample was soaked in 50 ml of RO-water and was dispersed with 10 ml of 10 % sodium hexametaphosphate. The sample was stirred gently after every 20 minutes for 4 hours to achieve complete dispersion of fine fraction. The dispersed sediment sample was wet sieved through 230-mesh (63 mμ) sieve in a soft jet of RO-water. The –63μm fraction was collected in a clean 1000 ml measuring cylinder. Sufficient care was taken to limit the washing volume to < 1000 ml. The volume was finally made to 1000 ml before starting the pipette analysis.

The +63μm fraction (sand) retained on the sieve was transferred to a pre-weighed 50 ml beaker, dried at ~80° C, and weighed. The –63μm fraction (clay + silt) in the measuring cylinder was subjected to pipette analysis. The –63μm fraction was stirred vigorously with the help of a perforated disc-stirrer for about 2 minutes. The time is noted down soon after the stirring is stopped. A 100 ml of settling mixture containing clay fraction was pipetted from designated depth-level in the cylinder at defined time-intervals depending upon the ambient temperature of the settling medium. The clay fraction was transferred to pre-weighed beakers and dried at ~50°C. The dried clay fraction was weighed and stored in the plastic vials for the further analysis. The weight of the clay fraction was corrected for the weight of dispersant. The weights of clay and sand fractions were subtracted from the original weight of the sample to obtain the silt content. Further, the weight of each fraction was translated in to weight percent. Several duplicate samples were also analysed to assess the precision of the results, which is within ± 3 %.

4.2. Sediment grain-size measurement:

The continental shelf core GC-02 was analysed for detailed grain-size distribution using a Malvern Mastersizer-2000 Laser Particle Analyser. The Mastersizer basically works on the Fraunhofer model and Mie theory. The former can predict the scattering pattern that is created when a solid opaque disc of known size is passed through a laser beam, while the latter theory predicts the way the light is scattered by spherical particles. But in nature the particles are not regular as considered by the above fundamental models. However, the key point here is that, if the size of a particle and other details of its structure are known, one can predict the way it scatters the light. In other words, each particle has its characteristic scattering pattern that is different than any other size particles. The Mastersizer works precisely backwards on the above theory. It actually captures the scattering pattern from a field of particles passing through a laser beam and calculates the sizes of the particles responsible for creating characteristic scattering patterns.

As particle size proxy was required to monitor the changes in detrital grain input from the fluvial activity, it is necessary to remove the carbonate skeletons from the sediment. Therefore, the sediment was completely decarbonised in mild HCl (0.5

N), washed repeatedly with RO-water to remove the traces of acid, dispersed in an ultrasonic bath and fed to the optical unit of the Mastersizer. The detector array of the Mastersizer takes several snap-shots of scattering produced by the particles settling through the analyser beam at particular time. The inbuilt Malvern software converts the scattering pattern in to the volume concentration using Beer-Lambert Law and expressed as percent. The volume percentages are used for interpretations without any conversions because the aim is to monitor relative variation of specific size-band particles rather than quantifying them for absolute grain-size distribution. The replicate measurements of few random samples suggest that the precision of the results is within ±1% of the distribution volume of a given size-band. The organic matter however was not removed from the sediment before size-analysis.

4.3. Calcium carbonate analysis

In the regions away from the hydrothermal activity and atmospheric dust sources, the sedimentary carbonate is normally derived from calcite secreting planktonic organisms. The areas in the vicinity of river discharge contain significant amount of continental silicate detritus. Hence, the down-core variation of these components provide first hand information about the past productivity and river intensity, which in turn are dependent upon the summer monsoon strength in the EAS. The flux of biogenic calcite is also a useful tool to assess past productivity because it minimises the bias due to dilution by terrigenous material and variations in sedimentation rates if the preservation is complete. Dried and accurately weighed salt-free sediment was reacted with 0.1 N HCl until the complete evolution of the CO_2. The leachate was centrifuged and decanted in to volumetric flask and diluted with 18 mohm deionised water. The diluted solution was analysed for Calcium (Ca) in a Perkin-Elmer® OPTIMA-2000 DV ICP-OES. The measured Ca was translated in to $CaCO_3$ using a conversion factor of 2.497. Accuracy of the measurement was assessed by analysing AR-grade synthetic $CaCO_3$ powder treated in the same way as the samples. The duplicate measurements of the sample leachates and the treated in the same way as the samples. The duplicate measurements of the sample leachates and the synthetic-$CaCO_3$ standard suggested that the analytical precision was within ±1 % and the accuracy was within ±2 %. The same leachates were also used for analysing Aluminum (Al). There is a possibility of HCl leaching the clay particles in the sediment. However, there are no reports demonstrating the corrosive effect of very mild-HCl on the clays. Therefore, I assume that the strength of the acid used (0.1 N HCl) for carbonate dissolution is the optimum strength to leach-out the carbonate and particle scavenged metals from the water column leaving behind the clays unaffected (see Banakar et al., 1998).

4.4. Sedimentary stable isotope analysis

4.4.1. Calcite oxygen- and carbon-isotopes:

Oxygen has three naturally occurring stable isotopes, ^{16}O (abundance 99.763 %), ^{17}O (abundance 0.0375 %) and ^{18}O (abundance 0.1995 %). Because of the higher abundance and the greater mass difference, the $^{18}O/^{16}O$ ratio is normally determined, which may vary in natural samples by about 10% or in absolute numbers from about 1:475 to 1: 525. As a result of fractionation during evaporation, the vapour tends to enrich with $H_2{}^{16}O$ relative to $H_2{}^{18}O$ leaving the reservoir (ocean) enriched with $H_2{}^{18}O$. When water vapour condenses to produce precipitation the fractionation is in the opposite sense, i.e., the water condensing from vapour and then precipitating is enriched with $H_2{}^{18}O$ relative to the remaining vapour. Hence, the first condensed rain is more enriched with $H_2{}^{18}O$ than the later rains. The greatest fractionation is however evident during the evaporation. Thus, the atmospheric evaporation-precipitation cycle results in net fractionation of oxygen isotopes and precipitated water is richer in $H_2{}^{16}O$ than the seawater from which it was evaporated. On a global scale, when ^{16}O-enriched water vapour is precipitated as snow and builds up to form glaciers and ice-caps, then the oceans will have lost proportional amount of ^{16}O along with fresh water until the ^{16}O enriched water locked in continental ice is released back to the ocean by melting. Therefore, the $^{18}O/^{16}O$ of the ocean produce distinct responses to the climate change. In other words the global oceans are ought to exhibit higher $^{18}O/^{16}O$ during the cold and dry glacial climate when the continental ice has waxed to a greater extent (more than 29% during the last glacial period compared to modern extent), and during the warm and humid interglacial climate the global oceans are replenished with ^{16}O due to waning of the ice sheets that have locked-in fractionated lighter-^{16}O from the ocean water. Such relative variations in the seawater $^{18}O/^{16}O$ ratios (higher during glacial periods and lower during interglacial periods) are preserved globally in the contemporary calcite skeletons secreted by the marine organisms such as foraminifera. In spite of large variation in absolute values of the $^{18}O/^{16}O$ exhibited by different species of the foraminifera depending on vital effects and their habitat, the general structure of the time-series calcite-$^{18}O/^{16}O$ in the sedimentary records over the world oceans is remarkably similar. This similarity rather suggests not only the global nature of the past climate change but also indicates the fidelity of the marine planktonic organisms to record such changes.

Carbon occurs in nature as highly reduced organic compounds in the biosphere to highly oxidized inorganic compounds such as CO_2 and carbonates. It comprise of two stable isotopes ^{12}C (natural abundance of 98.89%) and ^{13}C (natural abundance of 1.11%). The global seawater distribution of carbon-isotopic composition ($\delta^{13}C$) reflects the nutrient content and the marine photosynthesis (Kroopnick, 1985). The inter-oceanic thermohaline circulation (Broecker, 1991) is believed to convey the North Atlantic Deep-Water (NADW) and Antarctic Bottom-Water (AABW) $\delta^{13}C$ characters across the global oceans through overturning. However, in the surface ocean the source water $\delta^{13}C$ characteristics are modified to a greater extent due to ageing as it travels away from the source region and mixing with local water masses. The past climatic fluctuations in fact have affected the production of deep-water masses and hence the reservoir $\delta^{13}C$ composition, the details are out of the scope of the present study. Here, only the application of $\delta^{13}C$ in sedimentary biogenic material with respect to changes in local productivity is considered.

The carbon-isotopic fractionation basically is the result of both thermodynamic and kinetic processes acting simultaneously within the marine reservoir. In case of inorganic carbon associating with secretion of carbonate skeletons, the fractionation mechanism is by isotope equilibrium exchange reactions, which leads to enrichment of ^{13}C in carbonate. In organic matter, it is by the process of kinetic isotope effects i.e., during photosynthesis the light isotope ^{12}C concentrates in the synthesized organic matter leaving the ambient water enriched with ^{13}C. In other words, during high productivity episodes, the organic matter exhibits enrichment of light carbon and therefore, contemporary inorganic calcite secreted by the organisms from ^{13}C enriched ambient water should therefore exhibit relative enrichment of heavy carbon. The main isotope-discriminating steps during biological carbon fixation are 1) the uptake and intracellular diffusion of CO_2 and, 2) the biosynthesis of cellular components. The comprehensive details of the isotopes used for the present study are available in Hoefs (1997).

For the measurement of calcite carbon and oxygen isotope ratios, upper mixed layer dwelling planktonic foraminifera *Globigerinoides sacculifer (G. sacculifer)* (<30 m: Hemleben et al., 1989; Chaisson and Revello, 2000) was selected. Since the objective of the present work is related with the surface ocean processes and responses, this species is well suited. About 30-40 clean individuals of 250-350 μm size were picked under a binocular microscope from the coarse fraction (+63 μm) of the sediment sections. The tests were carefully observed under the microscope to avoid damaged specimen due to dissolution and specimen with terminal sacs. As the terminal sacs develop at deeper depths during their gametogenesis, the specimen with such sacs therefore may alter the surface water isotopic signals by contaminating with heavy-oxygen enriched signals inherent to colder deep ambient water (Hemelben et al., 1989). The sac-free specimen were transferred to thimbles, mildly crushed with a blunt pin in presence of a drop of ethanol to break-open the chambers, sonicated to remove fine detritus and dried at 50°C. The thimbles were placed in the numbered disc-holder of the reaction vessel, which was maintained under vacuum and connected to a glass transfer line having three cold fingers for three-step CO_2 purification.

The *G.sacculifer* tests were allowed to react completely in reaction vessel containing 100 % Phosphoric Acid maintained at 60° ± 1° C. The CO_2 released during the reaction (($3CaCO_3 + 2H_3PO_4 \Rightarrow 3CO_2\uparrow + 3H_2O + Ca_3(PO_4)_2$)) was purified thrice in the glass line maintained under vacuum. The liquid-nitrogen and a mixture of liquid-nitrogen and ethanol (to obtain solution having ~ –105° C temperature) were used respectively to trap moisture in cold-fingers and release only the CO_2. The purified CO_2 was analysed for oxygen- and carbon-isotopic ratios using a Finnigan MAT-251® mass-spectrometer. The measurement of $^{18}O/^{16}O$ and $^{13}C/^{12}C$ is done by using mass discriminator at 46 and 45 respectively against reference standard NBS-20 calibrated with PDB. The final isotopic ratios are expressed in PDB-calibrated scale (Table 2).

Table 2. Standards used for expressing isotopic compositions

Element	Description of standard	Standard
Calcite-O & C Organic matter-C	*Belemnitella americana* from the Cretaceous Peedee formation, South Carolina	PDB
Sedimentary-N	Air nitrogen	AIR

The stability of the equipment was obtained by repeatedly analysing an in-house standard Solenhoffen Limestone over the analytical period of three months (June-August, 2001) and the results were accurate and precise within ±0.02 ‰ (Table 3).

Table 3: Isotopic measurement results of the in-house Reference Standard (Solenhofen Limestone)

Sl. No.	$\delta^{18}O$ ‰ vs PDB	$\delta^{13}C$ ‰ vs PDB
1	-4.035 ± 0.011	-4.049 ± 0.012
2	-4.101 ± 0.011	-4.162 ± 0.009
3	-4.129 ± 0.018	-4.223 ± 0.012
4	-4.023 ± 0.016	-4.018 ± 0.008
5	-4.140 ± 0.018	-4.224 ± 0.015
6	-4.027 ± 0.021	-4.047 ± 0.013
7	-4.140 ± 0.015	-4.189 ± 0.008
8	-4.100 ± 0.028	-4.068 ± 0.011
9	-4.130 ± 0.015	-4.162 ± 0.016
10	-4.129 ± 0.023	-4.201 ± 0.008
11	-4.158 ± 0.020	-4.136 ± 0.015
12	-4.126 ± 0.012	-4.152 ± 0.017
13	-4.047 ± 0.014	-4.099 ± 0.003
14	-4.111 ± 0.019	-4.204 ± 0.009
15	-4.027 ± 0.029	-4.170 ± 0.009
16	-4.094 ± 0.034	-4.140 ± 0.009
17	-3.967 ± 0.026	-4.039 ± 0.014
18	-4.118 ± 0.024	-4.162 ± 0.007
19	-4.122 ± 0.035	-4.132 ± 0.014
20	-4.091 ± 0.028	-4.091 ± 0.015
21	-4.080 ± 0.012	-4.072 ± 0.012
Average:	**-4.090 ± 0.020**	**-4.130 ± 0.011**

4.4.2. Organic matter and carbon- and nitrogen- isotopes:

The different photosynthetic pathways distinctly fractionate C-isotopes, and the nitrogen fixation-denitrification processes leave distinct signals of nitrogen-isotopes in the sedimentary organic matter (Wada and Hattori, 1978). Therefore, it is possible to understand the past variation in organic production and its fate during oxidation and burial by studying the sedimentary organic matter. As such the organic carbon (C_{org}) and C/N ratios together provide fairly accurate information about the marine productivity, if the organic matter has escaped diagenetic alterations in the water column during its export to the seafloor or after burial in to the sediment. Therefore, well-preserved organic matter (normally evident by moderate to high organic carbon content in sediment) can be a measure of the photic zone productivity. The Redfield ratios of C/N are useful to evaluate the contribution of terrestrial organic matter in the marine sediment (Peters et al., 1978). The marine sedimentary biomarkers such as alkenones (di-, tri- and tetra-unsaturated ethyl and methyl ketones) are proved to be reliable indicators of marine productivity (Ikehara et al., 2000), as they are refractory to the settling or burial diagenesis unlike organic carbon (Brassell, 1993). Keeping this potential in mind, one core (GC-08) was subjected to detailed measurement of organic components and their isotopes to reconstruct the past climate driven productivity and OMZ-variations.

The finely powdered (-250 um) bulk sediment was decarbonised with 1 N HCl until carbonate fraction was removed quantitatively. The decarbonised fraction was washed repeatedly with de-ionised water to remove the traces of acid. The carbonate-free fraction was dried at 60°C. Accurately weighed dried sediment fraction was analysed for C_{org} and N in Fison® NA-1500 Elemental Analyser. The C- and N-isotopes were also measured simultaneously by flow-injection method using online Finnigan® MAT252 mass-spectrometer after combusting the sample and converting particulate-C and -N in to their gaseous components. The results of isotopic ratios are expressed as PDB calibrated units for C-isotopes and atmospheric-N_2 calibrated units for N-isotopes (Table 2). The accuracy of the results as obtained by repeated measurement of amino acid reagents and reference standards are within ±2% for C- and N-contents and within ±0.2 ‰ for C- and N-isotopes.

4.4.3. Alkenone extraction and measurement:

Alkenones forms a family of temperature-sensitive lipids comprising a series of C_{37}-C_{39} di-, tri-, and tetra-unsaturated ethyl- and methyl-ketones synthesised by the *Prymnesiophyceae* group of unicellular coccolithophorid algae, particularly *Emiliana huxleyi* species in the mixed layer (Volkman et al., 1980). These organic compounds are highly refractory to the diagenesis during or after their export to the seafloor. Additionally, the unsaturation index of the alkenones was found to be sensitive to the ambient water temperature at which they are synthesised. These properties rendered the alkenones as potential proxy for both SST and marine productivity see Brassell, 1993; Prahl et al., 1998; Yamamoto et al., 2000). In the recent past several researchers have used the alkenones extensively in palaeoclimate studies (see Cayre and Bard, 1999 and references therein).

Accurately weighed fine powders of dried sediment (1-2 grams) were taken in centrifuge tubes and the organic molecules were extracted in Dichloromethane-Methyl alcohol mixture under sonification. The extracted molecules were subjected to chromatographic separation of alkenones following the methods described by Yamamoto et al. (2000). Exactly 50 μl of internal standard ($C_{36}H_{74}$) containing 0.05 g/l of C_{36} to yield 5 ng in the eluted alkenone fraction was used as spike. The third (toluene eluted) fraction containing alkenones and internal standard were dried under nitrogen stream and the residue dissolved in ultrapure hexane, transferred to collapsible vials, loaded on the autosampler and analysed on a Hewlett-Packard®

Gas-Chromatograph. The results of the measurement compared to an in-house standard are within ±3%. The sum of di- and tri- ethyl and methyl ketones (Σalkenones) is considered here as the proxy for productivity. The unsaturation index ($U^{k'}_{37}$) was calculated from the concentration of di- and tri-unsaturated alkenones using Brassell et al. (1986) equation: [C37:2MK]/([C37:2MK]+[C37:3MK). The SST was then obtained using the calibration of Prahl et al. (1988):

$U^{k'}_{37}=0.034T+0.039$, where T is the SST in °C.

4.5. Estimation of excess- Al and -Mn:

The sedimentary scavenged-Al may be useful to support the other productivity proxy data, and particulate Mn-oxide is useful in understanding the redox conditions of the water. The details of particle scavenged-Mn and -Al and their potential application in marine geochemical processes are available in Banakar et al. (1998); Dickens and Owen (1994); Murray and Leinen (1993). The scavenged elements can be estimated from bulk sediment composition by subtracting the detrital silicate bound contents (Murray and Leinen, 1993; Banakar et al., 1998). However, extremely mild acid leaching can extract the particle surface bound and authigenic oxide bound scavenged metals from the bulk sediment providing an opportunity of direct measurement such scavenged phases of metals from seawater.

The 0.1 N HCl leached fraction from the bulk sediment (used for carbonate measurement) was utilized to estimate the excess-Al and –Mn content. A Perkin-Elmer® Optima DV-2000 ICP-OES was used for the analysis following three point calibration obtained by multi-element standards of Sigma-Aldrich®. A synthetic standard was prepared for estimation of accuracy and precision of the results. The analysed results are accurate and precise within ±3%.

5. Results

The down-core records of sediment texture, calcite-oxygen and -nitrogen isotopes, sedimentary organic components and their isotopes, and sedimentary inorganic components exhibit in general smooth variations suggesting at the outset a) the variations are natural and b) the sediment cores are free from post depositional perturbations such as bioturbation or turbidite or slumping. These characters of the present sedimentary records would help in reconstructing the past oceanic responses to the climate change with reasonable confidence. In the following sub-sections, I describe the salient features of the results separately for each sediment core.

5.1. Age-model and chronology

SK 117/GC08 (Figure 2):

The $\delta^{18}O_{G.sacculifer}$ in the core-top section is –1.37 ‰. The lowest value of the entire down-core record is at a depth of 15 cm (-1.65 ‰). The down-core fluctuations of the $\delta^{18}O_{G.sacculifer}$ are marginal up to 19 cm depth. From 19 cm the $\delta^{18}O_{G.sacculifer}$ rapidly increases to ~0.4 ‰ and further down up to 90 cm varies within a narrow range of ~0.2 ‰. The heaviest (0.47 ‰) $\delta^{18}O_{G.sacculifer}$ is recorded at 75 cm depth. From 90 cm to 123 cm these values significantly decrease from 0.47 up to –0.33 ‰ and remain more or less constant ~0.2 ‰ up to 280 cm depth. The second and third lowest $\delta^{18}O_{G.sacculifer}$ events are located at 329 cm (-1.10 ‰) and at 397 cm (-1.19 ‰).

The down-core $\delta^{18}O_{G.sacculifer}$ profile shows well-defined Marine Oxygen Isotope Stages (MIS). The age model is constructed by tuning the down-core $\delta^{18}O_{G.sacculifer}$ profile to the low latitude SPECMAP stack (Bassinot et al. 1994), which is a modified version of the original SPECMAP of Imbrie et al., (1984). This enabled to demarcate the Holocene/LGP boundary (11 Ka) at 25 cm; LGP/MIS3 (24 Ka) at 105 cm; MIS 3/4 (57 Ka) at 227 cm; and MIS 4/5 (71 Ka) at 290 cm. The marine isotopic stage boundaries are drawn at the mean of the highest and lowest oxygen isotopic values between the two adjacent warm and cold oxygen isotope events defined in the SPECMAP. Four tie-points are used to evolve fairly accurate age model, viz., 1) The Last Glacial Maximum (LGM) occurring at 18 Ka identified at 75 cm exhibiting the latest heaviest oxygen isotope event (0.47 ‰), 2) occurrence of the well-dated Youngest Toba Tuff (YTT) at ~ 72 Ka (Ninkovitch et al., 1978) identified by the presence of abundant YTT-characteristic glass-shards (Pattan et al., 2000) at 297 cm, and 3) the interstadials of MIS5, viz., MIS5.1 occurring at 330 cm and MIS5.3 at 397 cm dated to be 79 Ka and 97 Ka respectively (Bassinot et al., 1994).

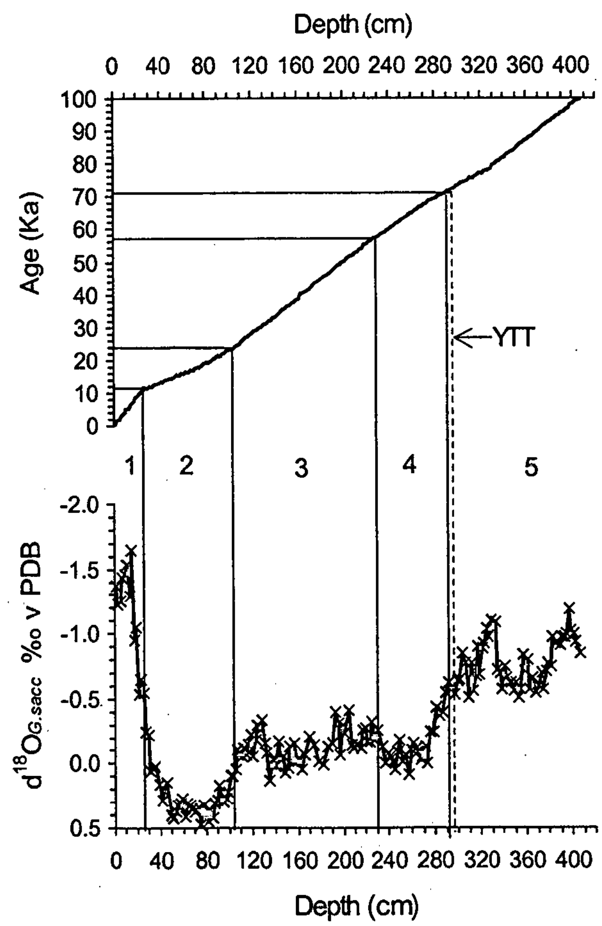

Figure 2: Marine oxygen isotope stage (MIS) boundaries recognized in the SK117-GC08 core. The age model (upper panel) is derived from tuning the *G.sacculifer* oxygen isotope depth curve to the tropical-stack SPECMAP. The horizontal and vertical lines indicate depth-age relationship. The numbers are the marine oxygen isotope stages. The core covers last 100 Ky time-span. YTT=Youngest Toba Tuff that occurs at 297 cm depth in core. Two lighter oxygen-isotope peaks in MIS5 are the two warm interstadials 5.1 and 5.3 separated by colder stadial 5.2.

SK-129/CR-04 (Figure 3):

The $\delta^{18}O_{G.sacculifer}$ in the core-top section is –1.82 ‰ and remains more or less uniform up to 32 cm where it begins to increase rapidly down-core reaching ~0.00 ‰ at 70 cm forming the peak of the heaviest $\delta^{18}O_{G.sacculifer}$. The lightest $\delta^{18}O_{G.sacculifer}$ in the entire down-core profile occurs at 358 cm (-2.14 ‰). The lighter $\delta^{18}O_{G.sacculifer}$ peak is located at 15 cm depth (-2.04 ‰). The isotopic values remain more or less constant at around –0.6 ‰ from 90 cm to 230 cm but with a marginally heavy $\delta^{18}O_{G.sacculifer}$ ~200 cm. A decrease from –1.55 ‰ to -2.2 ‰ is evident between 230 cm and 380 cm. This increase contains three distinct increasingly lighter $\delta^{18}O_{G.sacculifer}$ peaks down-core (i.e., at ~258 cm, at ~308 cm, and at ~356 cm). Further down-core the profile exhibits heavy $\delta^{18}O_{G.sacculifer}$ similar to that found ~70 cm depth. Thus a distinct transition from the heavy $\delta^{18}O_{G.sacculifer}$ to light $\delta^{18}O_{G.sacculifer}$ is evident between 400 cm and 360 cm depths in core. The structure of this transition is quite similar to that found between the 70 cm and 30 cm depths in the core.

The above-described depth versus $\delta^{18}O_{G.sacculifer}$ profile of SK129-CR4 core is tuned to the low latitude SPECMAP stack (Bassinot et al., 1994). Thus identified marine oxygen isotope boundaries are, Holocene/LGP boundary (11 Ka) at 40 cm, LGP/MIS3 (24 Ka) at 94 cm, 3/4 (57 Ka) at 181 cm, 4/5 (71 Ka) at 220 cm and 5/6 (122 Ka) at 358 cm. Several tie points are also used to evaluate the precision of the age model. They are, 1) the LGM (18 Ka) at 70 cm depth, 2) Youngest Toba Tuff (~72 Ka) at 224 cm, 3) Last Appearance Datum (LAD) of *G. ruber* (pink variety) (120 Ka) at 354 cm and, 4) the interstadials of MIS5, viz MIS5.1 (79 Ka), MIS5.3 (97 Ka) and MIS5.5 (122 Ka) at 258 cm, 308 cm, and 358 cm depths respectively. The derived age model for SK129-CR4 indicates that the core covers the last 148 Ka.

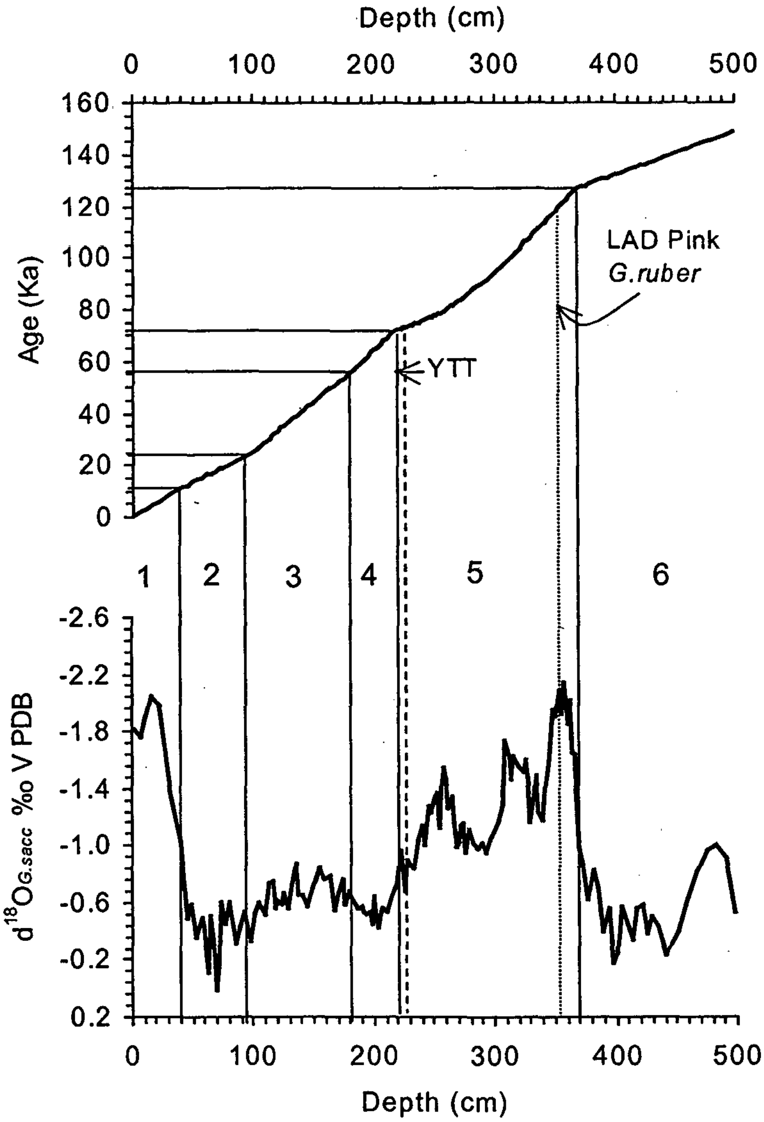

Figure 3: The age model for SK129-CR04 core. The vertical and horizontal lines are the marine oxygen isotope stage boundaries recognized in the core with corresponding ages as defined in the SPECMAP. The vertical lines with labels are the independent tie-points in the form of YTT (~72 Ka) located at 228 cm depth and the last appearance datum of *G. ruber* (pink variety) at 352 cm dated to be 120 Ka (Thompson and Duplessy, 1982). Clearly defined LGM and interstadials of MIS5 (5.1, 5.3, and 5.5) provided additional control points for the age model. The numbers are the marine oxygen isotope stages.

SK-117/GC-02 (Figure 4):

The core top $\delta^{18}O_{G.sacculifer}$ is –1.83 ‰, which is nearly uniform with marginal fluctuations down-core up to ~20 cm. Further down the $\delta^{18}O_{G.sacculifer}$ increases rapidly to –0.6 ‰ at ~85 cm. From 85 cm down to ~350 cm the increase is rather gentle (from –0.6 ‰ to 0.2 ‰). The lightest $\delta^{18}O_{G.sacculifer}$ of the entire core (–2.04 ‰) is recorded at 11 cm depth and the heaviest $\delta^{18}O_{G.sacculifer}$ (0.18 ‰) is at 293 cm. Further down-core the $\delta^{18}O_{G.sacculifer}$ decrease to –0.45 ‰ at 386 cm (bottom of the core) from 0.17 ‰ at 347 cm depth.

The comparison of the $\delta^{18}O_{G.sacculifer}$ depth-profile with the SPECMAP suggests that the core appears to cover a maximum of 24 Ka, i.e., the Holocene and LGP. The Holocene and the LGP boundary and the isotopic variation within this time-span can be appreciated by referring to the compressed inset and the exploded versions of the isotope-depth profiles together in Figure 4. The Holocene/LGP boundary (11 Ka) is located at 44 cm depth and LGP/MIS3 boundary (24 Ka) appears to be at 386 cm depth. There were no independent tie-points available to verify the accuracy of this age model, but based on the structure of the isotope-depth profile, the derived age model appears to be fairly accurate. The latest heaviest $\delta^{18}O_{G.sacculifer}$ (0.18 ‰) at 293 cm depth is considered as the LGM. However, the AMS ^{14}C dating would help to overcome any ambiguity if at all evident in the present age model.

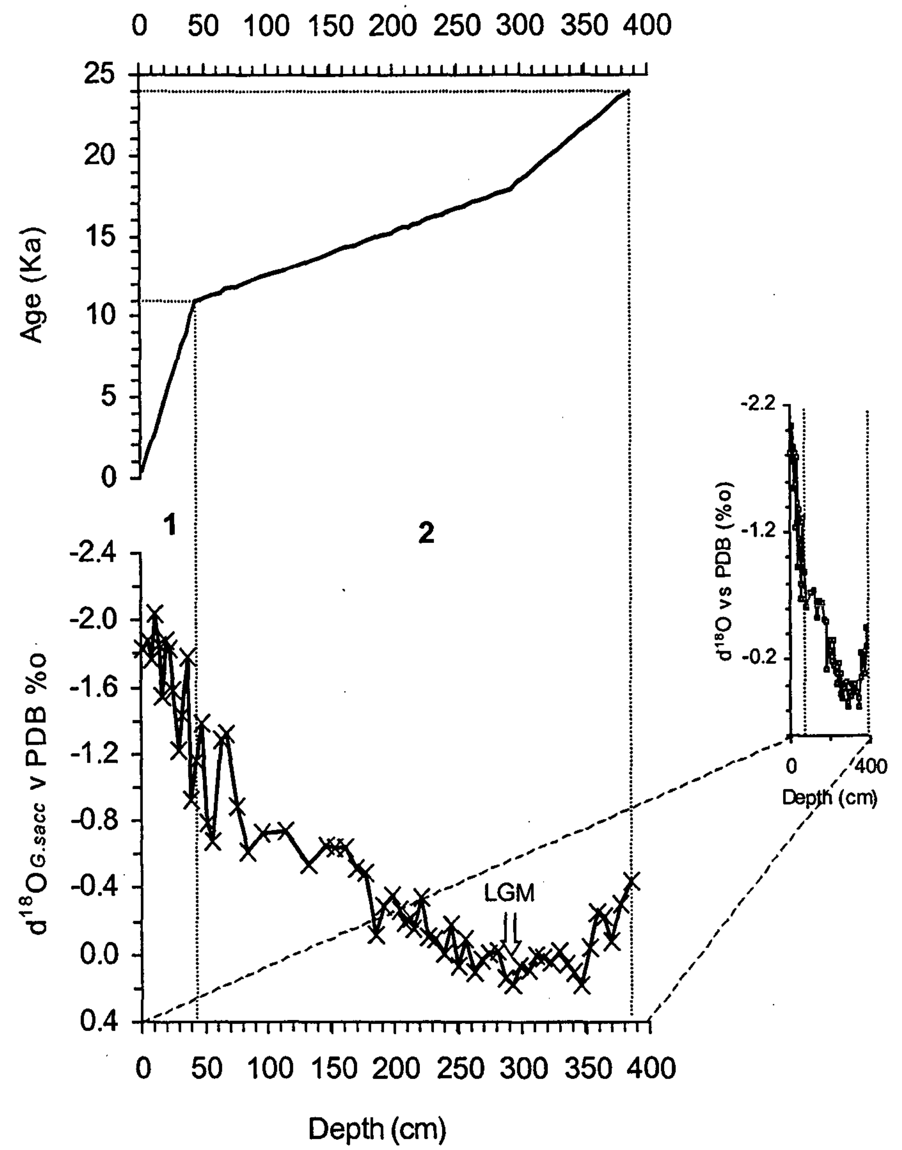

Figure 4: Depth versus oxygen isotope profile used for the Age-Model of SK117/GC-02 core. The compressed inset on the right-hand-side is presented for ready comparison with the SPECMAP. The upper exploded panel is the depth-age curve used to define the age-model. Vertical and horizontal broken lines indicate the marine oxygen isotope stage boundaries and corresponding ages. LGM=Last Glacial Maximum (~18 Ka) identified as the latest heaviest oxygen-isotope event in the depth profile.

5.2. Sedimentation rates:

The changes in marine sedimentation rates in the proximity of continents provide preliminary clues about the past variation in aeolian dust, fluvial erosion input, and the marine productivity (Prins et al., 2000; Sirocko et al., 1993). The sedimentation rates are essential to estimate the mass accumulation rates of the components at the seafloor, which eliminates the bias (due to dilution effect) associated with interpreting direct weight concentrations in sediments with varying physical properties. In the present case, the sedimentation rates in GC2 and GC8 from the shelf and slope off Goa are expected to provide a cumulative scenario of fluvial erosion input from the Mandovi-Zuari river draining the hinterland of Goa (part of Deccan Mountain belt), continental dust input mainly from the adjoining Indian peninsula by the winter monsoon winds and the water column productivity. On the other hand, sedimentation rates in the third core (CR4) would dominantly indicate changes in productivity, because this core is far removed from the land and the winter monsoon wind influence is less dominant. The calculated sedimentation rates using the depths at which various isotope stage boundaries are defined, isotope stage boundary timings, and the total thickness of the sediment represented by the each isotope stage are presented in Table 4.

Table 4: Linear sedimentation rates

Core	Sedimentation rate (cm/ky)					
	Holocene	LGP	MIS-3	MIS-4	MIS-5	MIS-6
SK117/GC02	4.0	25.6				
SK117/GC08	2.3	6.1	3.8	4.0	4.6	
SK129/CR04	3.6	4.4	2.6	2.2	3.1	4.1

From Table 4 it is clear that the sedimentation rates in all the three cores are highest during the LGP. The Holocene sections exhibit moderately varying sedimentation rates, i.e., 2-4 cm/ky in all the cores. The GC-02 core (continental self) shows extremely high sedimentation rate (by ~6 times) during the LGP than during the Holocene. The deep-water core (GC-08) from the same longitude exhibits three times higher rate of sedimentation during the LGP than during the Holocene. The southern EAS deep-water core (CR-04), on the other hand shows marginal increase during the LGP. This core records nearly similar sedimentation rate during the penultimate glacial period (MIS6) as that during the LGP. In the GC08 the sedimentation rates during the MIS5 through MIS3 time-slice are same (~4 cm/ky) and are nearly two times higher than the Holocene.

5.3. Sediment texture

SK117/GC08 (Figure 5):

In general the +63 μm (sand) fraction exhibits decreasing trend down-core. The variation is of an order of magnitude (between ~25 % and ~2 %). The Holocene section contains high percentage (Av. ~22%) than the sections corresponding to

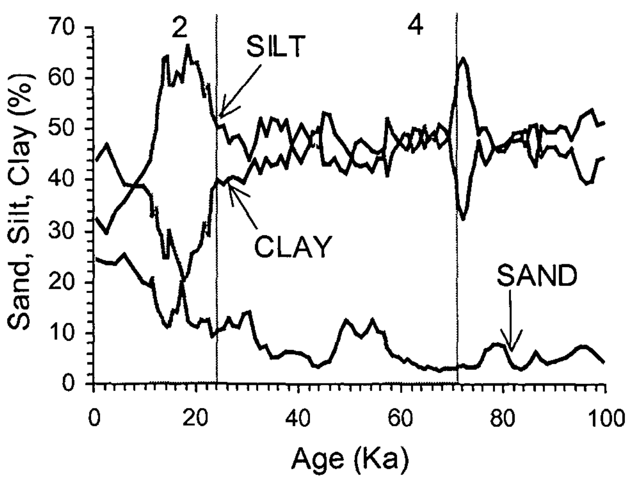

Figure 5: Temporal distribution of the three sediment fractions in continental slope core off Goa (SK117/GC-08). Note the mirror image variation in silt and clay fractions independent of the sand fraction. The minimum clay and maximum silt characterize the LGP. Where as, the maximum sand characterizes the Holocene. The vertical shaded bars are the glacial stages defined by the age model.

other time periods. The LGP contains on an average ~10 % sand but with a peak of ~20 % at ~16 Ka. The MIS3 period exhibits two minor peaks of sand at ~30 Ka (14 %) and ~50 Ka (12 %) separated by broad trough of nearly 20 ky time-span. The sand content in the MIS4 and MIS5 sections is the lowest (~3%) of the entire record without any significant variation.

The silt- and clay-fractions exhibit an interesting mirror-image temporal-trend independent of sand. The clay content varies between 20% and 50 %. The dominant fraction of the sediment is the silt, which varies between 40 % and 65 %. The LGP interval exhibits highest silt content (~65%) and lowest clay content (~20%). The Holocene period records ~42% silt and ~35% clay. Nearly equal content (~45%) of both these fractions dominate the rest of the time period prior to the beginning of the LGP. The only significant feature of the pre-LGP silt-clay variation is the second highest silt-lowest clay pairing (62% vs 32%) at around the closure of MIS5.

SK129/CR04 (Figure 6):

Down the core, the sand fraction increases from 20 % (core-top) to 38 % at ~9 Ka, reduces to ~18 % (~16 Ka), and remains more or less constant ~20% through the MIS3 period. A further reduction by ~10 % through the MIS4 section results in the lowest (~7 %) sand content at ~72 Ka. The second peak of ~40 % sand is located at MIS5.5 (~122 Ka) and further down-core reduces to ~10 % through the MIS6. Interestingly, the sand fraction monotonously increases through all the three glacial events leading to peaked concentration at the commencement of succeeding warm events. The structure of the temporal sand profile for the Holocene and the MIS5.5 appear to be very similar. The silt and sand exhibit more or less opposite trend. The prominent low-silt events in the core are identified at ~9 Ka (40 %), ~82 Ka (45 %) and ~ 123 Ka (36 %), where as, the high-silt events are located at 17 Ka (59 %) and 73 Ka (~72 %). The rest of the silt distribution varies marginally around 50 % throughout. Even though the clay is second abundant sediment fraction, it follows partly the sand and partly the silt. There are three low clay events located at ~15 Ka (22 %), ~ 72 Ka (28 %) and ~ 125 Ka (31 %). Overall marginally high clay content is restricted to the warm stages like Holocene and the MIS5.

Figure 6: Temporal variation of the three sediment fractions in southern-EAS continental slope core (SK129/CR04). Note the opposite trends in the silt and sand variation. The block arrow indicates that the MIS6 continues beyond the core record. The vertical shaded bars with numbers are the glacial stages as defined by the age-model.

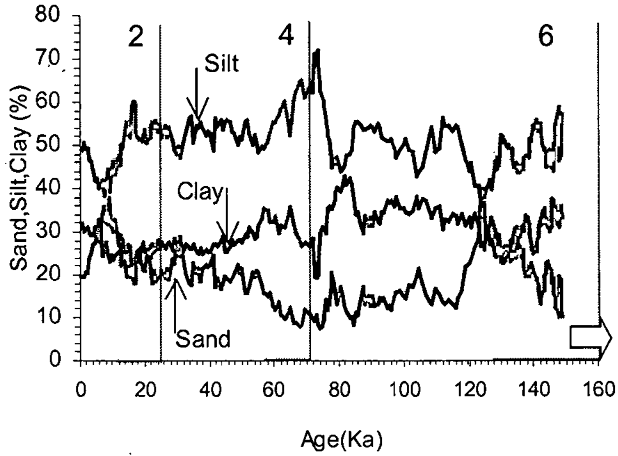

SK117/GC02 (Figure 7):

Except for few spikes around the beginning and closure of the LGP, the sediment fractions exhibit smooth variation. The variation of sand fraction is exactly opposite to both silt and clay, which are strongly coherent with each other in the core. The Holocene section exhibits highest content of sand (~80 %) and reaches the lowest of <5 % at ~11 Ka. At the commencement of the LGP, the sand content is very low (<10 %) and drastically increases between ~21 Ka and ~18 Ka (i.e., around

Figure 7: The Last Glacial to Holocene variation in the sediment fractions of the SK117/GC-02 core. Note the alternating dominance of coarse (sand) and fine (silt & clay) fractions at around the beginning of the LGP and the Holocene. The upward arrows on the age-axis indicate prominent events of coarse-fine reversals.

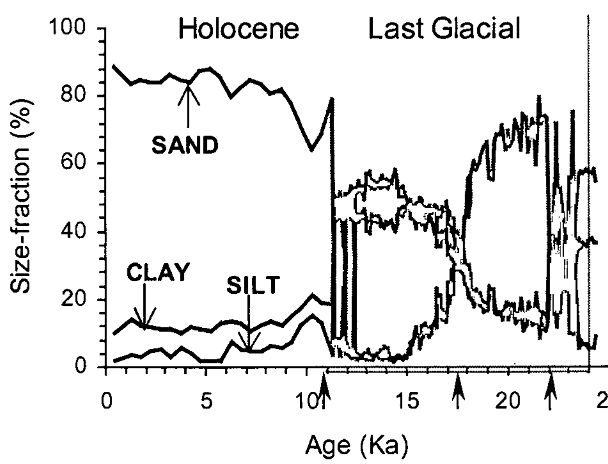

LGM) to as high as >60 %. On the other hand, the lowest silt and clay contents are recorded during the Holocene followed by during the early part of the LGP (~22 Ka-~18 Ka), which overtake the sand dominance at ~18 Ka until ~11 Ka. The overall clay fraction is higher (~12 %) than the silt (~3 %) in the Holocene interval. Where as, during the LGP the clay and silt contents are nearly equal and vary between 20 % and 40 %.

5.4. Time-series record of sedimentary inorganic components

5.4.1. Calcium carbonate

SK117/GC08 (Figure 8):

The calcium carbonate (henceforth only carbonate) content varies from 18 % to 49 %. There are four elevated carbonate intervals in the core, which are at around the latest Holocene, mid-LGP, early-MIS3 and MIS5.3. A fifth peak of ~35% carbonate is at MIS5.1, which is formed due to two lowest content (<20 %) troughs of carbonate at the commencement of MIS4 and at the MIS5.2. The former peaks exhibit nearly constant carbonate content of ~45 %. The other characteristics of the carbonate distribution in this core are, a) a drastic increase through the Holocene and MIS4, and marginal variation (within ±5 %) during the LGP through MIS3 time-slice, and b) extreme variations (~20 % to ~45 %) through MIS4 and in MIS5.

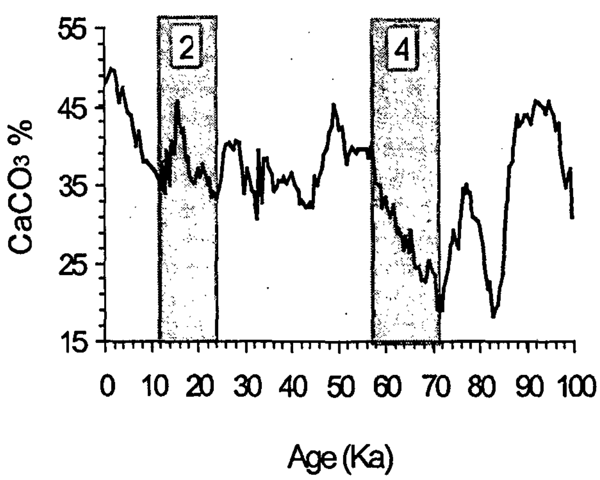

Figure 8: Temporal variation of calcium carbonate in the SK117/GC08 core. Note the distinctly elevated carbonate in the post-MIS4 period, which begins to increase from ~20% at the commencement of MIS4 and reaches a high of ~45 % in the earliest MIS3. The largest variation is found during the MIS5 period.

SK-129/CR04 (Figure 9):

The average carbonate content in the core is ~50 % with a minimum at ~72 Ka. The Holocene through MIS3 section exhibits relatively narrow variation within ±5 % around an average of 55 %. The carbonate content shows a monotonous increase through the MIS4 from ~25 % at the commencement to ~50% at the closure. The MIS5 section on the other hand contains three high carbonate peaks separated by three low carbonate troughs. The structure of the carbonate variation during the MIS5 though appears to resemble the stadial-interstadial pattern recognized in the oxygen isotope curves, but do not exactly correspond to their timings. The high-low carbonate events are rather located at the transition of stadial-interstadial events in MIS5. A common feature in carbonate variation during all the three glacial events is that of increasing trend through the glacial period towards the succeeding warm intervals.

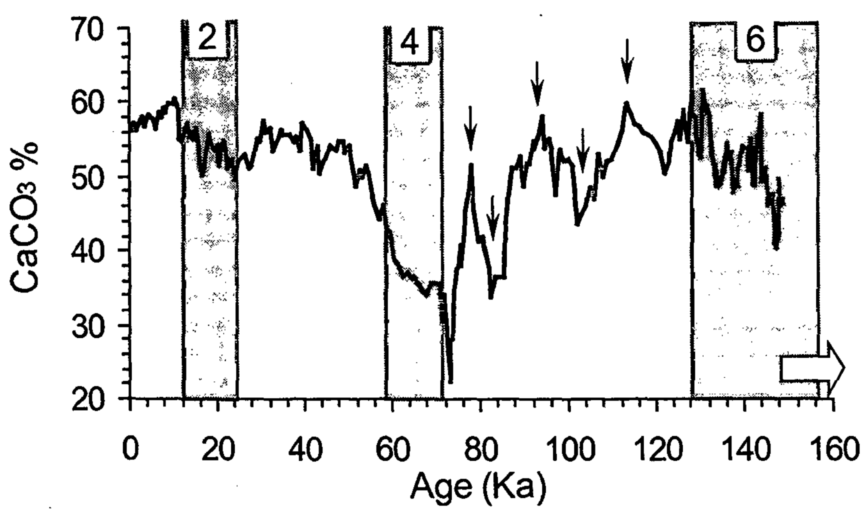

Figure 9: Temporal variation in carbonate content of the SK129/CR04 core from the southern-EAS region. Note the drastic increase of carbonate content through the MIS4 and the typical stadial and interstadial type structure in the MIS5 (downward arrows). Block arrow indicates that the MIS6 continues further down-core. The shaded bars are the glacial periods numbered at the top.

SK117/GC02 (Figure 10):

The Holocene average carbonate content is ~80 % without significant variations except for a rise at ~5 Ka. On the other hand, the LGP section records extreme variation. The LGP begins with a drastic increase from 20 % (at ~ 24 Ka) reaching to 60 % (at ~ 22 Ka) (i.e., 40 % increase in 2 kyr span). The rise continues gradually up to a maximum of ~70 % at ~17 Ka. During the latest part of the LGP (15 Ka onwards) the carbonate content gradually decreases to ~55 % at its termination.

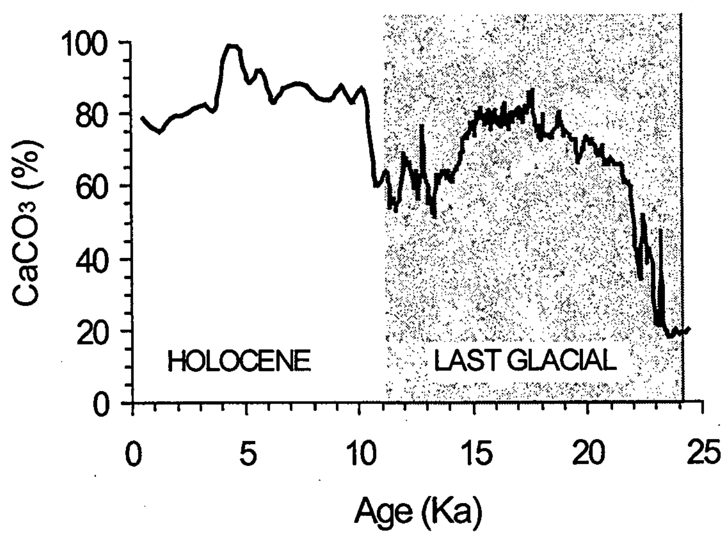

Figure 10: The carbonate variation during the LGP through the Holocene recorded in SK117/GC02 core. Note a drastic increase (from ~20 % to as high as 60 %) in the carbonate content during beginning of the LGP.

5.4.2. Particulate-Mn and scavenged-Al variation (Figure 11):

The particulate Mn-oxide and the detrital silicate unsupported-Al (scavenged-Al) could be the indicators of water column redox conditions and surface water productivity respectively (Banakar et al., 1998; Dickens and Owen, 1994; Murray and Leinen, 1993). The core exhibits highest Mn_{excess} (~250 ppm) in the earliest part of the LGP decreasing to ~40 ppm at around 15 Ka. Further later, it increases to ~100 ppm in the latest part of the LGP, followed by monotonous decrease to 50 ppm through the Holocene. The Al_{excess} variation in this core is nearly similar to that of the Mn_{excess}. The lowest concentration troughs in the time-series are centred ~17 Ka.

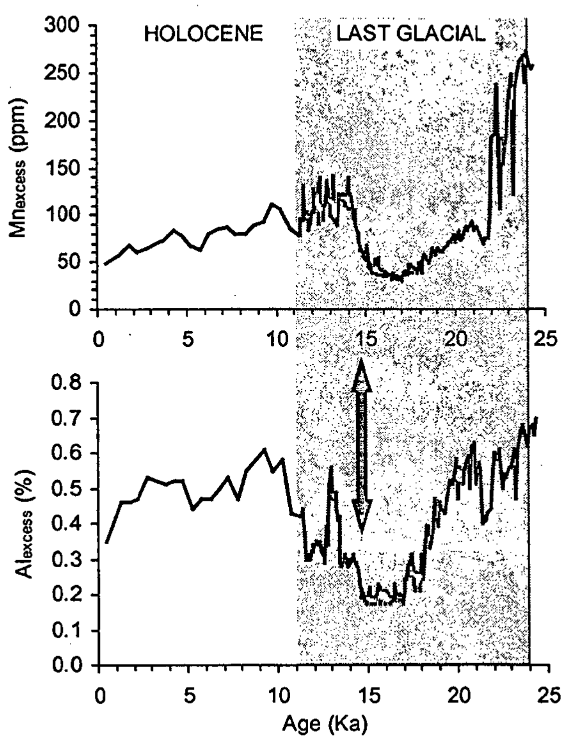

Figure 11: Sedimentary Al_{excess} and Mn_{excess} variation in continental shelf core (GC02). The shaded area is the time period covered by the LGP. The double head arrow marks the beginning of increase in excess Al & Mn around the beginning of deglaciation.

5.5. Time-series records of sedimentary organic components:

The data of sedimentary organic components comprising organic carbon (C_{org}), total nitrogen (N_{tot}), and alkenones was obtained for only one deep-water core (GC08) due to certain analytical constraint. I am aware of this limitation because modern biogenic-flux across the deep Arabian Sea greatly varies in space (Haake et al., 1993; Nair et al., 1989). Nevertheless, the present data-set for the GC-08 forms the nearly complete climate proxy record and hence should be able to provide important clues regarding EAS responses to past climate variability.

5.5.1. Sedimentary organic carbon and nitrogen (Figure 12):

The temporal variation of C_{org} and N_{tot} exhibit strictly similar trends as normally expected for the unaltered marine organic matter (Peters et al., 1978). The carbon is enriched nearly by an order of magnitude than the nitrogen. The C_{org} ranges from 0.5 to 1.8 %, while the N_{tot} varies between 0.06% and 0.21% in the core. During the major part of the LGP and MIS3 both these components are distinctly higher than the mean contents of 1% and 0.13% respectively in the core. In the MIS3 section the C_{org} and N_{tot} attain highest concentrations (up to 1.8% and 0.21% respectively). The C_{org} content in the Holocene is not only less than the core average, but also is the second lowest average content (~0.8%). Through the MIS4, both the components gradually decrease from ~1.2% and 0.15% to 0.5 % and 0.07 % respectively. The MIS5 stadial exhibits higher C_{org} and N_{tot} (~1.2% and 0.16% respectively) than the interstadials (~0.5% and 0.06%). The C_{org} and N_{tot} in the LGP are distinctly higher than the Holocene.

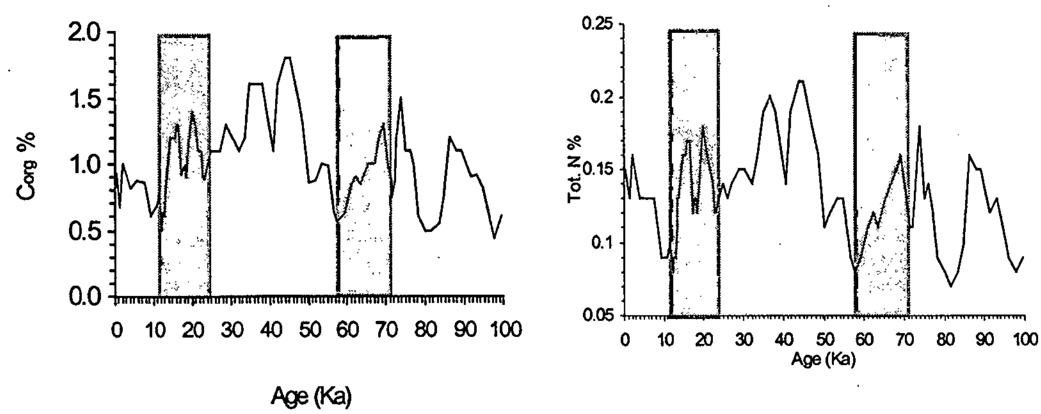

Figure 12: The temporal variation of the sedimentary organic-carbon and total-nitrogen in GC08. The replicated behaviour of these components suggests negligible fractionation. The carbon content is nearly 8 times higher than the nitrogen, nearly in accordance with the Redfield Ratio for marine organic matter (~7).

5.5.2. Alkenone variation during the LGP to Holocene (Figure 13):

The temporal variation of the Σalkenones (sum of di- and tri-unsaturated ketones C37, C38 and C39) exhibit extremely low content in the Holocene section (<0.1 ppm) as compared to very high concentrations up to 1.6 ppm in the LGP. The Holocene- Σalkenones show nearly constant value (<0.1 ppm), while in the LGP the content ranges between 0.6 ppm (~18 Ka) to ~1.5 ppm (~20 Ka & ~14 Ka). The average Σalkenones content in the LGP (~1 ppm) is higher by an order of magnitude than the Holocene. The actual rise in Σalkenones appears to begin around the commencement of the LGP and reaches the peaked concentration at the beginning of the deglaciation.

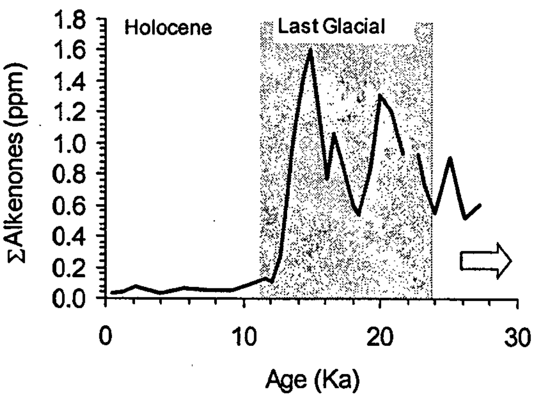

Figure 13: Temporal variation of Σalkenones during the last 27 Ka in GC08. The concentrations in the LGP sections are enriched by an order of magnitude compared to the concentrations in the Holocene. The block arrow indicates that the MIS3 continues further down-core. The shaded vertical bar is the LGP.

5.5.3. Time-series record of organic carbon isotopes ($\delta^{13}C_{org}$) (Figure 14):

The temporal variation of sedimentary $carbon_{org}$ isotopes is within –19 ‰ and –17 ‰. The most depleted $\delta^{13}C_{org}$ are evident around the latest Holocene, mid-MIS3, commencement of MIS4, and at MIS5.2 with a value of ~ -19.3 ‰. The enriched $\delta^{13}C_{org}$ is evident at the commencement of the Holocene (~17.7 ‰) and at around MIS5.1 (~18.1 ‰). The $\delta^{13}C_{org}$ curve exhibits steep slopes leading to rapid peak and troughs. The most prominent and largest excursion of around 2.4 ‰ is noticed in the Holocene section, where the $\delta^{13}C_{org}$ with ~ -17 ‰ at the beginning of the Holocene

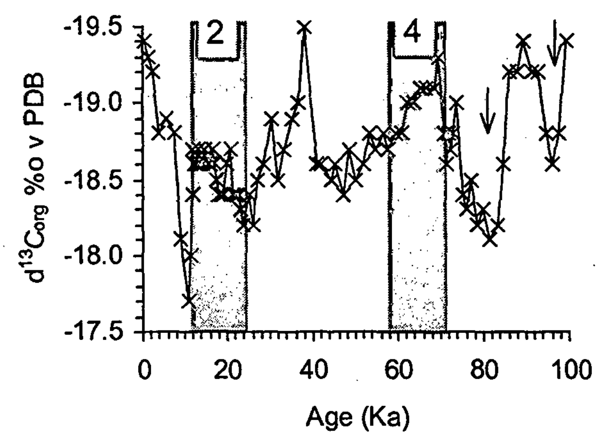

Figure 14: The $\delta^{13}C_{org}$ variation during the last 100 Ky recorded in GC08 core. Equally depleted $\delta^{13}C_{org}$ events are evident at the latest Holocene, mid-MIS3, early-MIS4, and mid-MIS5. The downward arrows indicate higher$\delta^{13}C_{org}$ around the MIS5 interstadials (5.1 & 5.3) than during the stadial (5.2).

decreases to ~ -19.5 ‰ in the latest Holocene (core top) section. Both the interstadials of MIS5 exhibit distinctly enriched $\delta^{13}C_{org}$ than the stadial.

5.5.4. Time-series record of sedimentary nitrogen isotopes ($\delta^{15}N$) (Figure 15):

The sedimentary nitrogen isotopes ($\delta^{15}N$) show distinct alternating enrichment and depletion during the last 100 Ky. Similar to the sedimentary organic-

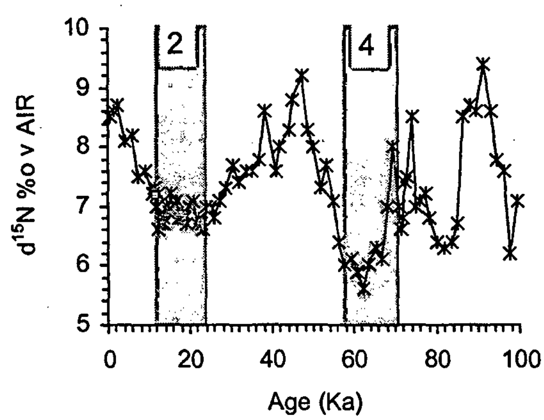

Figure 15: The temporal record of the sedimentary nitrogen isotopes in GC08 core. The variation defines several enrichment and depletion events.

carbon isotopes, the LGP section exhibits near uniform concentration of the $\delta^{15}N$ (~7 ‰). Prominent peaks and troughs are evident throughout the pre-LGP period. The lowest $\delta^{15}N$ (5.8 ‰) is evident in MIS4 followed by MIS5.1 and MIS5.2 interstadials.

The MIS5.1 and MIS5.2 low $\delta^{15}N$ events are separated by a maximum enrichment (9.4 ‰) event centred on MIS5.2. The MIS3 section also contains a prominent peak of enriched $\delta^{15}N$ (~9.2 ‰) at ~45 Ka. Through the Holocene the $\delta^{15}N$ increases from ~7 ‰ at it's commencement to 8.5 ‰ in the recent most (core-top) section. Another important aspect of the $\delta^{15}N$-temporal record is that the enrichment events appear to have spaced at about 45 Ky intervals, if relatively less prominent intruding peak at ~72 Ka is ignored.

5.6. Time-series record of *G. sacculifer* carbon isotopes (Figure 16):

The temporal record of the calcite carbon isotopes obtained from the skeletons of the *G.sacculifer* exhibit large scatter. Nevertheless, few distinct trends are noticeable. Therefore, to bring-out those trends the data is smoothed by two point running averages.

In the GC-08 core (panel A) the $\delta^{13}C_{G.sacculifer}$ variation exhibits a decreasing trend through both the glacial stages (LGP and MIS4), where it decreases from ~1.1‰ at their commencement to ~0.6 ‰ at their closure. A monotonous increase from 0.6 ‰ to 1.05 ‰ is evident through the MIS3. However, during the Holocene and the MIS5 the $\delta^{13}C_{G.sacculifer}$ fluctuations are rather gentle (within ±0.3 ‰) around an average of 0.9 ‰. These minor fluctuations within both the warm periods do not exhibit any discernible trends. The lowest $\delta^{13}C_{G.sacculifer}$ are evident around 13 Ka and 56 Ka.

The $\delta^{13}C_{G.sacculifer}$ variation in CR04 core (Panel B) is more complex. The fluctuations through the last ~100 Ky are within a narrow margin of ±0.3 ‰ around an average of ~1.2 ‰. The MIS4 exhibits minimum variation of <0.2 ‰ as compared to the rest of the 100 Ky time-span. The most interesting and the prominent feature in this core is a major positive shift from ~0.6 ‰ at ~128 Ka, to ~1.3 ‰ at ~100 Ka. This 0.7 ‰ shift is nearly double than those recorded in other time-slices in the core and marks a major event in the last 150 Ky $\delta^{13}C_{G.sacculifer}$-record. Prior to this shift, in the latest part of the MIS6, the $\delta^{13}C_{G.sacculifer}$ remains ~0.8 ‰ with a fluctuation of ±0.3‰. Thus there are two levels of $\delta^{13}C_{G.sacculifer}$ trends in the core, viz., the enriched $\delta^{13}C$-trend (~1.2 ‰) during post-100 Ka period, and depleted $\delta^{13}C$-trend (0.8 ‰) prior to the Glacial Termination 2 (GT2) (or the commencement of MIS5 warm period). Thus the GT2 marks a major positive shift in the calcite carbon isotopes.

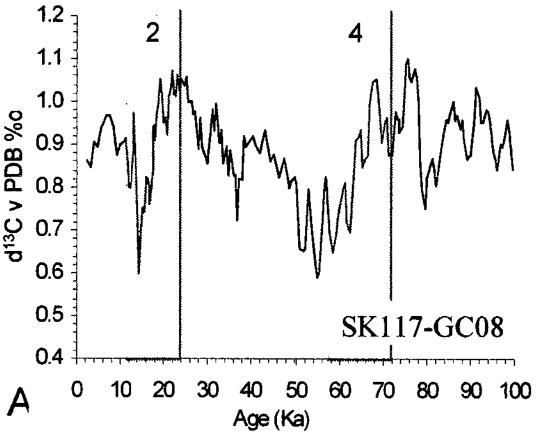

Figure 16: Time-series *G.sacculifer* calcite-$\delta^{13}C$ record in the Eastern Arabian Sea sediment. The two long-term records of the deep-water cores (A & B) exhibit nearly comparable temporal variation suggesting robustness of the carbon-isotopic record despite large fluctuations. The last glacial fluctuations appear more complex than during the Holocene in the high-resolution record of the GC02 core. Note a major positive shift of the $\delta^{13}C_{G.sacculifer}$ at the Glacial Termination 2 through the MIS5 in the CR4 (B). Panel A = GC08, Panel B = CR04 and Panel C = GC-02.

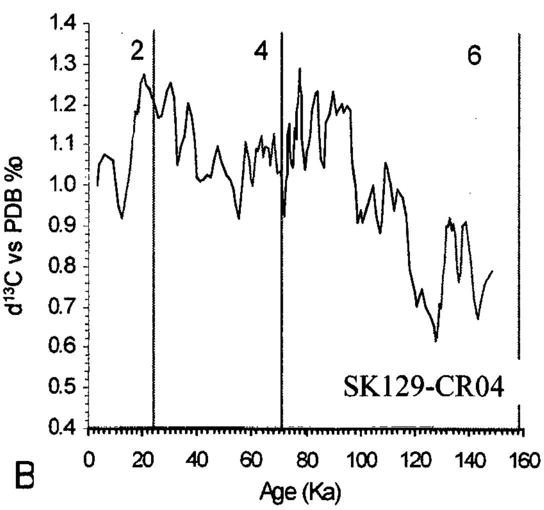

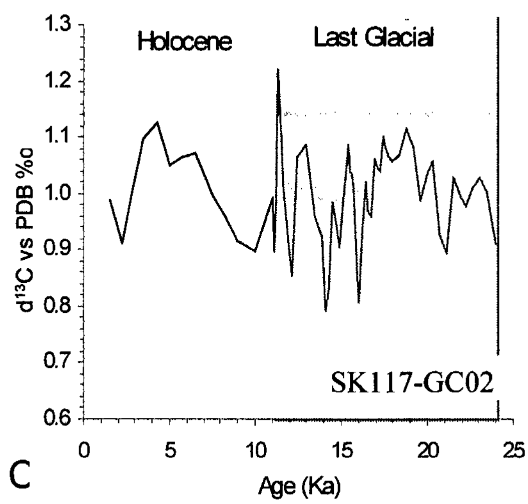

The high-resolution $\delta^{13}C_{G.sacculifer}$ curve in GC02 core does not exhibit any distinct variations (Panel C). The overall range of variation is between 0.8 ‰ and 1.2 ‰ with an average of 1 ‰. The Holocene record contains a gradual change with only one $\delta^{13}C_{G.sacculifer}$ -enriched event of ~1.1 ‰ at ~ 5 Ka flanked by two -depleted events of 0.9 ‰ at ~2 Ka and ~10 Ka. The later half of the LGP (17-11 Ka) contains high frequency fluctuations of ±0.4 ‰. In contrast the earlier half of the LGP shows a gradual variation within ±0.2 ‰.

6. Discussion

In this section, sedimentary responses of the Holocene-Glacial period are presented first, as this record is available for all the three sediment cores, followed by the discussion on long-term responses based on the two deep-water cores (GC08 & CR04). As mentioned in the previous section, the multi-proxy data of the GC08 core are considered as the central evidences for the cumulative response of the EAS to climate change. The emphasis is given on themes of coupled responses rather than discussing each core individually based on each proxy, as the present cores provide an opportunity for a comprehensive understanding of changes in the entire EAS. The relevant data is provided at the end as Appendix. To extract the information on past changes in local E-P or salinity, the $\delta^{18}O$-correction required for subtracting the global ice-volume (or global sea level) effect from the composite calcite-$\delta^{18}O$, the presently available most precise sea level reconstruction by Shackleton (2000) (Figure 17) has been used.

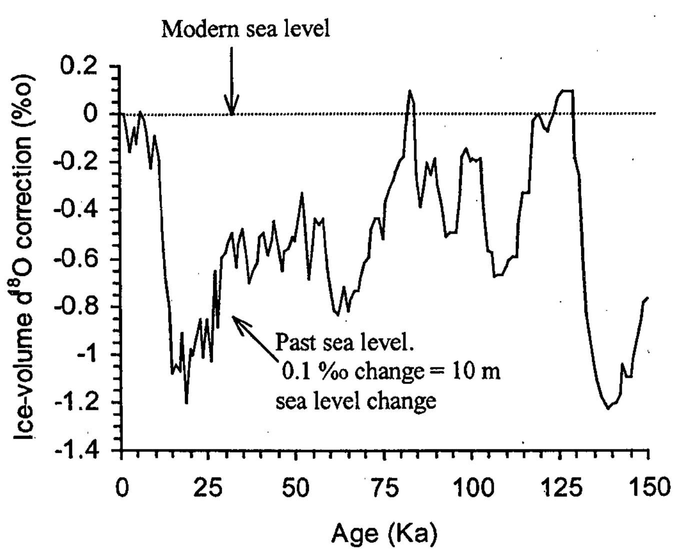

Figure 17: The seawater $\delta^{18}O$ variation due to global ice-volume or sea level variation through time (Shackleton, 2000). This curve was used for correcting the *G.sacculifer* $\delta^{18}O$ data for global ice effect.

6.1. $\delta^{18}O_{G. sacculifer}$, salinity, and monsoon linkage:

Variations in the Indian summer monsoons produce dramatic changes in sea surface salinity (hereafter salinity) structure because the salinity adjustment between the high-salinity Arabian Sea and low-salinity BOB largely depends upon the seasonally reversing monsoon system (Prasad, 2001; Prasannakumar and Prasad, 1999; Shetye et al., 1991). Therefore, the salinity budget of those two basins is dependent upon the annual variation of the E-P (Prasad, 2001). Irrespective of the mode of salt-exchange between the two basins such as, complex cross-equatorial mode of exchange through cross-equatorial cell (Jensen, 2001; 2003), or straightforward exchange between the two basins by reversing rhythmic monsoon surface circulations (Shankar et al., 2002; Shetye et al., 1991), the summer precipitation and winter evaporation largely determine the salt-budget in the region.

On one hand, the Quaternary monsoon system of the Arabian Sea was shown to have responded to the changing solar radiation or insolation pattern that has caused the glacial-interglacial cycles (Prell, 1984); on the other hand, the variation in the monsoon associated tropospheric aerosols derived from the Asian and the Arabian continents are believed to have played a major role in triggering the Dansgaard-Oeschger type rapid climate fluctuations recorded in the Greenland ice-cores (see Overpeck et al., 1996). The connection between the Greenland climate fluctuations and the Arabian Sea monsoon climate has been identified beyond reasonable doubt (Schulz et al., 1998; Hong et al., 2003). These studies indicate the importance of the Indian monsoons as a feedback for the global climate oscillations.

The planktonic foraminifera calcite oxygen isotopes have been the main source of information generated so far on the past variations in Indian monsoons in response to climate change (see Duplessy, 1982; Naidu and Malmgren, 1996; Niitsuma et al., 1991; Kutzbach et al., 2000; Rostek et al., 1997; Sarkar et al., 2000a & b, and references therein). The $\delta^{18}O$ of foraminiferal calcite secreted in equilibrium with the ambient seawater contains three climatic signals (details in Methods section). They are, changes in the volume of global continental ice, local-SST and local-salinity (Epstein et al., 1953; Shackleton and Opdyke, 1973). The effect of global ice volume remains uniform throughout the world oceans. Where as, the SST and salinity largely depend upon the local processes. Urey (1946) estimated a change of 0.2 ‰ calcite-$\delta^{18}O$ for every 1°C change in ambient water temperature, which has been confirmed by several subsequent culture experiments. On the other hand, the salinity and calcite-$\delta^{18}O$ relationship appears more complex and region specific (Delaygue et al., 2001; Duplessy, 1982; Rostek et al., 1993). However, the salinity and the seawater-$\delta^{18}O$ in general are directly related (Delaygue et al., 2001). When the ice-volume effect is global in nature and the past-SST variation in the EAS region is nearly uniform (Cayre and Bard, 1999; Sonzogni et al., 1998; Rostek et al., 1997), then the time-series planktonic calcite-$\delta^{18}O$ corrected for global ice volume should be able to reflect the local salinity variation over the time covered by the present sedimentary records. Even though the off-Goa cores (GC-02 and GC-08) do not exactly represent the northern-EAS, for convenience and clarity they are considered as northern cores in relative sense with the southern-EAS core (CR-04) (Figure 1).

The modern salinity in the GC-02 and CR-04 locations is nearly similar ~34.8 psu, while at the GC-08 location is ~35.8 psu (Levitus and Boyer, 1994 and NOAA Web, 2002). Where as, the annual average SST is similar at all the three locations (~28°C). In such a surface hydrographic set-up the core-top $\delta^{18}O_{G.sacculifer}$ should also reflect an agreement with the local salinity. The former two core-top $\delta^{18}O_{G.sacculifer}$ are nearly similar (-1.83 ‰ and –1.82 ‰ respectively), and lighter than the core-top value of the GC-08 (-1.37 ‰; Figure 18 A and 2, 3, 4) suggesting low-salinity regime in the former two core locations and high-salinity regime in the latter location in accordance with the modern salinity set-up. Therefore, the time-series $\delta^{18}O_{G.sacculifer}$ difference (contrast) between these cores may effectively demonstrate the changes in salinity regime through time. Thus, the ice-corrected (hereafter 'residual')-$\delta^{18}O_{G.sacculifer}$ would reasonably depict the local salinity changes. The EAS experiences in general, mixing of two salinity end-members in the upper mixed layer. They are, the high salinity end-member ASHSW originating due to excess evaporation (>E-P) in the northernmost Arabian Sea, and the low salinity end-member BOB-water originating in the northern BOB due to excess freshwater flux. The presence of these two end-members spreading in opposite directions as two distinct salinity fronts (Prasannakumar and Prasad, 1999; Shetye et al., 1993) result over 2 psu salinity difference between the northernmost and southernmost Arabian Sea (Figure 1). The low salinity BOB-water advected in to the EAS by the PCC is dominant source of freshening the modern EAS. The PCC is also responsible for sharply deflecting the zonally (E-W) trending isohalines towards north in the EAS (see Wyrtki, 1973; Prasannakumar and Prasad, 1999; Duplessy, 1982, and references there in) (Figure 1). The northward deflection of the isohalines is the characteristic of the EAS. Therefore, any shift in the salinity pattern in the EAS should have a direct link with the relative importance of ASHSW and BOB-fresh water input (PCC) in maintaining the salinity balance in the region.

The full-Holocene/LGP averaged residual-$\delta^{18}O_{G.sacculifer}$ contrasts in the three cores is 0.7 ± 0.1 ‰, wherein the northern-EAS deep-water core GC-08 shows highest contrast of 0.8 ‰ and southern-EAS deep-water core CR-04 shows lowest contrast of 0.6 ‰ (Figure 18 B) suggesting that the northern region has witnessed relatively higher salinity change than the southern region during the last 24 Ka. When the Holocene-peak and LGM-peak are considered, that contrast is much larger (>1‰). The inter-location (i.e., between the cores) residual-$\delta^{18}O_{G.sacculifer}$ contrasts during the past relative to the present can be used to understand the EAS-characteristic isohaline shift. To appreciate the following discussion, it may be necessary to characterize the locations of the sediment cores.

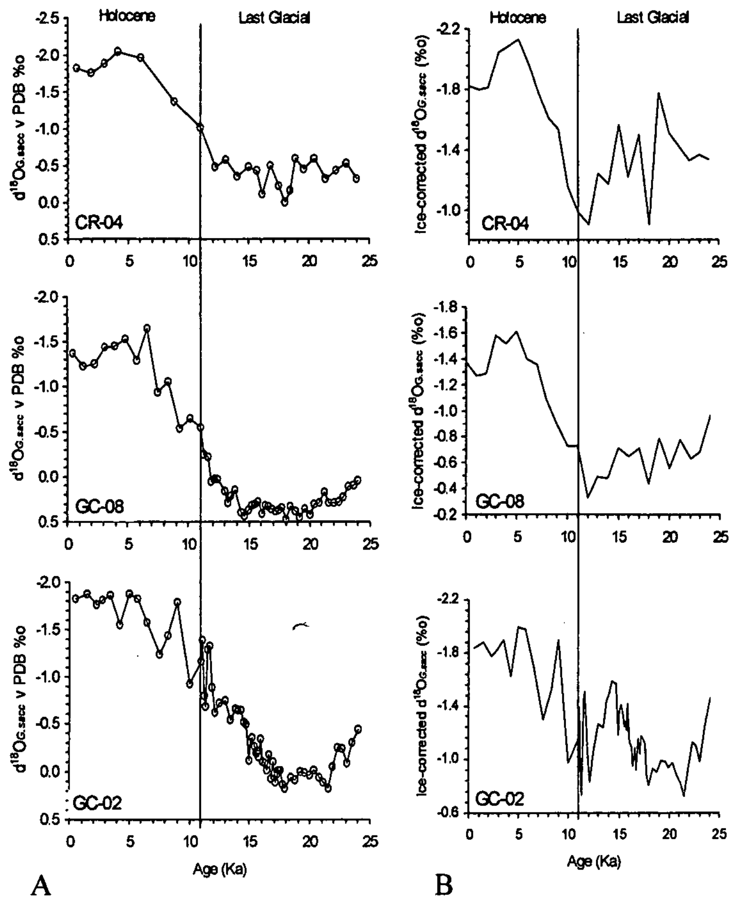

Figure 18: Holocene-Last Glacial Period variation of $\delta^{18}O$ in three EAS sediment cores (A), and their respective global ice-volume corrected patterns (B). The ice-volume corrected $\delta^{18}O$ would provide the record of the relative changes in the local salinity, when the modern SST and its past variations are considered to be nearly uniform in the region.

The CR04 and the GC02 are located in the southern and northern portion of the low-salinity tongue respectively. The GC08 is located around 200 km west of the GC02 and comes under the influence of southward spreading ASHSW. Though it is very difficult to isolate the GC08 totally from the influence of the low-salinity tongue, the salinity structure of the basin suggests that its location has dominant influence of the ASHSW than the influence of the low salinity tongue. These location-characteristics are clearly reflected in the relatively heavier $\delta^{18}O_{G.sacculifer}$ in GC08 core-top than the nearly similar $\delta^{18}O_{G.sacculifer}$ in CR04 and GC02 core-tops (Figure 18A). The full-Holocene residual-$\delta^{18}O_{G.sacculifer}$ contrast between northern-EAS deep- and shallow-water cores (GC08 & GC02 respectively) and northern- and southern-EAS deep-water cores (GC08 & CR04 respectively) are similar ~0.45 ‰. Whereas, that difference between the northern-EAS shallow-water (GC-02) and southern-EAS deep-water (CR-04) cores is minimum (~0.1 ‰). These differences in $\delta^{18}O_{G.sacculifer}$ clearly suggest that the location of GC08 is under high salinity regime and the locations of CR04 and GC02 are under the low salinity regime throughout the Holocene. That is, the PCC effect is distinctly visible all along the near-coast region of the EAS through the entire Holocene. These Holocene residual-$\delta^{18}O_{G.sacculifer}$ patterns change during the LGP. The differences between the northern deep-water (GC08) and southern deep-water (CR04) cores increases to ~0.8 ‰ and the northern shallow-water (GC02) and southern deep-water (CR04) cores increases to ~0.3 ‰ (Figure 18 B). These shifts in residual-$\delta^{18}O_{G.sacculifer}$ contrasts towards higher values between northern and southern regions probably indicate that the northward deflection of the isohalines in the EAS has reduced during the LGP and they were mostly in east-west direction aligning with the general zonal trend across the Arabian Sea. In the northern-EAS continental shelf core (GC02), the signals of fresh water input from the Deccan Rivers might have also been incorporated. Therefore, the emphasis is given to the changes observed in the two deep-water cores because their locations are considerably away from the direct influence of the Deccan River discharge. Additionally, these two cores are well suited to understand the relative variation between two salinity end-members viz., ASHSW (high salinity northern end-member) and PCC activity (low-salinity southern end-member).

After having recognized the overall changes in the salinity regime through residual-$\delta^{18}O_{G.sacculifer}$ contrasts during the Holocene-LGP, a salinity contrast curve for the past 100 Kyr utilizing northern- and southern-EAS deep-water cores (GC-08 & CR-04 respectively) is constructed. This curve may help understanding the changes in salinity structure in the EAS due to variations in inter-basin communication through characteristic SMC and WMC-PCC circulation driven by the climate sensitive Indian monsoon system.

The $\delta^{18}O_{G.sacculifer}$ of both the cores were first interpolated to 1 Ky time-scale to match the Shackleton's (2000) ice-volume correction curve (Figure 17). Then the ice-volume correction was applied to each interpolated data-point of both the cores to obtain residual-$\delta^{18}O_{G.sacculifer}$ (Figure 19).

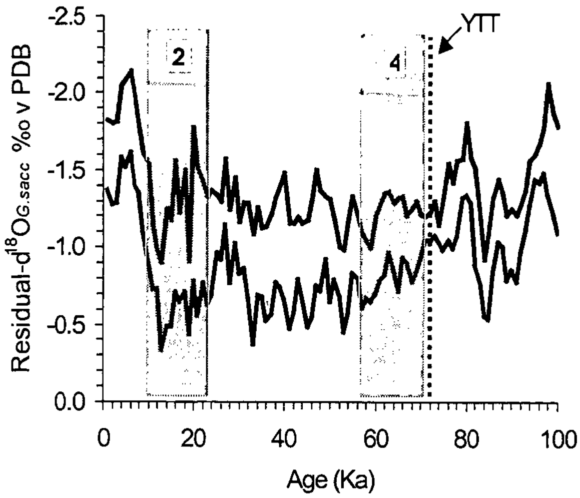

Figure 19: The ice-volume corrected (residual)-$\delta^{18}O_{G.sacculifer}$ curves for the northern (GC-08: red) and southern (CR-04: blue) sediment cores. The consistently heavier isotopic curve of the northern core than the southern core clearly indicates high-salinity regime in the former location throughout the last 100 Ky than in the latter location. Therefore, the time-series contrast between these two records should be able to demonstrate the changes in past-salinity gradient in the EAS region.

The time-series residual-$\delta^{18}O_{G.sacculifer}$ records (Figure 19) are comparable to the palaeosalinity curves reconstructed for the southern-EAS (see Rostek et al., 1993) and the BOB (see Kudrass et al., 2001). This similarity suggests that, a) the time-series residual-$\delta^{18}O_{G.sacculifer}$ variations in the present cores are largely the responses of regional salinity changes in the past, and b) the differences in past-SSTs in space and time within the EAS were not significantly different (Sonzogni et al., 1998), hence uniform effect of the site-specific SST component on $\delta^{18}O_{G.sacculifer}$ of the EAS. Additionally, the residual-$\delta^{18}O_{G.sacculifer}$ in the northern-EAS remains heavier than in the southern-EAS throughout the last 100 Kyr suggesting that the former location has been perennially under high-salinity than the latter location.

The residual-$\delta^{18}O_{G.sacculifer}$ in the northern-EAS is -1.6 ‰ at around the peak-Holocene (~6 Ka) and -0.4 ‰ at around the LGM, while the southern-EAS records –2.1 ‰ and –1 ‰ respectively (Figure 19), i.e., a contrast of ~1.1 ‰. This contrast, in addition to local salinity change contains the LGM-SST drop of ~2°C particularly in the vicinity of our core locations (Cayre and Bard, 1999; Sonzogni et al., 1998; Rostek et al., 1997). A similar lowered SST of ~2 °C during the LGM was also obtained by $U_K^{37'}$ - thermometry for the northern-EAS core (GC-08).

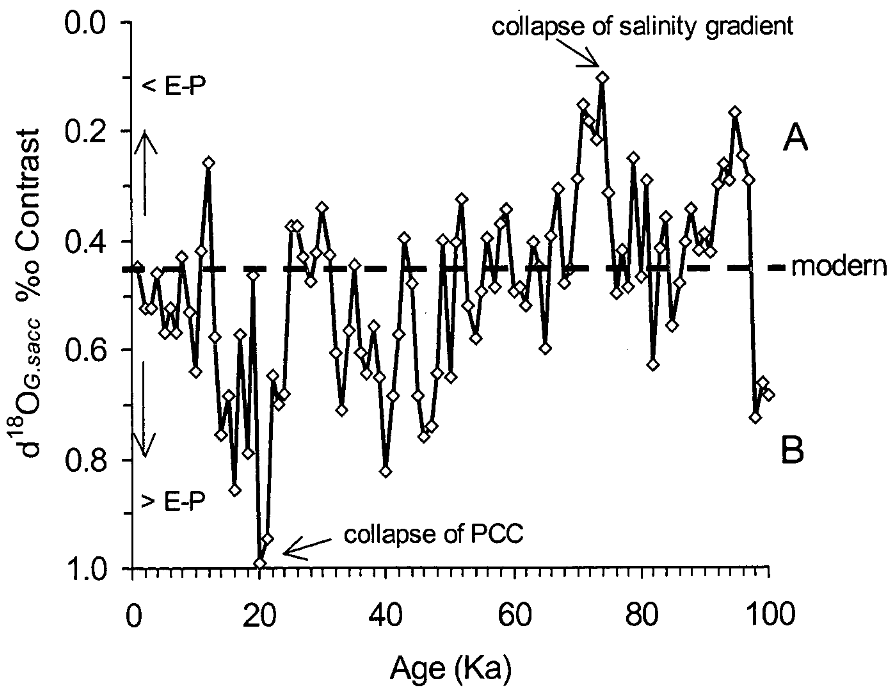

Figure 20: Residual-$\delta^{18}O_{G.sacculifer}$ contrast between northern- and southern –EAS derived using GC08 & CR04 sediment cores. The horizontal dashed-line indicates the modern contrast as recorded by the core-top sections. The lower sector 'B' marks the increased E-P (or reduced summer monsoon rains), and the upper sector 'A' marks the reduced E-P (or increased summer monsoon rains) than the modern conditions in the region.

A 2°C SST drop during the LGM would increase the *G. sacculifer* calcite-$\delta^{18}O$ by ~0.4 ‰ (Duplessy et al., 1981). Subtracting this SST-effect from the residual-$\delta^{18}O_{G.sacculifer}$ contrasts yields a remainder of ~0.7 ‰ accountable for the Holocene-LGM local salinity change. The $\delta^{18}O_{G.sacculifer}$ contrast of ~0.45 ‰ between the two core tops (see Figure 20) can be considered as a measure of modern salinity difference of ~1 psu between those two corresponding locations. Then, a 0.7 ‰ Holocene-LGM contrast would translate in to ~1.5 psu salinity change at both the locations, which approximately in agreement with the overall salinity increase of ~2 psu during the LGM in the only available past-salinity record from the entire Arabian Sea region (MD900963 from the southern-EAS: Rostek et al., 1993, see Figure 1). This general agreement between the present averaged isotopic records and the previously published salinity reconstructions indicates the level of confidence with which the present residual-$\delta^{18}O_{G.sacculifer}$ could represent the past salinity variation in the study region.

Considering the surface hydrography in the EAS, the fluctuations in the north-south residual-$\delta^{18}O_{G.sacculifer}$ contrast can be associated with the relative variations in the intensity ASHSW and BOB-freshwater influx (PCC strength), in turn the monsoon intensity. Because, the northern Arabian Sea origin ASHSW and the southern Arabian Sea origin low salinity tongue caused by the BOB-water influx are solely responsible for the salinity structure of the EAS. Hereafter, the residual-$\delta^{18}O_{G.sacculifer}$ contrast is often referred as the 'salinity contrast' for clarity, because the SST variations in the past over the region are assumed to be nearly uniform (Cayre and Bard, 1999; Rostek et al., 1997; Sonzogni et al., 1998), which have contributed regionally more or less similar temperature sensitive signals.

The average salinity-contrast is highest for the LGP ($\delta^{18}O_{contrast}$ ~0.7 ‰), high for the Holocene and MIS3 ($\delta^{18}O_{contrast}$ ~0.5‰), moderate for the MIS4 and MIS5.2 ($\delta^{18}O_{contrast}$ ~0.4‰) and lowest for MIS5.1and MIS5.3 ($\delta^{18}O_{contrast}$ ~0.2 ‰), which translate in to overall variation within ~1.5 psu in the last 100 Ky, considering the core-top contrast of 0.45 ‰ as an equivalent of the modern salinity difference of ~1 psu between those locations. In other words, the geographical salinity contrast between northern- and southern-EAS during the LGP was highest ~1.5 psu, while during the interstadials of MIS5 was nearly half of the modern contrast, suggesting at the outset a largest salinity gradient during the former period and smallest gradient during latter period. However, the time-series salinity-contrast profile contains much larger amplitude oscillations ($\delta^{18}O_{contrast}$ of 0.1 ‰ to 1 ‰) on shorter time-scales (<5 ky: Figure 20), suggesting rapid and much greater changes in the past salinity gradient in the EAS region accounting for an order of magnitude fluctuations (i.e., the salinity gradient varied between a minimum of ~0.2 psu and a maximum of ~2.2 psu as compared today's ~1 psu).

Before invoking the probable causes for fluctuations in the salinity-contrast between northern- and southern-EAS, it is necessary to identify the dominant contributing factors to the salinity changes at each of those two locations. Assuming nearly uniform effect of overhead precipitation due to vigorous surface circulations in the region, the northern location salinity change can be influenced largely by both the ASHSW and PCC. On the other hand, the variation in the intensity of WMC-PCC carrying BOB-low salinity water alone can affect the salinity change in the southern location, since the influence of ASHSW on the surface salinity structure gradually diminishes due to gradual sinking along with its southward advection. By the time the ASHSW reaches the southern-EAS region its influence is limited to the depth beyond the mixed layer (see Prasannakumar and Prasad, 1999). Keeping this modern hydrographic set-up as a framework, the changes in the geographical salinity-contrast between northern- and southern-EAS (within the low-salinity tongue), therefore could be the result of relative changes in the activity of two salinity end-members viz., ASHSW (high-salinity end-member) and WMC-PCC (low salinity end member).

The north-south salinity-contrast in the EAS would increase when the northern location comes under enhanced influence of ASHSW, and the contrast would decrease when it comes under the enhanced influence of PCC. The alternative combinations, which hypothetically can produce the changes in the salinity-contrast are, 1) increased influence of ASHSW on northern location and WMC-PCC on southern location would increase the contrast, and 2) decreased influence of ASHSW on northern location and WMC-PCC on southern location would reduce the contrast. The simultaneously increased or decreased influence of the ASHSW on northern location and PCC on southern location at a given time is not possible considering the hydrographic set-up in the EAS, because, they operate in opposite sense to reduce the effect of each other on the northern location. In that an increased PCC would automatically reduce the influence of ASHSW on northern location. On the other hand, the intensified ASHSW will not have any significant influence in southern location mixed layer. Intensified PCC means the strengthening of the low salinity tongue, is associated with the intensified summer monsoons. Therefore, when the ASHSW intensifies (reduced freshwater flux or >E-P) the north-south salinity-contrast in the EAS is increased and when the WMC-PCC is intensifies (increased freshwater flux or <E-P) the contrast is decreased. This concept provides the preamble for understanding the past variation in the summer monsoon intensity utilizing the salinity-contrast between northern and southern regions of the EAS.

Presently the annual evolution of the summer monsoon is the main force driving almost all circulation changes in the northern Indian Ocean, where weak winter monsoons have less significant role (see Shankar et al., 2002). However, the Indian monsoons have witnessed dramatic changes during the LGP. For example, a) mean position of the summer monsoons is believed to have shifted southward resulting in reduced time-span of summer monsoons (Sirocko et al., 1991), and b) the CLIMAP-GCM models when forced with glacial boundary conditions such as reduced SST, increased continental albedo, and decreased atmospheric CO_2-level, resulted over 30% reduced southerly wind velocity and summer monsoon precipitation (Prell and Kutzbach, 1992), suggesting significantly weakened summer monsoons. The additional supports for weakened summer monsoons during the glacial periods emerge from, 1) large scale climate models for the modern conditions have suggested that an intense winter and extended snow cover over the Tibet and Himalayas during the spring (generally expected scenario of glacial climate) delays and weakens the following summer monsoon (Yang, 1996), and 2) minimum surface water-$\delta^{18}O$ contrast between the Arabian Sea and the BOB during the LGP (Duplessy, 1982) suggested greatly reduced fresh water transfer from the Arabian Sea to the Indian sub continent (Schulz et al., 1998). Within the LGP sections of the sedimentary records from the northern Indian Ocean, the indications of enhanced sea surface salinity based on faunal analysis (Cullen, 1981) and oxygen-isotope based reconstructions (Rostek, 1993), and dominant Mediterranean type pollens characteristic of arid climate (Van Campo et al., 1982) strongly suggest either the intensification of winter monsoons or winter monsoons were the only dominant seasonal feature.

The increased salinity contrast between the northern and southern region of the EAS during the LGP appears to have associated therefore with greatly diminished fresh water input from the BOB and Deccan Rivers responsible for freshening the northern region. Near disappearance of the low salinity tongue along the west coast of India during the LGM (see 18 Ka salinity gradient for the Arabian Sea in Duplessy, 1982) not only supports the above interpretation but also suggests broken communication between the Arabian Sea and the BOB. All these evidences are clearly in contrast with the previously hypothesised intensification of low-salinity BOB water transfer into the Arabian Sea during the LGM (Sarkar et al., 1990). The southward shift of the summer monsoon mean-axis during the LGM (Sirocko et al., 1991) appears to have still maintained low salinity regime in the southern region of the EAS despite the collapse of inter-basin communication but by summer monsoon overhead precipitation. The southward shift of the summer monsoon axis also potentially has to result in significant increase of E-P in the northern region by reduced precipitation there. Such variation through time may have been responsible for maintaining the observed high-salinity regime in the northern EAS and the low-salinity regime in the southern EAS. In fact, the CLIMAP models have shown that the western equatorial Indian Ocean has received increased precipitation during most of the glacial periods of the last 150 Ky (Prell and Kutzbach, 1987). The present study and previous models indicate that in spite of weakened summer monsoons during climate cooling cycles affecting both the basins and Indian subcontinent, the sustained equatorial precipitation has kept the CR04 core location in the southern-EAS out of the freshwater drought unlike in GC08 core location.

The dominant winter monsoon winds during the glacial periods are expected to enhance the formation of the ASHSW in the northern Arabian Sea due to increased E-P. The cumulative effect of such meteorological and hydrographic changes is to enhance the salinity build-up in the northern-EAS as compared to the southern-EAS. The increased salinity contrast during the LGM therefore was due to reduced freshening of the Arabian Sea and BOB due to weakened summer monsoon precipitation. The alongshore pressure gradient in the EAS (Shetye et al., 1991) might have decreased due to weakened summer monsoons during the LGM resulting in the diminished low-salinity tongue (or PCC) due to reduced flow of low-salinity BOB water (Shankar et al., 2002; Shetye et al., 1990; 1991). The diminished low-salinity tongue of the LGM thus not only rendered the northern-EAS to come under the increased influence of the intensified ASHSW, but also reduced the northward deviation of the isohalines in the region (see Duplessy, 1982).

The strengthening of the summer monsoon should result in reduced salinity contrast between northern- and southern-EAS. This reasoning is in agreement with both the summer monsoon influence on circulation of the Arabian Sea and the glacial-interglacial monsoon variations. During the interglacial periods both the basins were well connected and the BOB was significantly fresher than the glacial periods, hence an enhanced increase of the salinity in southern location relative to northern-EAS is not at all feasible. These observations and reasoning provide a clear scenario for the EAS that, the north-south salinity contrast fluctuations within the low-salinity tongue of the EAS through time have been the summer monsoon forced changes in the intensity of ASHSW and PCC at the northern location. Therefore, the variation in the geographical salinity contrast of the EAS region has monitored the past changes in the Indian summer monsoon intensity, in that intense summer monsoons resulted in reduced salinity-contrast, while the weakened summer monsoon resulted in increased salinity-contrast. The high-frequency high-amplitude fluctuations in the salinity-contrast observed within the main climate events prior to the Holocene (Figure 20) might be indicative of the instability of the past summer monsoons.

Various palaeoceanographic records and models suggest that the Asian monsoon system was established by the late Miocene when the Himalayan mountains attained half of their present height probably following the main boundary thrust at ~10 Ma (Banakar et al., 2003) to induce characteristic monsoon circulations (Filippelli, 1997; Prell and Kutzbach, 1992). Even though the monsoons established long before, their unstable nature appears to be rather a rule than exception because most of the last 100 ky time period covered under this study has witnessed highly irregular summer monsoons on millennial time-scale. However, the Holocene period is devoid of such high frequency-high amplitude oscillations in the salinity-contrast variation (Figure 20) suggesting significantly stabilized monsoon régime since it's beginning. Considering the coherent behaviour of the summer monsoons with the D-O type Greenland Climate fluctuations (see Leuschner and Sirocko, 2000; Schulz et al., 1998), the observed instability in the pre-Holocene salinity-contrast further may lend a support for the above link. However, it is not possible to identify those individual D-O type high-frequency climate events in the present sedimentary record of the salinity-contrast due to poor time-resolution.

From Figure 20 it is also evident that on several occasions during the last 100 kyr EAS has witnessed more intense summer monsoons than the Holocene. The closing of the last warm period (MIS5: ~73 Ka) appears to have forced near collapse of the salinity gradient in the EAS as evident in lowest salinity-contrast ($\delta^{18}O_{contrast}$ ~0.1 ‰ i.e., equivalent to just over 0.2 psu salinity contrast), probably due to very intense summer-monsoons, and vigorous PCC than today, i.e., greatly intensified and significantly expanded low-salinity tongue in the EAS. The warmest MIS5 and the coldest LGM (~20 Ka) mark two extreme summer monsoon scenarios in the EAS as evident in respectively lowest and highest salinity-contrasts ($\delta^{18}O_{contrast}$: ~0.1 ‰ and 1 ‰). The latest intensification of the summer-monsoon precipitation and strengthening of the PCC has taken place with commencement of the Holocene evident in the reduced salinity-contrast ($\delta^{18}O_{contrast}$ from ~1 ‰ at LGM to ~0.3 ‰ at ~11 Ka; i.e, from ~2.2 psu to ~0.6 psu (Figure 20). As mentioned earlier the fully developed Holocene (since ~8 Ka) has experienced more stable summer monsoons and the PCC activity as evident in marginal variation of the salinity-contrast within <0.4 psu (i.e., residual-$\delta^{18}O_{contrast}$ <0.15 ‰). This observation appears to be in disagreement with the earlier studies, which have invoked large fluctuations in the strength of the summer-monsoon precipitation during the Holocene (Thamban et al., 2001), and E-P (Sarkar et al. 2000). However, unless some kind of quantification of the relative changes in the monsoon precipitation and the corresponding salinity-contrast variation in the EAS is achieved, it may be difficult to assess the actual variation in the past summer monsoon intensity. It is interesting to note from Figure 20 that after the collapse of the salinity gradient in the EAS due to extremely intense summer monsoons at the interstadial MIS5.1 (~73 Ka) has quickly re-established to the modern level within around 5 Ky (i.e., the commencement of MIS4). The near collapse of the salinity gradient during the last warm period (MIS5) may also suggest exceptionally vigorous surface water exchange between the Arabian Sea and the BOB. The period between ~73 Ka and ~25 Ka has witnessed moderate fluctuations in the summer monsoon intensity as evident in moderate variations in the salinity-contrast. Most of the last glacial cycle (LGP+MIS3+MIS4) has witnessed weaker summer monsoons than the Holocene. *(See the cartoon on next page for the likely scenario of the salinity structure in the EAS with varying PCC or the low-salinity tongue)*

6.2. Silicate-detritus in sediment and summer rains on land:

In the previous section a relationship of past salinity-contrast fluctuations in the EAS with the summer monsoon intensity is brought out. The summer monsoon rains on the Indian peninsula feed large network of seasonal rivers rapidly draining the Deccan Mountains, which discharge considerable amount of fresh water and silicate-detritus in to the EAS (over 73 km^3/y: Rao, 1979). Therefore, it is possible to understand the past changes in the summer monsoon intensity utilizing the strength of the Deccan Rivers as means. The variation in the intensity of the Deccan Rivers can be assessed by their ability to erode the drainage area. In other words, the abundance of the coarse silicate material they transport to the continental shelf region depends on their strength. By monitoring the sediment grain-size variation through time at a location of the continental shelf in the proximity of discharge point of any Deccan Rivers, one can qualitatively assess the past variation in the strength of those rivers. Here, utilizing the time-series variation in volumetric changes of grain-size of the GC02 core in three size-windows (2 μm, 10 μm, and 100 μm), an attempt is made to reconstruct the past erosion strength of the Deccan rivers vis-à-vis summer monsoon intensity. One such river couple, viz., Mandovi-Zuari, which discharges around 1.3 km^3/y of freshwater in to the EAS off Goa, is considered as the representative of the Deccan Rivers. The GC02 core is located about 200 km off the discharge point of these rivers and hence is under the direct influence of those rivers as far as fluvial sediment input is concerned. Moreover, the core-site is far isolated from the major dust source such as Arabia and hence the contribution of the aeolian material is not significant (Sirocko et al., 1991). The Indus sediment influence (Prins and Weltje, 1999) at this location may be ignored because of the shallow water continental shelf set-up. Therefore, the relative variation in the coarse and fine

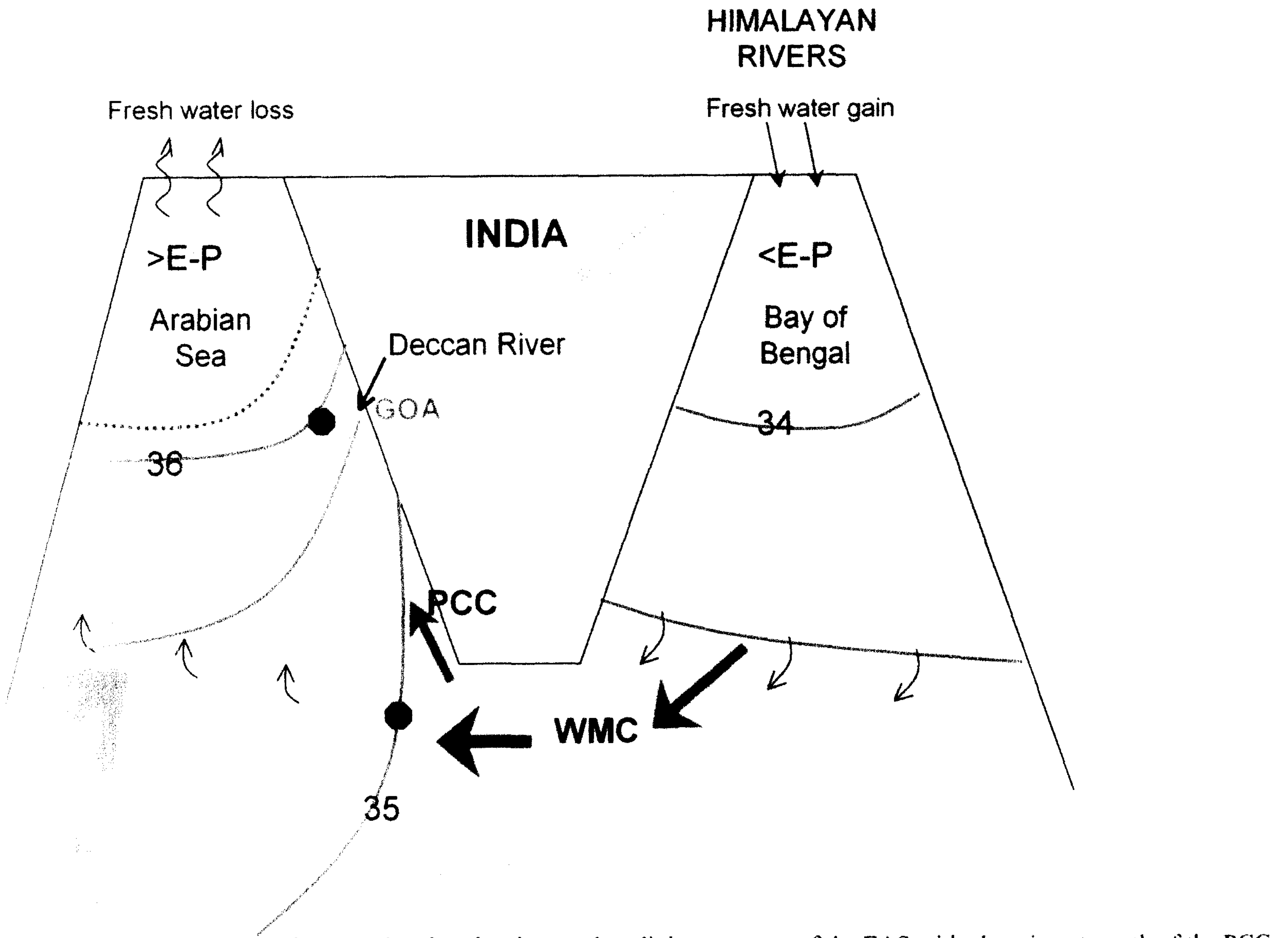

Cartoon showing the changes in salinity structure of the EAS with changing strength of the PCC. The likely scenario of the 36 psu isohaline with stronger PCC (blue dotted line) and with weaker PCC (yellow dotted line). Grey arrows are summer and winter winds. Red lines are the modern isohalines. Filled circles are the northern-EAS (GC08) and southern-EAS (CR04) sediment cores grain-sizes would reasonably suggest the changes in the strength of Deccan River network in-turn the intensity of the summer monsoon rains on the Indian peninsula.

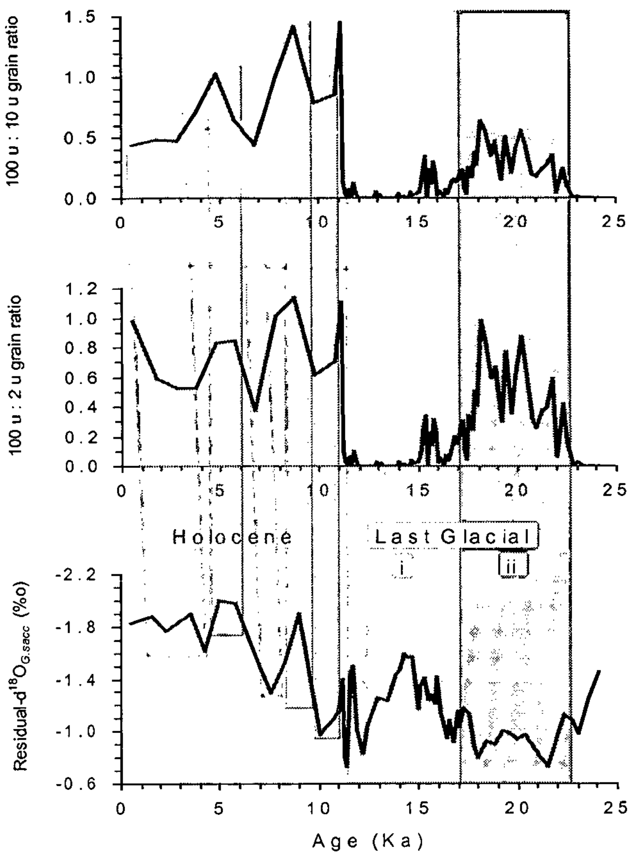

Figure 21: Residual-$\delta^{18}O_{G.sacculifer}$ record compared with the grain-size variation in continental shelf core GC-02. The blue shaded bars indicate correspondence between the coarse to fine grain ratios and residual-$\delta^{18}O_{G.sacculifer}$ during the Holocene, in which the decreased $\delta^{18}O_{G.sacculifer}$ events invariably correspond with the dominance of larger grain-size suggesting higher erosion of the Deccan Mountains due to relatively intense summer monsoon rains on land (increased freshwater flux). On the other hand, the grey shaded bars in the LGP section exhibit opposite relationship to the Holocene. In that, during the Event-I, the decreased $\delta^{18}O_{G.sacculifer}$ overlaps the lowest coarse grain abundance, probably due to melt-water input from the Himalayan glaciers during the deglacial episode (16 Ka to 11 Ka). The Event-II probably marks the period of intense aridity and strong winter winds around the LGM due to which the coarser grain abundance increased with concurrent increase in $\delta^{18}O_{G.sacculifer}$.

The geographical salinity-contrast in the EAS covering last 25 Ka (Figure 20), suggests that the summer monsoons were as intense as today at ~4 Ka and ~8 Ka but were more intense at around commencement of the Holocene (12-11 Ka). These events are separated by slightly weakened monsoon periods ~2-3 Ka, 5-7 Ka, and ~10 Ka. The events of increased summer monsoons recorded by the salinity-contrast must also reflect as the decreased residual-$\delta^{18}O_{G.sacculifer}$ events in the GC02 core, if the Deccan Rivers have responded to those events. In fact, they are evident in the residual-$\delta^{18}O_{G.sacculifer}$ record but with certain mismatched timings (Figure 21). This mismatch is acceptable because, a) the salinity-contrast was based on interpolated time-scale of 1 Ky of two deep-water cores, but the GC02 residual-

$\delta^{18}O_{G.sacculifer}$ profile is based on high-resolution data, and b) differences in water-depths at different core locations might have induced some uncertainty in their age comparison. I restrict the discussion on the age-uncertainty only to the observed marginal miss-match, due to non-availability of the ^{14}C-dates. Nevertheless, when the residual-$\delta^{18}O_{G.sacculifer}$ of the GC02 are averaged on 1 ky time-scale then all the lowered salinity-contrast and the decreased residual-$\delta^{18}O_{G.sacculifer}$ events (depicting stronger summer monsoon associated high freshwater flux) show good agreement.

The increased summer monsoon rains are expected to increase the coarser to finer grain-ratios in the shelf sediment. The 100 μm : 10 μm and 100 μm : 2 μm grain-ratio in the core particularly during the Holocene do exhibit significant increases occurring at 11 Ka, 9 Ka and 5 Ka (Figure 21) in concordance with the increased summer monsoons recorded as salinity-contrast events in the EAS. The observed relationship between decreased residual-$\delta^{18}O_{G.sacculifer}$ and the increased coarse-versus fine grain-ratios clearly suggests that the Mandovi-Zuari river couple was relatively intense at around those times. This relationship drastically reverses during the LGP (24 Ka -11 Ka). The 100 μm : 10 μm and 100 μm : 2 μm grain-ratios surprisingly exhibit inverse relationship with the residual-$\delta^{18}O_{G.sacculifer}$ during the LGP in contrast to that observed during the Holocene. From 15 Ka to 12 Ka, the decreased 100 μm : 10 μm and 100 μm : 2 μm grain-ratio correspond to decreased residual-$\delta^{18}O_{G.sacculifer}$, while the increased 100 μ : 10 μ and 100 μ : 2 μ grain-ratio between 22 Ka and 17 Ka correspond to increased residual-$\delta^{18}O_{G.sacculifer}$ (Figure 21). The decreased residual-$\delta^{18}O_{G.sacculifer}$ event at ~15 Ka is also evident in other two deep-water cores (Figure 20) suggesting that the event is robust and occurs in the entire EAS.

The decreased residual-$\delta^{18}O_{G.sacculifer}$ at ~15 Ka should have been associated with the increase in the 100 μm : 10 μm and 100 μm : 2 μm grain-ratio in the core, if that signal was due to increased fresh water flux as a result of intensified summer monsoon rains. But the minima in 100 μm : 10 μm and 100 μm : 2 μm grain-ratios during this time period (Figure 21) suggest rather significantly weakened Mandovi-Zuari river couple indicating weakened summer monsoon rains in the region. Overall LGP has witnessed greatly reduced summer monsoons (Duplessy, 1982; Prell and Kutzbach., 1987; Sirocko et al., 1991; Naidu et al.,1996; Sarkar et al.,2001; Rostek et al., 1997; Kudrass et al., 2001; Shimmield et al., 1990, and references therein). The higher geographical salinity-contrast at ~15 Ka in the EAS (Figure 20) also indicates weaker summer monsoons (> E-P). The western Indian continental shelf (EAS-region) sediment properties in fact have suggested weakened summer monsoons around that time than the Holocene (Nair and Hashimi, 1980). Therefore, the decreased residual-$\delta^{18}O_{G.sacculifer}$ at ~15 Ka is not associated with the intensified summer monsoon precipitation. Nevertheless, that period has significance in terms of melt water pulses (MWPs). The period between 10.5 Ka and 14.5 Ka ^{14}C-ages has witnessed four deglacial MWP events in the north Atlantic (Keigwin et al., 1991). The 14.5 Ka and 10.5 Ka events have been identified as major MWPs producing global signals (Bard et al., 1990; Brunnberg, 1995). Even though, the GC02 chronology lacks the ^{14}C-dating, the decreased residual-$\delta^{18}O_{G.sacculifer}$ at ~15 Ka associating with minimum coarse to fine grain ratios might be the result of MWPs, particularly from the Himalayan Glaciers during the LGM-Holocene deglaciation. If the Bølling interstadial (~14 Ka), which followed the Antarctic warming (Wilson et al., 2000) had the global effect, then there is a possibility of increased melting of the Himalayan ice, feeding mega-rivers such as Indus, Ganges, Brahmaputra (in turn Arabian Sea and BOB) with ice-locked extremely low $\delta^{18}O$ freshwater even in the absence of stronger summer monsoon rains. It is interesting in this context to note that the southern-EAS deep-water core (CR-04) and the northern-EAS continental shelf core (GC02) contain signals of reduced residual-$\delta^{18}O_{G.sacculifer}$ at ~15 Ka (Figure

18). A precise chronology based on ^{14}C-dating would help resolve and confirm these MWP signals in the EAS, which until then would remain speculative.

The period around 20 Ka is marked by the intense dry climate as evident in the significant increase in the north-south salinity-contrast (or E-P) in the EAS region (Figure 20). This period was globally significant for the lowered sea level by ~120 m due to extensive waxing of the continental ice sheets (Shackleton, 2000; Fairbanks, 1989). The observed heaviest residual-$\delta^{18}O_{G.sacculifer}$ in the entire EAS (Figure 18) is in accordance with such climate scenario, but surprisingly the coarse- to fine-grain ratios exhibit increased values in the shelf region (Figure 21). A significant increase in silt content in both northern-and southern-EAS deep-water cores (Figure 5 and 6) and sharp increase in sand content of northern-EAS shelf core (Figure 7) during most part of the LGP provide support to the above grain-ratio variation. Such increase in the coarser-grain abundance is not expected either in the shelf core or in the deep-water cores during the time of weakened summer monsoons during arid-LGP, because the Deccan Rivers' erosion ability should have been diminished significantly.

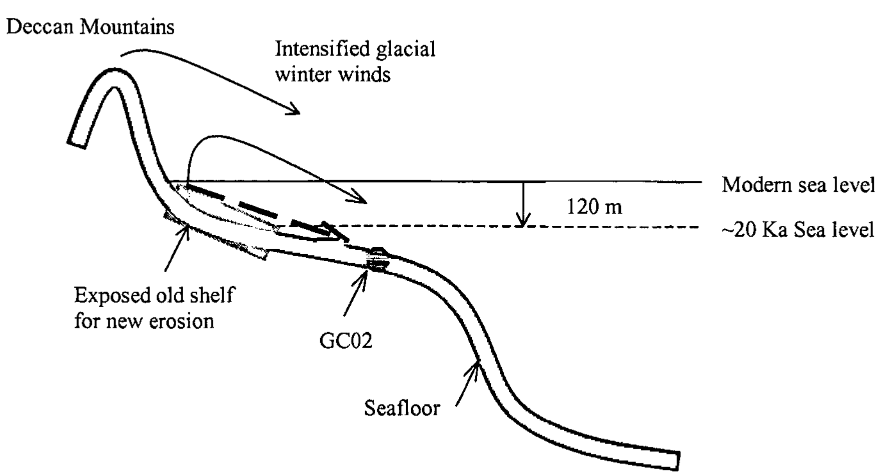

Figure 22: Cartoon drawing showing the exposed continental shelf during the lowered sea level, which could have acted as a source of coarse grain sedimentary material to the GC02 site.

The increased coarse to fine grain-ratios around the LGM (~20 Ka) can be explained alternatively by invoking the exposed continental shelf due to lowered sea-level (see Figure 22). The lowering of the sea level by ~120 m during the LGM must have exposed the modern inner shelf and hence the modern outer shelf (GC02 location at 225 m depth) was converted in to shallow inner shelf around that time. Thus the coarse-grain dominant detritus deposited on the palaeo-inner shelf prior to ~20 Ka ought to have subjected to new erosion regime. Therefore, the subsequent erosion by then intensified winter winds of the LGP (Rostek et al., 1997; Riechart et al.,1998 and references therein) and to certain extent further seaward extended river activity, though had greatly weakened, might have transferred the relict coarse sedimentary material to the GC02 location. The possibility of enhanced transport of the Deccan Mountain erosion products by strengthened winter winds also might have contributed to the increased coarse grain material in the sediment deposited during the LGP. Thus the coarse-grained material supply to the EAS has increased during the LGP in spite of the diminished fluvial activity due to reduced summer monsoons.

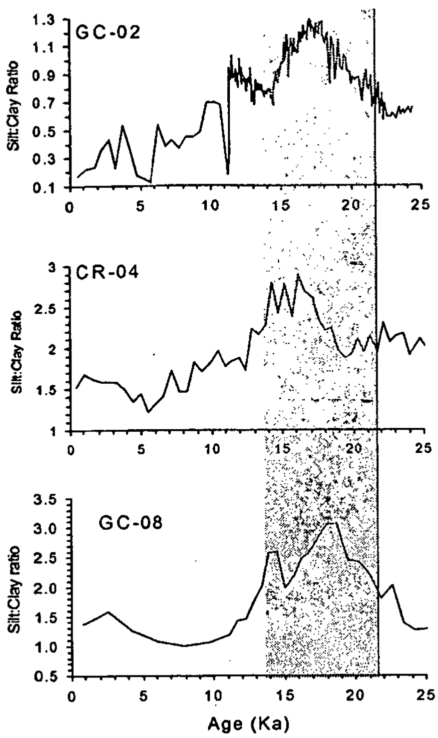

Figure 23: Increased silt:clay ratios during the last glacial period (shaded) in all the three sediment cores from the EAS suggest increased transport of continental weathered products by stronger winter winds blowing towards the Arabian Sea.

The silt : clay ratios calculated using the sedimentary fraction contents (Figures 5, 6 & 7) in all the three cores from the EAS also exhibit increased trends between 15 Ka and 20 Ka (Figure 23). Such near concordant increase of the coarser material in the sediment all over the EAS region strengthens the above views invoking intensified glacial winter winds and exposed continental shelf resulting in the enhanced coarse material transport further off in to the sea. Presently unavailable detrital grain morphology would be able to resolve the exact mode of material transport to the sea during the LGP. Therefore, the sediment cores from the EAS provide interesting clues for the past linkage between monsoon precipitation, Deccan River strength, and continental erosion in response to the climate variation.

6.3. Past-monsoon driven productivity changes in the EAS

6.3.1. The Controversy:

The strong winds of summer monsoons promote mixing of water in offshore regions leading to entrainment of the deep nutrient rich waters to the surface resulting in the development of intense upwelling zones along the coasts of Somalia, Oman and India (Banse and McClain, 1986; Currie et al., 1973; Haake et al., 1993; Rao et al., 1989; Wyrtki et al., 1973). The moderate upwelling has been observed in the northern and eastern Arabian Sea during the winter monsoons also (Banse, 1987; Brock et al., 1991; Qasim, 1982). The monsoon wind driven upwelling induces increased productivity. The seasonal productivity is highest in the western region, gradually reducing eastward during the summer monsoons, whereas, the EAS experiences high productivity during the winter monsoons in addition to the summer monsoon peaked productivity (Haake et al., 1993).

I have already mentioned briefly in the introduction chapter about the contrasting views on monsoon driven productivity patterns across the Arabian Sea on glacial-interglacial time-scales. In the sedimentary records of the western Arabian Sea upwelling region, interglacial high- and glacial low-productivity trends have been observed previously. The interglacial high productivity in the western region (Emeis et al., 1995; Naidu and Malmgren, 1996; Shimmield et al., 1990; Spaulding and Oba, 1992), as well as in the southeastern region of the Arabian Sea (Pattan et al., 2003) have been suggested based on various proxies. The increased water column denitrification during the interglacial periods was interpreted as indicative of intense OMZ due to elevated productivity across the Arabian Sea (Altabet et al., 1999). As the strong summer monsoon winds drive upwelling and associated productivity in the western region where the winter monsoons do not have much influence, the interglacial high productivity may be in accordance with the Indian monsoon dynamics. But the entire Arabian Sea in general or southeastern region in particular showing the elevated productivity only during the interglacial is debatable because the summer monsoon driven upwelling cells are largely develop off Somalia and Oman but not over the entire Arabian Sea.

The enhanced glacial productivity in the EAS indicated by the past OMZ reconstructions and biomarkers (Cayre and Bard, 1999; Rostek et al., 1997; Schulte et al., 1999) questioned the views suggesting in general high productivity in the interglacial Arabian Sea as a whole. This interglacial high-productivity coupling may not hold good to the EAS region as it also comes under the direct influence of the northeasterlies, which can induce upwelling during the winter. The east-west difference in present day productivity has already been observed in the Indo-FRG sediment trap experiments, which clearly demonstrated a productive EAS during the winter-monsoons also, unlike only a summer maximum biogenic-flux in the western region (Haake et al., 1993). The recently conducted sediment trap experiments by the National Institute of Oceanography, in the continental shelf to upper continental slope regions of the EAS covering the present day OMZ (200 m - 1100 m) have brought out very interesting observation that suggest seasonally independent organic matter flux within the experimental depth range (Paropkari et al., 2003, personal communication). This experiment strongly argues that, in spite of the modern weak winter winds compared to the summer monsoon winds, effect of the former on the productivity is distinct in the EAS region and forces to recognise the importance of the winter monsoons in determining the average annual biological activity of the region. Therefore, increased glacial productivity in the EAS (Cayre and Bard, 1999; Rostek et al., 1997; Schulte et al., 1999) that largely hinges on the hypothesis that invokes intensified winter monsoon and weakened summer monsoon during the LGP (Duplessy, 1982) is well justified. In the following sections the multiple proxies are used to evaluate the EAS productivity in response to oscillated monsoon dynamics.

6.3.2. Biogenic calcite and productivity:

The accumulation of biogenic calcium carbonate on the seafloor mainly depends on surface water productivity, dissolution through the water column and on the seafloor, and dilution by the non-carbonate fraction such as terrigenous matter. The carbonate-flux (carbonate mass-accumulation rate) at the seafloor has been extensively used as a reconnaissance for marine productivity. But, its application is valid only if the preservation is complete. It has been shown by several workers that the past climate induced variations in the preservation of carbonate complicated the approach. Berger et al. (1982) and Curry and Cullen (1997) have demonstrated that the progressive dissolution of foraminiferal calcite leads to the weakening and fragmentation of their tests, i.e., the loss of skeletal-calcite. The increased corrosiveness of the deep-waters during the climate cooling cycles has been shown to dissolve the biogenic calcite to great extent (Gröger et al., 2003 and references therein). Such preservation problems may lead to the underestimation of the productivity. Therefore, it becomes mandatory to examine the planktonic calcite tests to confirm the proper preservation before utilizing it for productivity interpretations. The coarse-fraction of the studied cores at all the intervals were carefully examined under the microscope. The shell-damage and fragmentation due to dissolution were not significant. Particularly, the *Gr. menardii* tests were intact and the abundance of keel (indicating destroyed shell walls) and fragmentation were rare in almost all the sections suggesting insignificant dissolution and good preservation (Ku and Oba., 1978). However, mechanical fragmentation caused due to processing of the sample was noticed and can be differentiated from the shell damage process. Additionally, the seafloor depths (<3000 m) at the studied core locations are much shallower than the carbonate lysocline in the region (~4000 m).

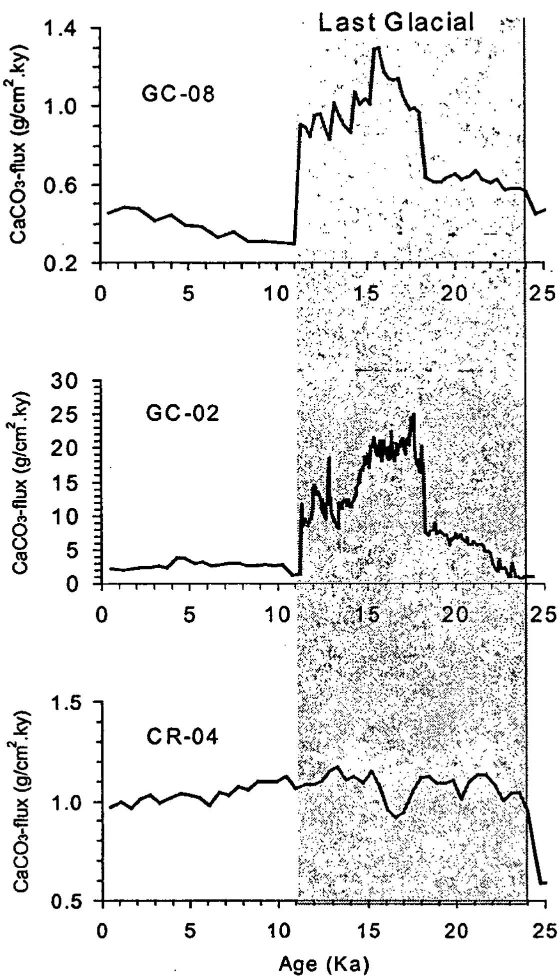

Figure 24: Holocene-LGP carbonate-flux variation in the EAS. The northern-EAS cores (GC02 & GC08) exhibit distinctly higher flux during most of the LGP, whereas, the southern core (CR04) records nearly uniform flux since the beginning of the last glaciation.

The possibility of aeolian dust carbonate from the Arabian Deserts may be ruled out in the study region because the dust input to the EAS has been shown to be negligible compared to the western and central regions (Sirocko et al., 1991). Therefore, calcium carbonate variations in the EAS region represent the productivity changes related to monsoon intensity.

The Holocene sections in the two northern-EAS cores (GC08 and GC02) exhibit almost similar trends, while the southern-EAS core (CR04) shows nearly uniform carbonate-flux since the commencement of the LGP (Figure 24). There is rapid increase in the productivity in the northern-EAS at around the LGM as evident in the sharp increase of $CaCO_3$-flux in GC02 (from 7 to 25 g/cm^2.ky) and GC08 (0.7 to 1.3 g/cm^2.ky). Where as, the productivity has remained constant through the LGP-Holocene in the southern-EAS region as evident by the nearly unchanged flux recorded in the CR04 core (~1.0 g/cm^2.ky). Both the northern-EAS cores exhibit peaked production at ~16 Ka. Thus at the outset it appears that the surface water biological productivity was distinctly higher during the LGP in the EAS. Even though the southern-EAS core exhibits nearly uniform productivity signal through the LGP and the Holocene, the increase appears to have commenced at the closure of the previous period (MIS3) (Figure 24), suggesting that the increase in productivity has in fact begun with the commencement of the LGP, but well-sustained through the Holocene in the southern-EAS.

The long-term productivity changes recorded in two deep-water sediment (GC08 and CR04) exhibit almost similar trend from the MIS3 through MIS5 (Figure 25). A nearly uniform $CaCO_3$-flux during the MIS3 is evident in both the cores. The last warm period (MIS5) however, exhibits higher productivity roughly around the colder-stadial. The later part of the penultimate glacial period (MIS6) recorded in the CR04 exhibits distinct maximum of $CaCO_3$- flux (~2 g/cm^2.ky as against ~1 g/cm^2.ky of the LGP-Holocene) (Figure 25) suggesting significantly higher productivity during the penultimate glacial period (MIS6) than during the warm periods.

The higher productivity during the LGM is also evident in the time-series Al_{excess} that exhibits elevated content between 25 Ka and 19 Ka. The corresponding Mn_{excess} on the other hand shows well-oxygenated waters in the shelf region at the beginning of the LGM (24-22 Ka) (Figure 11). The high-oxygenation during the early part of the LGM suggests a possibility of weaker OMZ in spite of high productivity. This particular issue is addressed in the Section 6.3 dealing with the denitrification. However, the observations based on the Mn_{excess} and Al_{excess} need to be considered with caution because the GC-02 core is from a shallow water where rapid changes in geochemical cycling of the scavenged metals is common due to high very high export production and large supply of terrigenous matter.

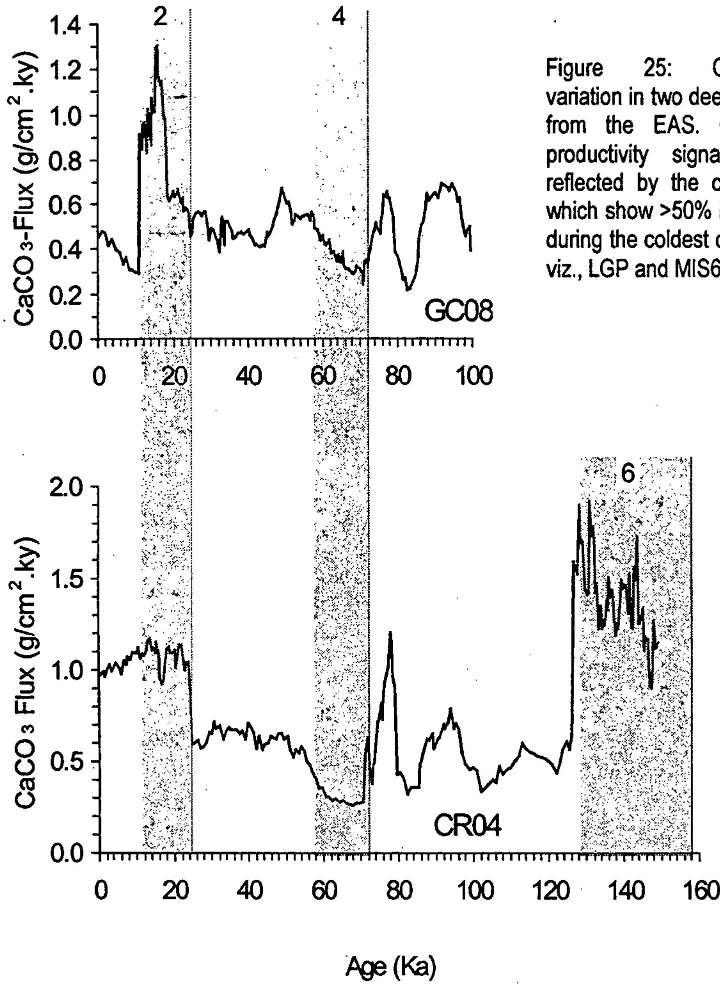

Figure 25: Carbonate-flux variation in two deep-water cores from the EAS. Glacial high-productivity signals are well reflected by the carbonate-flux, which show >50% increased flux during the coldest climate events viz., LGP and MIS6.

6.3.3. Sedimentary organic matter and productivity:

Variation in the intensity of summer- and winter-monsoons on glacial-interglacial time-scale has influenced the productivity in the EAS as evident in the carbonate-flux changes. The high carbonate-flux during the coldest MIS6 and LGP (Figure 25) warrants detailed assessment of the past productivity in the EAS region with the help of other widely used organic matter (OM) proxies. Because, the present results are not in agreement with the general view suggesting increased productivity during the warm and wet interglacial periods, when the summer monsoons were intense and winter-monsoons were weak.

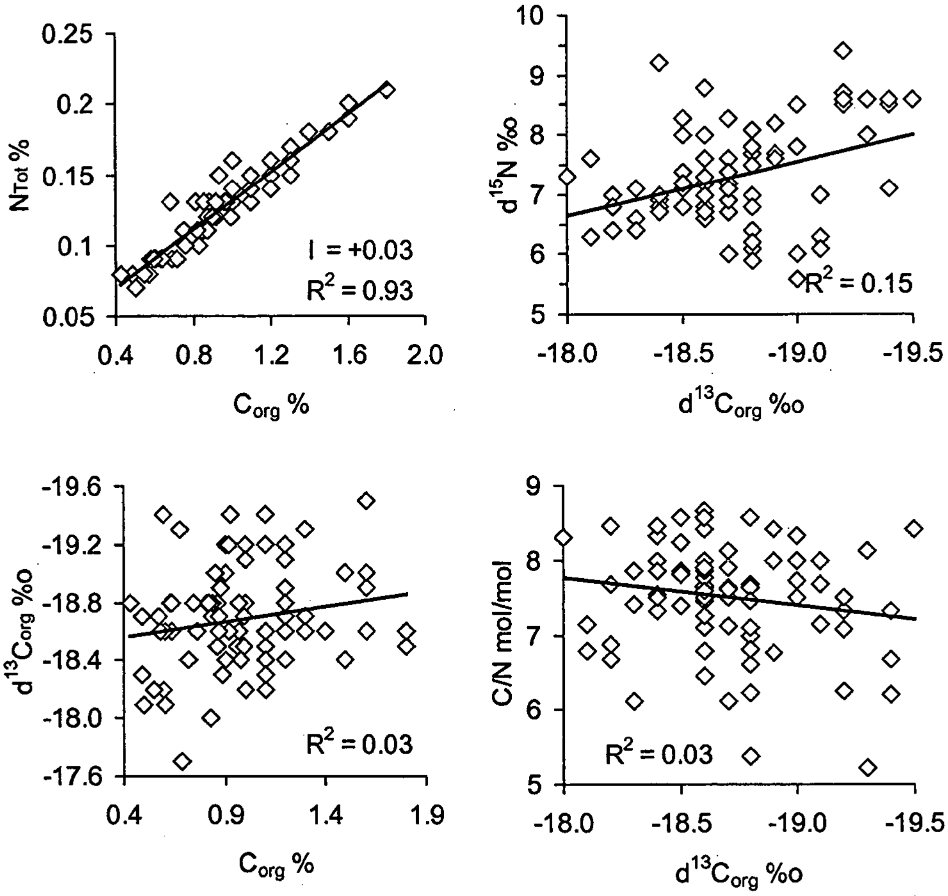

Figure 26: The association between various productivity proxies of the organic matter. The R^2 values tending towards 1 suggest increasing coherency in mutual variation of the proxies concerned due to increasing dominance of one process governing the variation.

Before considering the sedimentary-OM as palaeo-productivity indicator, it is necessary to demonstrate that the preservation of the OM in the sediment of the study region is adequately satisfactory. A good preservation of OM in the EAS region may be reasonably assumed based on the following observations, a) a previous study from the southern-EAS (sediment core: MD900963) has yielded excellent correlations between the C_{org} and various refractory biomarkers (Schulte et al., 1999); and b) the presence of poorly oxygenated (~1 ml/lit O_2) Indian Central Water in the intermediate depth (Olson et al., 1993) may not favour degradation of OM. The close association of the biomarkers with the C_{org} clearly indicates that the OM in the EAS sediment is rather unaltered. Nevertheless, it is necessary to establish the fidelity of the present OM-based proxies. For this purpose few simple inter-relationships between the different proxies (Figure 26) are evaluated.

The Redfield ratio of C/N for marine-OM is ~7 and for terrestrial-OM is ~35 (Ikehara et a., 2000; Reichart, 1997; Walsh et al., 1981). In the present core the C/N ratios vary around 7 indicating dominance of the marine-OM. The C/N ratios however can vary greatly depending upon the degree of preservation and mixing with high C/N terrestrial-OM. The C/N ratios as high as 30 in the OM dominated by marine origin have been found to be the result of diagenesis (Walsh et al., 1981). If the diagenesis has altered the OM content of the present sediment, then the C and N should vary randomly yielding very poor mutual association because the latter element fractionates during the settling- and burial-diagenesis (Walsh et al., 1981). A very strong linear positive association (R^2=+0.93) between those two elements (Figure 26) and their ratios lower than 9 (Figure 27e) rule-out any such alterations and confirm good preservation of the OM. The marginally higher C/N ratios (>7) and the offset in the intercept of the best-fit (0.03 % on N-axis: Figure 26) may suggest the presence of small amount of terrestrial-OM in the sediment. Using the C/N ratios of the marine- and terrestrial-OM (~7 and ~35 respectively) as two end-members of the mixing line, a maximum of 9 % of terrestrial-OM can be expected in the core. This would affect the carbon- and nitrogen-isotopic ratios in the OM to a maximum of 0.2 ‰, which is within the analytical uncertainty. The additional support for good preservation and purity of the marine-OM can be obtained by its isotopic relationships.

a) If the varying proportion of terrestrial-OM of significantly lighter-C and –N isotopes and higher C/N ratio has altered the marine-OM of significantly heavier-C and –N isotopes and lower C/N ratio, then such alteration should produce a sympathetic relationship between $\delta^{13}C$ and $\delta^{15}N$ and inverse relationship between $\delta^{13}C$ and C/N ratios (see Ganeshram et al., 2000).

b) According to Rayleigh's fractionation kinetics, the diagenetic alteration should result in the preferential loss of ^{12}C and ^{14}N of the sedimentary-OM leaving behind the residual-OM enriched with ^{13}C and ^{15}N. Therefore, if the decreased OM content in the sediment was due to the diagenetic breakdown, then the decreased OM should correlate with the increased $\delta^{13}C$, and the $\delta^{13}C$ and $\delta^{15}N$ should correlate sympathetically (Ganeshram et al., 2000; Kienast et al., 2001).

None of the above inter-relationships are evident in Figure 26 and hence are indicative of near pristine nature of the OM in the EAS and the studied cores in fact have recorded the changes in marine production with remarkable fidelity. The distinguishing isotopic features of the well-preserved, non-contaminated sedimentary-OM such as significantly heavier $\delta^{13}C$ and $\delta^{15}N$ of the tropical marine-OM (~-20 ‰ and ~5 ‰ respectively) as compared to the terrestrial C3-OM (~-27 ‰ and ~2 ‰ respectively) (see Figure 27c & d: and Altabet et al.,1999; Fontugne and Duplessy, 1981; Jasper and Gogosian, 1990; Rau et al., 1989; Sigman et al., 1997; Sweeney and Kaplan, 1980) provide further confirmation in favour of well-preserved sedimentary-OM inventory in studied core.

The phytoplankton preferentially fractionates ^{12}C during the synthesis of the organic matter leaving the surface ocean ΣCO_2 enriched with ^{13}C (Kroopnick, 1985) and the plankton-calcite precipitated in equilibrium with that water should preserve the enriched ^{13}C signal. Therefore, enhanced marine productivity at a given time is expected to associate with increased $\delta^{13}C$ in the planktonic foraminifera calcite. The vital effects modifying the expected equilibrium are assumed to remain uniform for the time-slice covered by the core. Therefore, the fluctuations in C_{org}–flux and the $\delta^{13}C_{calcite}$ together should be able to represent the past changes in productivity. The upwelling may alter the $\delta^{13}C$ inventory of the surface water and hence the $\delta^{13}C$ composition of both the organic matter and calcite. However, the organic-inorganic fractionation mechanism still remains the same and hence would not affect the relative changes on glacial-interglacial time-scales.

It is evident from the co-varying C_{org}-flux and $\delta^{13}C_{calcite}$ (Figure 27a & b) that the productivity in general was highest during the LGP, higher during MIS3 through MIS4, and stadial of MIS5 than the Holocene. The $\sum$alkenones in the LGP section exhibit nearly three-times higher content than at the closure of MIS3 and over an order of magnitude higher content than in the Holocene (Figure 28). The alkenones are highly refractory for diagenetic alterations and hence are faithful indicators of the marine productivity (Brassell, 1993). Therefore, the enrichment of the $\sum$alkenones in the LGP time-slice than the two adjacent warm periods demonstrates distinctly increased productivity in the EAS during that time.

The productivity minima have occurred during the terminations of the last two glacial periods (LGP and MIS4) and at the interstadials of MIS5 (i.e., ~80 Ka and ~97 Ka) (Figure 27). This observation implies that the climate warming episodes appear to have commenced when the marine productivity has reached its ebb. The association of high productivity largely with the cold events supports the previously proposed hypothesis of increased nutrient injection in to the photic zone of the EAS due to strengthened winter monsoons (Cayre and Bard, 1999; Rostek et al., 1997; Schulte et al., 1999; Thamban et al., 2001).

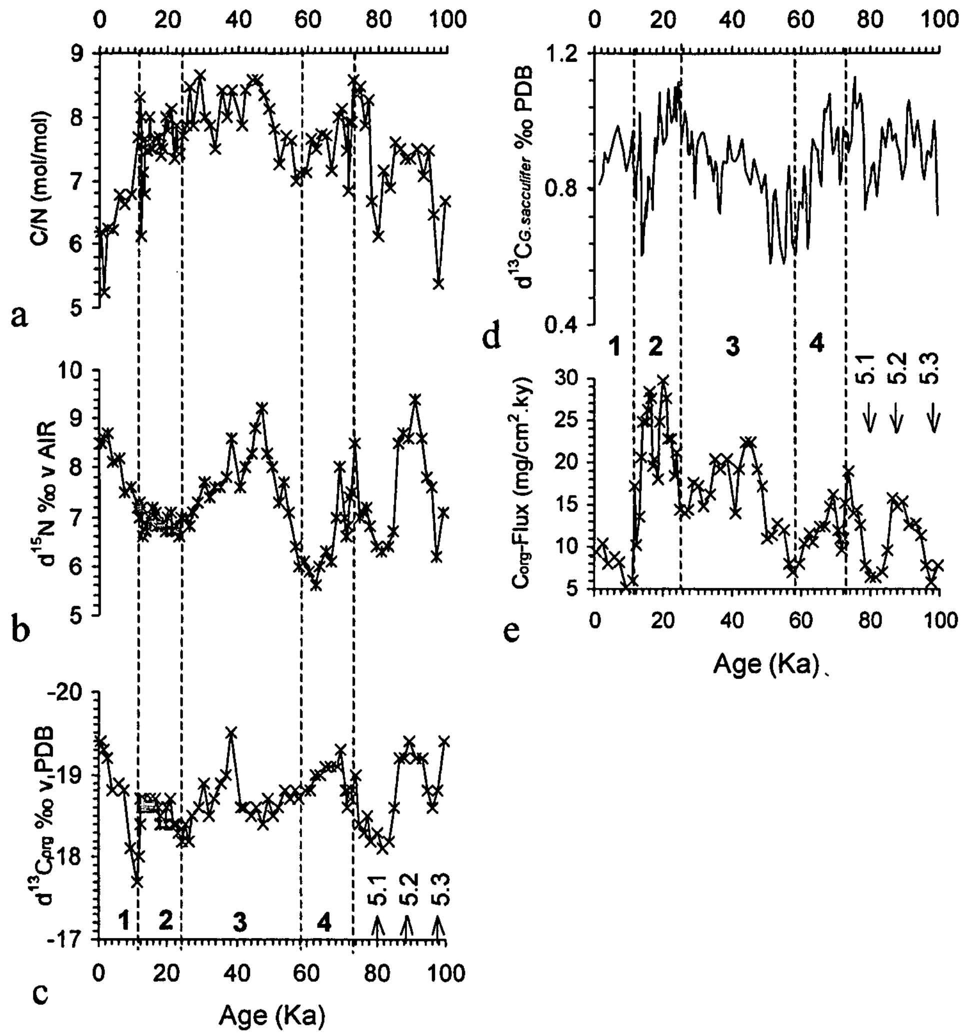

Figure 27: The time-series variation of the various organic and inorganic proxies of the marine productivity. The proxies invariably suggest higher marine production during cold climate, despite the presence of certain amount of terrestrial organic matter in the sediment of the EAS.

Weakening of the WMC and PCC during the glacial times (i.e., reduced low-salinity water flux in to the EAS from the BOB) appear to have weakened the surface layer stratification facilitating injection of the deep-water nutrient in to the euphotic zone. Additionally, the intensified winter-monsoon winds blowing over the Indian peninsula towards the EAS (see Figure 1) might have enriched the photic waters of the Indian margin with Fe-rich dust derived from the basaltic and lateritic terrains of the Deccan enhancing the possibility of complete utilization of the injected nutrients (Martin, 1990), thus greatly increasing the glacial productivity.

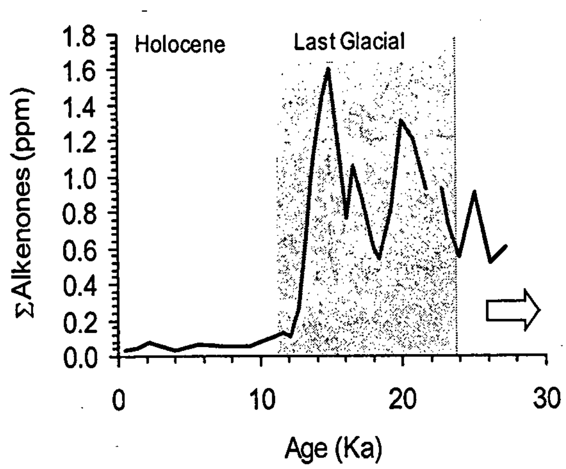

Figure 28: The alkenones synthesized by the prymnesiophyta group of algae are refractory to the post-burial diagenesis. Therefore, alkenone content in the sediment is most reliable proxy for the marine productivity. Distinctly higher content of the total-alkenones in the Glacial-EAS sediment strengthens the view based on other proxies suggesting higher Glacial-productivity.

This interpretation is supported by, a) elevated particle flux to the deep-EAS during the coldest SSTs of 1988/89 associated with strongest winter monsoons, and b) the definite role of winter monsoons in the inter-annual variability of the particle fluxes in the EAS unlike the western region, which is governed by the strength of summer monsoons (Haake et al., 1993). Interestingly, the recent study from the Oman Margin sedimentary records have provided new clues for well-sustained high productivity even during the LGM climate due to strengthened winter monsoons (Tamburini et al., 2003), which probably have intensified the winter cooling and deep-winter mixing (Madhupratap et al., 1996; Reichart et al., 1998). The marginally higher C/N ratios (>7) during the last glacial cycle (~72 Ka - ~11 Ka: Figure 27e) suggesting relatively increased transfer of the terrestrial-OM to the EAS region perhaps may be indicative of intensified glacial cycle winter winds.

6.4. Eastern Arabian Sea productivity vis-à-vis global climate:

The strengthened biological pump has been considered most important mechanism that lowered the atmospheric-CO_2 leading into the cold and dry glacial periods from the warm and wet interglacials (see Sigman and Boyle, 2000). In the last decade the southern ocean sector primary productivity emerged as the driver of the global climate variability in general and atmospheric-CO_2 in particular. However, this view was challenged with the help of biogenic-opal and calcite-carbon and sedimentary-nitrogen isotope evidences, which rather indicated that the primary productivity was lower during the LGP than during the Holocene (Shemesh et al., 1993). The role of oceanic productivity in sequestering the atmospheric-CO_2 (i.e., climate variability) in to the deep-oceanic sedimentary reservoir is rather unquestionable considering the size of oceanic carbon reservoir. If the primary productivity was lower in the southern ocean during the LGP, then there must be some oceanic regions elsewhere, which must have regulated the biological pump with amazingly rhythmic toggle. In this regard it is tempting to suggest that the oceanic areas such as the EAS, where the preliminary evidences in support of strengthened biological pump during the LGP brought-out in this study, may have played an important role in regulating the global climate! It may be necessary to investigate the marginal seas of the tropical regions to assess whether the glacial high productivity was specific to the EAS alone, or the marginal seas of the glacial tropics have witnessed high productivity in general. If the latter is true, then the mechanism regulating the global climate is located right within the tropical region, where the high latitudes might have merely responded to the tropical climate forcing during the glacial cooling. This view needs to be tested with several other records from the global oceans, until then it remains a speculation.

6.5. Denitrification and past-productivity: a mismatch?

The water column denitrification records preserved in the sediment can be useful in understanding the past productivity. The present day Arabian Sea has an intense OMZ due to basin-wide high productivity and low oxygen intermediate water feeding the OMZ (Olson et al., 1993), making it one of the worlds largest marine denitrification regions (Codispoti, 1995; Naqvi, 1987). The bacterially mediated denitrification in the ocean is a process by which marine nitrate is reduced to gaseous species. Marine denitrification produces significant enrichment of $\delta^{15}N$ in subsurface nitrates (Codispoti and Christensen, 1985), and is reflected in the sinking organic particulates (Altabet et al., 1995). Therefore, the sedimentary-$\delta^{15}N$ record may provide an additional tool to understand past changes in the productivity if the intermediate water oxygenation has remained unaltered. However, this relationship is not straightforward as different processes may be involved in controlling the denitrification. For example, recently Ganeshram et al., (2002) suggested that the glacial productivity was low due to altered Redfield ratios of phosphorous and nitrogen in spite of increased nutrient- or iron-supply. On the other hand, Altabet et al., (2002) have shown that the denitrification and productivity go hand-in-hand even on millennial time-scale. As there is little isotopic fractionation associated with the sedimentary denitrification (Brandes and Devol, 1997), the sedimentary $\delta^{15}N$ should be able to faithfully preserve the record of water column denitrification.

The time-series $\delta^{15}N$ record of the EAS obtained from GC-08 core (Figure 27) accurately superimposes the $\delta^{15}N$ records of the western Arabian Sea (Altabet et al., 1995) and closely resembles the only other available $\delta^{15}N$ record from the EAS (Ganeshram et al., 2000). Similar structure in time-series $\delta^{15}N$ profiles with similar range of values (6-9 ‰) (Figure 29 and also see Altabet et al., 1999, Ganeshram et al., 2000) across the Arabian Sea suggest the basin-wide homogeneity in the $\delta^{15}N$ signals irrespective of greatly differing upwelling and productivity intensity (Haake et al., 1993). The observed regional homogeneity across the basin renders the link between productivity and denitrification a complex issue especially for the EAS in light of the increased glacial productivity. The glacial increase in the productivity should have produced increased enrichment of the $\delta^{15}N$, had the intermediate water redox conditions remained uniform throughout. The glacial decreases (~6 ‰) and interglacial increases (~8 ‰) in the $\delta^{15}N$ of the EAS (Figure 27 & also see Ganeshram et al., 2000; Suthhof et al., 2001) can be explained by significant change in mid-water oxygenation feeding the OMZ-depth during the glacial periods.

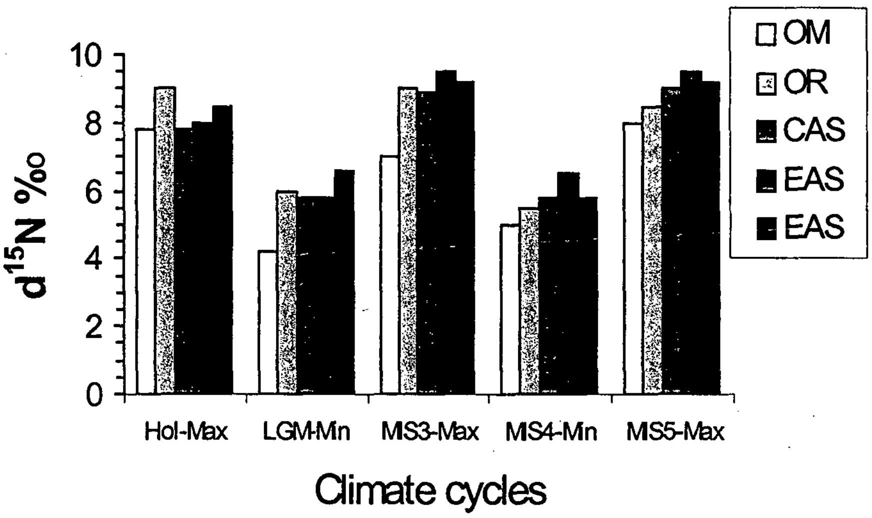

Figure 29: The sedimentary $\delta^{15}N$ records of the Arabian Sea. Note the marginal differences in the averaged peak-$\delta^{15}N$ events across the basin in spite of differing productivity pattern. OM=Oman Margin, OR=Owen Ridge, CAS=Central Arabian Sea,EAS=Eastern Arabian Sea. The black bar is the present data.

The Arabian Sea intermediate water presently consists of Persian Gulf Water with ~2.6 ml/L O_2 (2 Sv: sill-depth=~60 m), Red Sea Water with ~3.5 ml/L O_2 (0.5 Sv; Sill-depth=~140 m), and Indian Central Water with ~1 ml/L O_2 (6 Sv) (Olson et al., 1993; Wyrtki, 1973). Only the Indian Central water fed the OMZ of the LGM-EAS, as the Persian Gulf was desiccated and Red Sea water greatly reduced due to drop in sea level. This hydrographic condition coupled with the increased productivity during the LGP should further intensify and expand the OMZ in the EAS leading to an intensified denitrification rather than observed collapse of the OMZ (see Figure 27d).

Unless there was a perennial existence of the well-oxygenated water in the intermediate depths, the observed productivity-denitrification decoupling in the high productive glacial-EAS is simply not possible. The remarkably improved mid-water oxygenation during the time of isolation of the Persian Gulf and Red Sea probably has resulted by either the enhanced advection of oxygen rich southerly ventilated water (Wyrtki, 1973), or the intensified ASHSW and deep winter mixing. The deep winter mixing has already been invoked to explain the collapse of glacial-OMZ in the northern Arabian Sea (Reichart et al., 1998). The former possibility is unlikely, because by the time the southern source water penetrates in to the Arabian Sea, its oxygen is expected to deplete beyond the required level to diminish the OMZ. The intensified ASHSW in the northern Arabian Sea and its southward advection associating with enhanced deep winter mixing due to strengthened winter monsoons during the cold periods appear to have resulted effective ventilation of the mid-depth water in the EAS. Such vigorous ventilation could have satisfied the increased demand of oxygen due to elevated glacial-productivity and hence reduced the denitrification. Therefore, the latter hypothesis is a plausible mechanism to explain the reduced denitrification in the EAS in spite of increased productivity during the LGP. The reduced denitrification resulting in increased nitrate- and intensified winter monsoons increasing the Fe supply to the photic zone appear to have led to the complete utilization of increased nutrients.

The OMZ-oxygenation in the EAS could be evaluated with the help of particulate Mn-oxide or Mn_{excess} in the shelf core (GC02) because the present day OMZ sweeps over this region. The Mn_{excess} variation (Figure 11) is nearly similar to the alkenone variation in the GC08 (Figure 13), wherein both of them show very high values in the early part of the LGP. Interestingly, the Al_{excess} also shows similar variation (Figure 11) indicating high productivity (Banakar et al., 1998). This in fact supports the interpretation of decoupled productivity and denitrification, where the OMZ-depth might have remained well oxygenated (high Mn_{excess}) due to excellent ventilation during the LGP. However, in absence of such records from the other parts of the EAS, the above interpretation based on the similarity between GC02 and GC08 may remain speculative.

The most weakest denitrification events are evident during the moderately cold-MIS4 and warm-MIS5.1 and -MIS5.3 interstadials (Figure 27d) further complicating the generally believed denitrification and productivity linkage. If the Arabian Sea was more productive during the warm and wet climate periods than during the cold and dry periods as envisaged in many previous works based on the western Arabian Sea sediments, then why the denitrification intensity was weakest during both those type of climates? Why the milder cold period MIS4 shows lowest denitrification or practically non-existing OMZ than compared to the coldest-LGM, if the mid-depth oxygenation was improved only during the cold climates? Even though it is not a easy task to address these complexities with the aid of very limited data, at the out-set it is possible to suggest that, at several occasions in the past either the denitrification-productivity must have been decoupled or the basin-wide homogenisation process in the Arabian Sea due to highly vibrant thermocline might have modified the region and climate specific signals of the water column denitrification. The above-discussed conditions in the Arabian Sea hydrography probably have led to the observed mismatch between the sedimentary denitrification records and the climate-forced productivity changes.

Conclusions

7. Conclusions

The Eastern Arabian Sea bordering western India appears to be unique with respect to its response to the past climate change. In that, it shows quite contrasting features as compared to its western counter part. Few important interpretations derived from the present multi-proxy study are summarised below. These observations have significance in understanding the response of the Eastern Arabian Sea biogeochemical processes to the past climate change.

1. ***The*** north-south salinity gradient variation in the Eastern Arabian Sea, productivity patterns, and sedimentary properties reconstructed for the last 100,000 years provide a fairly consistent record of the biogeochemical responses of the region to the climate forced monsoon variations.
2. ***The*** salinity-gradient reconstruction based on the geographical contrast in the planktonic calcite-$\delta^{18}O$ has yielded higher gradient of ~2.2 psu for the last glacial maximum as compared to the present ~1 psu gradient between the studied locations. Nearly doubled salinity-gradient indicates that the poleward coastal current, which is responsible for maintaining the low-salinity in the study region, appears to have collapsed during that time. The collapse of this winter-spring circulation in the region possibly was the result of broken communication between the Bay of Bengal and the Eastern Arabian Sea. The greatly diminished summer monsoons during the last glacial period appear to have resulted in the broken communication between those two basins.
3. ***The*** events of lowest salinity gradient of ~0.2 psu during the last warm period (MIS5) clearly indicate that much stronger summer monsoons than the Holocene existed in the past, which have driven the coastal currents more vigorously. The vigorous coastal currents appear to have led to the disappearance of the salinity gradient in the Eastern Arabian Sea.

4. ***The*** salinity-gradient during the pre-Holocene period exhibits high-frequency large amplitude fluctuations as compared to the marginal variations in the Holocene time. This may be due to the fact that, the Holocene monsoon system has been considerably stable than the preceding period.
5. ***The*** coarse grain silicate detritus transport to the continental shelf by the Deccan Rivers was high during most of the Holocene as compared to the last glacial period indicating stronger summer-monsoons during the former period. On the other hand, the increased proportion of the coarse grains in the sediment during the early part of the last glacial period when the Deccan Rivers were weaker suggests that the relict material was transported further off from the exposed continental shelf at the time of lowered sea level stand.
6. ***The*** productivity in the Eastern Arabian Sea was significantly higher during the last glacial period than the Holocene and the last warm period (MIS5). The isotopic proxies of the productivity exhibit maxima at the commencement of the climate cooling events (glacial) and reach the minima around their termination. Such productivity patterns have significance because the beginnings of the climate warming episodes coincide with the ebbs in marine productivity.
7. ***The*** glacial-high productivity in the study region can be explained by the combination of enhanced deep-water nutrient supply to the photic zone and the adequate availability of limiting-micronutrient iron. Intensified injection of the deep-water nutrients into the surface water might have taken place when the fresh water flux in the region has greatly reduced (due to broken communication between Bay of Bengal and Eastern Arabian Sea) leading to weakening of upper water stratification. The large supply of iron must have been possible when the winter winds blowing from the Indian continent towards the Eastern Arabian Sea were intense. Such glacial scenario might

have led to the complete utilization of nutrients injected in to the surface layer and hence significantly increased glacial productivity.

8. ***As*** the biogenic opal and carbon-isotope evidences from the Southern Ocean sediment have revealed reduced primary productivity during the last glacial period, the increased tropical marine productivity gains importance. In that, the biological pump elsewhere than the Southern high latitudes must have to be strengthened to account for the glacial drop in the atmospheric carbon dioxide. In light of convincing evidences for the glacial high productivity in the Eastern Arabian Sea, it may be feasible to suggest that the tropical continental-margin environment have played crucial role in regulating glacial climate through strengthened biological pump.

9. ***The*** sedimentary record of nitrogen-isotopes suggests that the water column denitrification in the Eastern Arabian Sea was almost collapsed (i.e., the oxygen minimum zone disappeared) during the last glacial period. This region showing high productivity during the glacial time, the evidence for reduced denitrification is intriguing. However, the reduced denitrification may be a reason for increased nutrient availability to the photic zone from OMZ-depth. Secondly, the ventilation of the OMZ-water might have been very vigorous during the glacial time due to intensified deep-winter mixing that has resulted in satisfying the oxygen demand of increased export production. Therefore, the exceptionally excellent OMZ-depth ventilation during the last glacial period when the winter monsoons were intense might have led to great reduction in the water column denitrification.

References

8. References

Altabet, M.A., Francois, R., Murray, D.W. and Prell, W.L., 1995. Climate related variations in denitrification in the Arabian Sea from sediment $^{15}N/^{14}N$ ratios. *Nature,* 373: 506-509.

Altabet, M.A., Murray, D.W. and Prell, W.L., 1999. Climatically linked oscillations in Arabian Sea denitrification over the past 1 my: implications for the marine N cycle. *Paleoceanography,* 14: 732-734.

Banakar, V.K., Galy, A., Sukumaran, N., Parthiban, G. and Volvaiker, A.Y (Chodankar, A.R)., 2003. Himalayan sedimentary pulses recorded by silicate detritus within a ferromanganese crust from the Central Indian Ocean. *Earth and Planetary Science Letters,* 205: 337-348.

Banakar, V. K., Parthiban, G., Pattan, J. N. and Jauhari, P., 1998. Chemistry of surface sediment along a north-south transect across the equator in the Central Indian Basin: an assessment of biogenic and detrital influences on element burial on the seafloor. Chemical Geology, 147: 217-132.

Banse, K., 1987. Seasonality of plankton chlorophyll in the Central and northern Arabian Sea. *Deep Sea Research,* 34: 713-723.

Banse, K. and McClain, C.R., 1986. Winter blooms of phytoplankton in the Arabian Sea as observed by the Coastal Zone Colour Scanner. *Marine Ecology Progress. Sev,* 34: 201-211.

Bard, E., Hamelin, B., Fairbanks, R.G. and Zinder, A., 1990a. Calibration of the 14C timescale over the past 30,000 years using mass spectrometric U-Th ages from Barbados corals. *Nature,* 345: 405-410.

Bard, E., Hamelin, B. and Fairbanks, R.G., 1990b. U-Th ages obtained by mass spectrometry in corals from corals from Barbados: Sea level during the last 130,000 years. *Nature,* 346: 456-458.

Bassinot, F.C., Beaufort, L., Vincent, E., Labeyrie, L.D., Rostek, F., Müller, P.J., Quidelleur, X., Lancelot, Y., 1994. Coarse fraction fluctuations in pelagic carbonate sediments from the tropical Indian Ocean: A 1500-kyr record of carbonate dissolution. *Paleoceanography,* 9: 579-600.

Calvert, S.E., Douglas, F., Cowie, G.L., Schubert, C., Von Rad, U., Schulz, H., Berner, U. and Erlenkeuser, H., 1996. Late Pleistocene record of organic carbon accumulation in the northeastern Arabian Sea. *International Symposium on Geology and Geophysics of the Indian Ocean, Goa* (Abstract), pp. 60-61.

Cayre, O. and Bard, E., 1999. Planktonic foraminiferal and alkenone records of the last deglaciation from the eastern Arabian Sea. *Quaternary Research,* 52: 337-342.

Chaisson, W.P. and Ravello, A.C., 2000. Pliocene development of the east-west hydrographic gradient in the equatorial Pacific. *Paleoceanography,* 15: 497-505.

Chodankar, A. R., Banakar, V. K. and Oba, T., 2003. Past-salinity gradient variations in the eastern Arabian Sea: reconstructions from the sedimentary $\delta^{18}O_{G.sacculifer}$ records. Internat. Young Scientists Global Change Conf., Trieste, Italy, 16-19 Nov. p.27.

Clemens, S. and Prell, W.L., 1990. Late Pleistocene variability of Arabian Sea summer monsoon winds and continental aridity; eolian records from the lithogenic component of deep-sea sediments. *Paleoceanography*, 5 (2): 109-145.

Clemens, S., Prell, W.L., Murray, D., Shimmield, G.B. and Weedon, G., 1991. Forcing mechanism of the Indian Ocean Monsoon. *Nature*, 353: 720-725.

Codispoti, L.A., 1995. Biogeochemical cycles: Is the ocean loosing nitrate? *Nature,* 376: 724-727.

Codispoti, L.A. and Christensen, J.P., 1985. Nitrification, denitrification, nitrous oxide cycling in the eastern tropical south pacific ocean. *Marine Chemistry,* 16:277-300.

Cullen, J.L., 1981. Microfossil evidence for changing salinity pattern in the Bay of Bengal over the last 20000 years. Palaeogeography Palaeoclimatology Palaeoecology, 35: 315-356.

Currie, R. I., Fisher, A. E. and Hargreaves, P. M., 1973. Arabian Sea Upwelling. In: *The biology of the Indian Ocean,* B. Zeitzschel (ed),. Springer, Berlin, pp. 37-52.

Curry, W.B. and Cullen, J.L., 1997. Carbonate production and dissolution in the western equatorial Atlantic during the last 1 m.y. *Proceedings of ODP Scientific Results,* 154, 189-199.

Dansgaard, W., Johnsen, S.J., Clausen, H.B., Dahl-Jensen, D., Gundestrup, N. and Hammer, C.U., 1984. North Atlantic climatic oscillations revealed by deep Greenland ice cores. In: Climate Processes and climate sensitivity. Geophysical Monograph 29, Maurice Ewing Volume 5, edited by J.E. Hansen and T. Takahashi, American Geophysical Union, Washington D.C., pp. 288-298.

Dansgaard, W., Johnsen, S.J., Clausen, H.B., Dahl-Jensen, D., Gundestrup, N.S., Hammer, C.U., Hvidberg, C.S., Steffensen, J.P., Sveinbjörnsdottir, A.E., Jouzel, J. and Bond, G., 1993. Evidence for general instability of past climate from a 250-kyr ice-core record. *Nature,* 364: 218-220.

Delaygue, G., Bard, E., Rollion, C., Jouzel, J., Steivenard, M., Duplessy, J.-C., 2001. Oxygen isotope/salinity relationship in the northern Indian Ocean. *Journal of Geophysical Research,* 106: 4565-4574.

Demaison, G. and Moore, G. T., 1980. Anoxic environments and oil source bed genesis. *American Association of Petroleum Geologists Bulletin,* 64: 1179-1209.

Dickens, G. R. and Owen, R.M., 1994. Late Miocene-Early Pliocene manganese redirection in the central Indian Ocean: Expansion of the intermediate water oxygen minimum zone. *Paleoceanography,* 9: 169-181.

Dodge, R.E., Fairbanks, R.G., Benninger, L.K. and Maurrasse, F., 1983. Pleistocene sea levels from raised coral reefs of Haiti. *Science,* 219: 1423-1425.

Duplessy, J.-C., 1982. Glacial to interglacial contrast in the northern Indian Ocean. *Nature,* 295: 494-498.

Duplessy, J.-C., Bè, A.W.H., Balnk, P.L., 1981. Oxygen and carbon isotopic composition and biogeographic distribution of planktonic foraminifera in the Indian Ocean. *Paleogeography Paleoclimatology Paleoecology,* 33: 9-46.

Emeis, K-C., Anderson, D.M., Doose, H., Kroon, D., Schulz-Bull, D., 1995. Sea-surface temperatures and history of monsoon upwelling in the northwest Arabian Sea during the last 500,000 years. *Quaternary Research,* 43: 355-361.

Emiliani, C., 1955. Pleistocene temperatures. *Journal of Geology,* 63: 538-578.

Epstein, S., Buchsbaum, R., Lowenstan, H.A., Uray, H.C., 1953. Revised carbonate-water isotopic temperature scale. *Bulletin of Geological Society of America,* 64: 1315-1325.

Fairbanks, R.G., 1989. A 17000-year glacio-eustatic sea level record: influence of glacial melting rates on younger Dryas event and deep ocean circulation. *Nature,* 342: 637-642.

Filippelli, G.M., 1997. Intensification of the Asian monsoon and a chemical weathering event in the late Miocene-early Pliocene: Implications for late Neogene climate change. *Geology,* 25: 27-30.

Folk, R.L., 1968. Petrology of sedimentary rocks, *Hemphills, Austin.* 177 pp.

Fontugne, M.R. and Duplessy, J.-C., 1981. Organic carbon isotopic fractionation by marine plankton in the temperature range-1°C-31°C. *Oceanologica Acta,* 4: 85-89.

Ganeshram, R.S., Pederson, T.F., Calvert, S.E., McNeill, G.W., Fontugne, M.R., 2002. Glacial-interglacial variability in denitrification in the world oceans: causes and consequences. *Plaeoceanography,* 15: 361-376.

Gröger, M., Henrich, R. and Bickert, T., 2003. Glacial-interglacial variability in lower North Atlantic deep water: inference from silt grain-size analysis and carbonate preservation in the western equatorial Atlantic. *Marine Geology,* 201: 321-332.

Haake, B., Ittekkot, V., Rixon, T., Ramaswami, V., Nair, R.R., Curry, W.B., 1993. Seasonality and inter-annual variability of particle fluxes to the deep Arabian Sea. *Deep-Sea Research Part-I,* 40: 1323-1344.

Haake, B., Rixen, T., Reemtsma, T., Ramaswamy, V. and Ittekkot, V. D., 1996. Process determining seasonality and interannual variability of settling particle fluxes to the deep Arabian Sea. In: V. Ittekkot et al. (Eds.), *Particle fluxes in the ocean.* John Wiley and Sons, pp: 251-270.

Hasternath, S. and Greischar, L., 1991. The monsoonal current regimes of the tropical Indian Ocean: Observed surface flow fields and their geostrophic and wind-driven components. *Journal of Geophysical Research,* 96: 12619-12633.

Hays, J.D., Imbrie, J. and Shackleton, N.J., 1976. Variations in the Earth's orbit: Pacemaker of the ice ages. *Science,* 194: 1121-1132.

Heinrich, M., 1988. Origin and consequences of cyclic ice rafting in the northeast Atlantic Ocean during the past 130,000 years. *Quaternary Research,* 29: 143-152.

Hemleben, C., Spindler, M., Anderson, R.O., 1989. Modern planktonic foraminifera. *Springer-Verlag, NY.*, p. 363.

Hoefs, J., 1997. Stable isotope geochemistry. Springer-verlag, Germany, p. 201.

Hong, Y.T., Hong, B., Lin, Q.H., Zhu, Y.X., Shibata, Y., Hirota, M., Uchida, M., Leng, X.T., Jiang, H.B., Xu, H., Wang, H. and Yi, L., 2003. Correlation between Indian Ocean summer monsoon and north Atlantic climate during the Holocene. *Earth and Planetary Science Letters*, 211: 371-380.

Imbrie, J., Hays, J.D. Martinson, D.G., McIntyre, A., Mix, A.C., Morley, J.J., Pisias, N.G., Prell, W.L., Shackleton, N.J., 1984. The orbital theory of Pleistocene climate: support from a revised chronology of the marine $\delta^{18}O$ record. In: A. Berger et al (Eds.). Milankovitch and climate, Part-I, Plenum-Reidel, pp. 269-305.

Ikehara, M., Kawamura, K., Ohkouchi, N., Kimoto, K., Murayama, M., Nakamura, T., Oba, T. and Taira, A., 1997. Alkenone sea surface temperature in the Southern Ocean for the last two deglaciations. *Geophysical Research Letters*, 24: 679-682.

Ikehara, M., Kawamura, K., Ohkouchi, N., Murayama, M., Nakamura, T. and Taira, A., 2000. Variations of terrestrial input and marine productivity in the Southern Ocean (48°S) during the last two deglaciations. *Paleoceanography*, 15: 170-180.

Jasper, J. P and Gogosian, R. B., 1990. The sources and deposition of organic matter in late Quaternary Pigmy Basin. *Geochimica et Cosmochimica Acta*, 54: 1117-1132.

Jensen, T.G., 2001. Arabian Sea and Bay of Bengal exchange of salt and tracers in an ocean model. *Geopphysical Research Letters*, 28: 3967-3970.

Jensen, T.G., 2003. Cross-equatorial pathways of salt and tracers from the northern Indian Ocean: Modelling results. *Deep Sea Research-II*, 50: 2111-2127.

Kabanova, Y. G., 1968. Primary production in the northern part of the Indian Ocean. *Oceanology*, 8: 214-225.

Keigwin, L.D., Jones, G.A., Lehman, S.J. and Boyle, E.A., 1991. Degalcial meltwater discharge, North Atlantic deep circulation and abrupt climate change. *Journal of Geophysical research*, 96C: 16811-16826.

Keinast, M., 2000. Constant nitrogen isotopic composition of organic matter in the South China Sea during the last climatic cycle: Global implications. *Paleoceanography,* 15(2): 244-253

Kienast, M., Calvert, S. E., Pelejero, C. and Grimalt, O., 2001. A critical review of marine sedimentary $\delta^{13}C$-pCO_2 estimates: New palaeorecords from the South China Sea and a revisit of other low latitude $\delta^{13}C$-pCO_2 records. *Paleoceanography,* 15: 113-127.

Kroopnick, P.M., 1985. The distribution of $\delta^{13}C$ of ΣCO_2 in the world oceans. *Deep Sea Research,* 32: 57-84.

Kudrass, H.R., Hofmann, A., Doose, H., Emeis, K. and Erlenkeuser, H., 2001. Modulation and amplification of climatic changes in the northern hemisphere by the Indian summer monsoon during the past 80 k.y. *Geology,* 29: 63-66.

Ku, T-L. and Oba, T., 1978. A method for quantitative evaluation of carbonate dissolution in deep-sea sediments and its application to paleoceanographic reconstruction. *Quaternary Research,* 10: 112-129.

Leuschner, D. K. and Sirocko, F., 2000. The low-latitude monsoon climate during Dansgaard-Oeschger cycles and Heinrich Events. *Quaternary Science Reviews.*, 19: 243-254.

Levitus, S. and Boyer, T.P., 1994. World Ocean Atlas-1994. vol 5, Salinity, NOAA Atlas NESDIS 3, 99p, U.S. Govt. Print. Off. Washington DC.

Madhupratap, M., Kumar, S.P., Bhattatri, P.M.A., Kumar, M.D., Raghukumar, S., Nair, K.K.C. and Ramaiah, N., 1996. Mechanism of the biological response to winter cooling in the northeastern Arabian Sea. *Nature,* 384: 549-552.

Martin, J.H., 1990. Glacial-interglacial CO_2 change: the iron hypothesis. *Paleoceanography,* 5: 1-13.

Milankovitch, M. M., 1941. Canon of insolation and the ice-age problem. Beograd: Koniglich Serbische Akademie. (English translation by the Israel Program for Scientific Translations, published for the US Department of Commerce, and the National Science, Foundation, Washington, DC (1969).)

Murray, R.W., Leinen, M., 1993. Chemical transport to the seafloor of the equatorial Pacific Ocean across the latitudinal transect at 135oW: tracking the sedimentary major, trace and REE element fluxes at the equator and intertropical convergence zone. *Geochimica et Cosmochimica Acta,* 57: 4141-4163.

Muller, P. J., Schneider, R. and Ruhland, G., 1994. Late Quaternary PCO_2 variations in the Angola Current: evidence from organic carbon $\delta^{13}C$ and alkenone temperatures. In: Zahn, R., Pedersen, T. F., Kaminski, M. A., Labeyrie, L. (Eds.). *Carbon Cycling in Glacial Ocean: Constraints on the Ocean's Role in Global Change.* NATO ASI Series, Vol 17, Springer, Berlin Heidelberg New York, pp 343-366.

Naidu, P. D. and Malmgren. B.A., 1999. Quaternary carbonate record from the equatorial Indian Ocean and its relationship with productivity changes. *Marine Geology,* 161: 49-62.

Naidu, P.D. and Malmgren. B.A., 1996. A high-resolution record of late Quaternary upwelling along the Oman margin, Arabian Sea based on planktonic foraminifera. *Paleoceanography,* 11: 129-140.

Nair, R.R. and Hashmi, N.H., 1980. Holocene climatic inferences from sediments of the western Indian continental shelf. *Proc. Indian Academy of Sciences,* 89-A: 299-315.

Nair, R.R., Ittekkot, V., Manganini, S.J., Ramaswami, V., Haake, B., Degens, E.T., Desai, B.N., Honjo, S., 1989. Increased particle flux to the deep ocean related to monsoon. *Nature,* 338: 749-751.

Naqvi, S.W.A., 1987. Some aspects of the oxygen deficient conditions and denitrification in the Arabian Sea. *Journal of Marine Research,* 45: 1049-1072.

Ninkovitch, D., 1979. Distribution, age, and chemical composition of western Indonesia. *Journal of Volcanology and Hydrothermal Research,* 5: 67-86.

Niitsuma, N., Oba, T. and Okada, M., 1991. Oxygen and carbon isotope stratigraphy at Site 723, Oman margin. In: W. L. Prell et al (eds), *Proceedings of ODP Scientific Results,* 117, College Station, Tx., 321-341.

Oeschger, H., Beer, J., Siegenthaler, U. and Stauffer, B., 1984. Late glacial climate history from ice cores. In: Climate Processes and Climate Sensitivity (J.E. Hansen and T. Takahashi, eds.). Washington, DC: American Geophysical Union, pp. 299-306.

Olausson, E., 1965. Evidence of climatic changes in deep-sea cores, with remarks on isotopic palaeotemperature analysis. *Progress in Oceanography,* 3: 321-352.

Olson, D.B., Hitchcock, G.L., Fine, R.A. and Bruce, A.W., 1993. Maintenance of low oxygen layer in the central Arabian Sea. *Deep Sea Research Part-II,* 40: 673-685.

Overpeck, J., Rind, D., Lacis, A.C. and Healy, R., 1996. Possible role of dust induced regional warming in abrupt climate change during the last glacial period. *Nature,* 384: 447-449.

Paropkari, A. L., Babu, C. P. and Mascarenhas, A., 1992. A critical evaluation of depositional parameters controlling the variability of organic carbon in Arabian Sea sediments. *Marine Geology,* 107:213-226.

Pattan, J.N., Shane, P., Banakar, V.K., 1999. New occurrence of Youngest Toba Tuff in abyssal sediment of the Central Indian Basin. *Marine Geology,* 155: 243-248.

Pattan, J.N., Masuzawa, T., Naidu, P.D., Parthiban, G., Yamamoto, M., 2003. Productivity fluctuations in the southeastern Arabian Sea during the last 140 Ka. *Palaeogeography Palaeoclimatology Palaeoecology,* 193: 575-590.

Pedersen, T. F. and Calvert, S. E., 1990. Anoxia Vs. Productivity: What controls the formation of organic carbon-rich sediments and sedimentary rocks? *American Association of Petroleum Geologists Bulletin*, 74: 454-466.

Pedersen, T. F., Shimmield, G. B. and Price, N. B., 1992. Lack of enhanced preservation of organic matter in sediments under the oxygen minimum in the Oman margin. *Geochimica et Cosmochimica Acta*, 56: 545-551.

Peters, K. E., Sweeney, R. E. and Kaplan, I. R., 1978. Correlation of carbon and nitrogen stable isotope ratios in sedimentary organic matter. *Limnology Oceanography,* 23: 598-604.

Pettijohn, F.J., Potter, P.E. and Siever, R., 1972. Sand and Sandstones. Springer, New-York, p.618.

Prasad, T.G., 2001. Formation and seasonal spreading of water masses in the Arabian Sea based on Data Analysis and Modelling. Ph. D. Thesis, Hokkaido Univ., Japan. p. 131.

Prasanna Kumar, S. and Prasad, T.G., 1999. Formation and spreading of Arabian Sea high-salinity water mass. *Journal of Geophysical Research,* 104: 1455-1464.

Prahl, F. G. and Wakeham, S. G., 1987. Calibration of unsaturation patterns in long-chain ketone compositions for paleotemperature assessment. *Nature,* 330: 367-369.

Prahl, F. G., Muehlhausen, L. A. and Zahnle, D. L., 1988. Further evaluation of long-chain alkenones as indicators of paleoceanographic conditions. *Geochimica et Cosmochimica Acta,* 52: 2303-2310.

Prahl, F.G., de Lange, G.J., Lyle, M. and Sparrow, M.A., 1989. Post depositional stability of long-chain alkenones under contrasting redox conditions. *Nature,* 341: 434-437.

Prell, W.L. and Kutzbach, J.E., 1992. Sensitivity of the Indian monsoon to forcing parameters and implications for its evolution. *Nature,* 360: 647-652.

Prell, W.L. and Kutzbach, J.E., 1987. Monsoon variability over the past 150,000 years. *Journal of Geophysical Research,* 92 (D7): 8411-8425.

Prell, W.L., Hutson, W.H., Williams, D.F., Be, A.W.H., Geitzenauer, R. and Molfino, B., 1980. Surface circulation of the Indian Ocean during the last interglacial maximum, approximately 18,000 yr B.P. *Quaternary Rsearch,* 14: 309-336.

Prins, M.A. and Weltje, G.J., 1999. End-member modeling of siliciclastic grain-size distributions: The late quaternary record of eolian and fluvial sediment supply to the Arabian Sea and its paleoclimatic significance in: Harbaugh et al., (eds), Numerical experiments in stratigraphy: Recent advances in stratigraphic and sedimentologic computer simulations. SEPM, Spl. Publ. 62, p. 91-111.

Prins, M.A., Postma, G., Cleveringa, J., Cramp, A. and Kenyon, N.H., 2000. Controls on terrigenous sediment supply to the Arabian Sea during the late Quaternary: the Indus Fan. *Marine Geology,* 169: 327-349.

Prins, M.A., Postma, G. and Weltje, G.J., 2000. Controls on terrigenous sediment supply to the Arabian Sea during the late Quaternary: the Makran continental slope. *Marine Geology,* 169: 351-371.

Qasim, S.Z., 1977. Biological productivity of the Indian Ocean. *Indian Journal of Marine Sciences*, 6: 122-137.

Qasim, S.Z., 1982. Oceanography of the northern Arabian Sea. *Deep Sea Research,* 29: 1041-1068.

Rao, B. R. and Veerayya, M. 2000. Influence of marginal highs on the accumulation of organic carbon along continental slope off India. *Deep-Sea Research II,* 47: 303-327.

Rao, K. L. 1979. India's water wealth: Its assessment, uses and projections. Orient Longman, pp. 261.

Rao, R.R., Molinari, R.L. and Festa, J.F., 1989. Evolution of the climatological near-surface thermal structure of the tropical Indian Ocean. *Journal of Geophysical Research,* 94: 10801-10815.

Rau, G. H., Takahashi, T. and Marais, D. J. D., 1989. Latitudinal variation in plankton $\delta^{13}C$: Implications for CO_2 and productivity in past oceans. *Nature,* 341: 516-518.

Reichart, G., 1997. Late Quaternary variability of the Arabian Sea monsoon and oxygen minimum zone. *Ph.D.Thesis,* Univ. Utrecht, p. 171.

Reichart, G.J., Lourens, L.J., Zachariasse, W.J., 1998. Temporal variability in the northern Arabian sea oxygen minimum zone during the last 225,000 years. *Paleoceanography,* 13: 607-621.

Reichart, G.J., Dulk, M. den., Visser, H.J., van der Weijden, C.H. and Zachariasse, W.J., 1997. A 225 kyr record of dust supply, paleoproductivity and the oxygen minimum zone from the Murray Ridge (northern Arabian Sea). *Paleogeography Paleoclimatology Paleoecology,* 134: 149-169.

Rose, W. I. and Chesner, C. A., 1987. Dispersal of ash in the great Toba eruption. Geology, 15: 913-917.

Rostek, F., Ruhland, G., Bassinot, F. C., Muller, P. J., Labeyrle, L. D., Lancelot, Y. and Bard, E., 1993. Reconstructing sea surface temperature and salinity using $\delta^{18}O$ and alkenone records. *Nature,* 364: 319-321.

Rostek, F., Bard, E., Beafort, L., Sonzogni, C. and Ganssen, G., 1997. Sea surface temperature and productivity records for the past 240 kyr in the Arabian Sea. *Deep Sea Research II,* 44: 1461-1480.

Sarkar, A., Ramesh, R., Somayajulu, B. L. K., Agnihotri, R., Jull, A. J. T. and Burr, G. S., 2000. High resolution Holocene monsoon record from the eastern Arabian Sea. *Earth and Planetary Science Letters,* 177: 209-218.

Sarkar, A., Ramesh, R., Bhattacharya, S. K. and Rajagopalan, G., 1990. Oxygen isotope evidence for a stronger winter monsoon current during the last glaciation. *Nature,* 343: 549-551.

Schulte, S., Rostek, F., Bard, E., Rullkotter, J., Marchal, O., 1999. Variation of oxygen minimum and primary productivity recorded in sediments of the Arabian sea. *Earth Planetary Science Letters*, 173: 205-221.

Schulz, H., von Rad, U. and Erlenkeuser, H., 1998. Correlation between Arabian Sea and Greenland climate oscillations of the past 110,000 years. *Nature*, 393: 54-57.

Shackleton, N.J., 2000. A 100,000 year ice-age cycle identified and found to lag temperature, carbon-dioxide, and orbital eccentricity. *Science*, 289: 1897-1902.

Shackleton, N. J., Opdyke, N. D., 1973. Oxygen isotope and palaeomagnetic stratigraphy of equatorial Pacific core V28-238: Oxygen isotope temperatures and ice volume on a 105 and 106 year-sclae. *Quaternary Research*, 3: 39-55.

Shackleton, N.J., 1967. Oxygen isotope analyses and Pleistocene temperatures re-assessed. *Nature*, 215: 15-17.

Shankar, D., Vinayachandra, P. N. and Unnikrishnan, A. S., 2002. The monsoon currents in the north Indian Ocean. *Progress in Oceanography*, 52: 63-120.

Sharma, G. S., 1977. Upwelling off the southwest coast of India. *Indian Journal of Marine Sciences*, 7: 209-218.

Shemesh, A., Macko, S.A., Charles, C.D. and Rau, G.H., 1993. Isotopic evidence for reduced productivity in the glacial Southern Ocean. *Science*, 262: 407-410.

Shetye, S. R., Gouveia, A. D., Shenoi, S. S. C., Michael, G. S., Sundar, D., Almeida, A. M. and Santanam, M., 1990. Hydrography and circulation off the west coast of India during the southwest monsoon. *Journal of Marine Research*, 48: 359-378.

Shetye, S.R., Gouveia, A.D., Shenoi, S.S.C., Michael, G.S., Sundar, D., Almeida, A.M. and Santanam, K., 1991. The coastal current off western India during the northeast monsoon. *Deep Sea Research*, 38: 1517-1529.

Shimmield, G.B., Mowbray, S.R., Weedon, G.P., 1990. A 350 ka history of the Indian SW-monsoon: evidence from deep sea cores, northwest Arabian Sea. *Transactions of the Royal Society, Edinburgh, Earth Sciences*, 81: 289-299.

Sigman, D.M. and Boyle, E.A., 2000. Glacial/interglacial variations in atmospheric carbon dioxide. *Nature,* 407: 859-869.

Sirocko, F., Sarnthein, M., Lange, H. and Erlenkeuser, H., 1991. Atmospheric summer circulation and coastal upwelling in the Arabian Sea during the Holocene and last glaciation. *Quaternary Research*, 36: 72-93.

Sirocko, F., Sarnthein, M., Erlenkeuser, H., Lange, H., Arnold, M. and Duplessy, J. –C., 1993. Century scale events in monsoon climate over the past 24,000 years. *Nature*, 364: 322-324.

Sirocko, F., Garbe-Schonberg, D., McIntyre, A. and Molfino, B., 1996. Teleconnections between the subtropical monsoons and high-latitude climates during the last deglaciation. *Science*, 272: 526-529.

Sirocko, F. and Sarnthein, M., 1989. Wind-borne deposits in the Northwestern Indian Ocean: record of Holocene sediments versus modern satellite data. In: *Paleoclimatology and Paleometeorology: Modern and Past Patterns of Global Atmospheric Transport*, Leinen, M. and Sarnthein, M. (Eds.). NATO ASI Series (282), Kluwer, Dordrecht-Boston-London, pp. 401-433.

Slater, R. D. and Kroopnick., 1984. Controls on dissolved oxygen distribution and organic carbon deposition in the Arabian Sea. In: *Marine Geology and Oceanography of the Arabian Sea and Coastal Pakistan,* Haq, B. U. and Milliman, J. D. (Eds.). Van Nostrand Reinhold, New York, 305-313 pp.

Smith, S. L., Banse, K., Cochran, J. K., Codispoti, L. A., Ducklow, H. W., Luther, M. E., Olson, D. B., Peterson, W. T., Prell, W. L., Surgi, N., Swallow, J. C. and Wishner, K., 1991. U. S. JGOFS: Arabian Sea Process Study, *U. S. JGOFS Planning Report No. 13,* Woods Hole Oceanographic Intitution, Woods Hole, Massachusetts, 164 pp.

Sonzogni, C., Bard, E., Rostek, F., 1998. Tropical sea surface temperatures during the last glacial period: a view based on alkenones in Indian Ocean sediment. *Quaternary science Reviews,* 17: 1185-1201.

Spaulding, S.A., Oba, T., 1992. Association of late Pleistocene calcareous nonnofossil assemblages and ^{18}O and ^{13}C isotopic changes, ODP Leg 117, Oman Margin, Arabian Sea. Memoire Di Scienze Geology, Univ. Padova, XLIII, 389-407.

Suthhof, A. Ittekkot, V., Gaye-Haake, B., 2001. Millennial-scale oscillation of denitrification intensity in the Arabian Sea during the late quaternary and its potential influence on atmospheric N_2O and global climate. Global Biogeochemical Cycles, 15, 637-649.

Sweeney, R. E. and Kaplan, I. R., 1980. Natural abundance of ^{15}N as a source indicator of nearshore and marine sedimentary and dissolved nitrogen. *Marine Chemistry,* 9: 81-94.

Tamburini, F., Föllmi, K. B., Adatte, T., Bernasconi, S. M. and Steinmann, F., 2003. Sedimentary phosphorous records from the Oman Margin: New evidence of high productivity during glacial periods. *Paleoceanography,* 18: 15-14.

Thamban, M., Rao, P.C., Schneider, R.R., Grootes, P.M., 2001. Glacial to Holocene fluctuations in hydrography and productivity along the southwestern continental margin of India. *Palaeogeography Palaeoclimatology Palaeoecology,* 165: 113-127.

Urey, H.C., 1947. The thermodynamic properties of isotopic substances. *Journal of Chemical Society,* 562-581.

Van Campo, E., Duplessy, J.C. and Rossignol-Strick, M., 1982. Climatic conditions deduced from a 100 kyr oxygen isotope-pollen record from the Arabian Sea. Nature, 296: 56-59.

Volkman, J. K., Eglinton, G., Corner, E. D. S. and Sargent, J. R., 1980. Novel unsaturated straight chain C37-C39 methyl and ethyl ketones in marine sediment and coccolithophore Emiliana Huxleyi. In: Adavances in organic geochemistry (A.G.Douglas and J. R. Maxwell, Eds.). Pergamon, pp. 219-227.

Wada, E.M. and Hattori, A., 1978. Nitrogen isotope effects in the assimilation of inorganic nitrogenous compounds. *Geomicrobiology Journal,* 1: 85-101.

Walsh, J.J., Premuzic, E.T. and Whitledge, T.E., 1981. Fate of nutrient enrichment on continental shelves as indicated by C/N content of bottom sediments. In: Ecohydrodynamics. J.C.J. Nihoul (Ed). Elsevier, pp. 13-49.

Wyrtki, K., 1973. Physical oceanography of the Indian Ocean. In: The biology of the Indian Ocean. B. Zeitzschel (ed). Springer, Berlin, pp. 18-36.

Yamamoto, M., Yamamura, M., Tada, R., 2000. Late Quaternary records of organic carbon, calcium carbonate,, and biomarkers from Site 1016 off Point Conception, California margin. *ODP Scientific Results,* 167: 183-194.

Yang, S., 1996. Snow-monsoon associations and seasonal-interannual prediction. International Journal of Climatology, 16: 125-134.

You, Y. and Tomczak, M., 1993. Thermocline circulation and ventilation in the Indian Ocean derived from water mass analysis. *Deep Sea Research*, 40: 13-56.

Zielinski, G.A., Mayewski, P.A., Meeker, L.D., Whitlow, S., Twickler, M.S. and Taylor, K., 1996. Potential atmospheric impact of the Toba mega-eruption ~71,000 years ago. *Geophysical Research Letters*, 23: 837-840.

APPENDIX

(The following pages contain various data generated for this study. The depth-interval or the chronological data shall be made available if required for review. However, those details are presented in the age-models of the sediment cores for ready reference)

***G. sacculifer* oxygen- and carbon-isotopes in the Eastern Arabian Sea sediment**

(on PDB scale)

	SK129/GC02 core		SK129/GC08 core		SK117/CR04 core	
Section No	$\delta^{18}O$ ‰	$\delta^{13}C$ ‰	$\delta^{18}O$ ‰	$\delta^{13}C$ ‰	$\delta^{18}O$ ‰	$\delta^{13}C$ ‰
1	-1.829	1.122	-2.065	2.844	-2.301	4.691
2	-1.879	0.857	-2.115	2.562	-2.351	4.392
3	-1.763	0.964	-1.999	2.673	-2.235	4.506
4	-1.810	1.022	-2.046	2.737	-2.282	4.576
5	-1.860	1.169	-2.096	2.895	-2.332	4.747
6	-1.542	1.080	-1.777	2.790	-2.013	4.623
7	-1.874	1.022	-2.110	2.739	-1.022	4.580
8	-1.826	1.106	-2.062	2.827	-2.298	4.672
9	-1.579	1.040	-1.814	2.748	-2.050	4.580
10	-1.227	0.950	-1.462	2.640	-1.698	4.453
11	-1.432	0.964	-1.667	2.662	-1.902	4.483
12	-1.785	0.864	-2.021	2.567	-2.257	4.394
13	-0.922	0.932	-1.156	2.611	-1.391	4.411
14	-1.157	1.053	-1.392	2.748	-1.627	4.566
15	-1.383	0.739	-1.618	2.419	-1.853	4.222
16	-0.789	1.245	-1.023	2.940	-1.258	4.758
17	-0.675	1.196	-0.909	2.884	-1.143	4.695
18	-1.285	1.005	-1.520	2.701	-1.755	4.520
19	-1.320	1.021	-1.555	2.718	-1.790	4.540
20	-0.884	0.800	-1.118	2.468	-1.353	4.257
21	-0.616	0.906	0.210	2.572	-0.023	4.324
22	-0.723	1.220	-0.957	2.912	-1.191	4.726
23	-0.738	0.954	-0.972	2.628	-1.206	4.423
24	-0.537	0.962	-0.771	2.630	-1.005	4.418
25	-0.656	0.883	0.370	2.549	0.138	4.293
26	-0.643	0.705	-0.877	2.359	-1.111	4.132
27	-0.641	0.959	-0.875	2.630	-1.109	4.422
28	-0.517	1.009	-0.751	2.679	-0.985	4.471
29	-0.493	0.884	-0.727	2.544	-0.961	4.326
30	-0.117	0.923	-0.350	2.574	-0.584	4.345
31	-0.299	1.036	-0.533	2.701	-0.766	4.486
32	-0.360	1.056	-0.594	2.724	-0.828	4.513
33	-0.264	1.118	-0.497	2.787	-0.731	4.577
34	-0.191	0.960	-0.424	2.616	-0.658	4.392
35	-0.217	1.109	-0.450	2.776	-0.684	4.564
36	-0.153	0.912	-0.386	2.563	-0.620	4.334
37	-0.344	0.810	-0.578	2.461	-0.812	4.232
38	-0.107	0.807	-0.340	2.449	-0.573	4.211
39	-0.092	1.067	-0.325	2.726	-0.558	4.506
40	-0.010	0.977	-0.243	2.628	-0.476	4.399
41	-0.177	0.960	-0.410	2.615	-0.644	4.390

42	0.071	0.959	-0.161	2.605	-0.395	4.372
43	-0.098	1.166	-0.331	2.833	-0.564	4.620
44	0.106	0.931	-0.127	2.574	-0.361	4.338
45	0.027	1.147	-0.206	2.808	-0.439	4.590
46	-0.013	1.056	-0.246	2.713	-0.479	4.489
47	-0.020	1.111	-0.253	2.771	-0.486	4.552
48	0.141	1.016	-0.092	2.664	-0.325	4.432
49	0.179	1.096	-0.054	2.748	-0.287	4.521
50	0.059	1.037	-0.173	2.689	-0.407	4.462
51	0.089	1.191	-0.143	2.853	-0.377	4.635
52	-0.002	0.971	-0.235	2.621	-0.468	4.391
53	0.012	1.004	-0.221	2.656	-0.454	4.428
54	0.035	1.066	-0.198	2.721	-0.431	4.496
55	-0.016	1.050	-0.249	2.706	-0.482	4.482
56	0.058	0.801	-0.174	2.437	-0.408	4.193
57	0.108	0.988	-0.125	2.636	-0.359	4.403
58	0.173	1.065	-0.060	2.716	-0.293	4.486
59	-0.052	0.925	-0.285	2.574	-0.518	4.342
60	-0.259	1.026	-0.492	2.689	-0.726	4.472
61	-0.238	0.997	-0.471	2.657	-0.705	4.437
62	-0.085	1.062	-0.318	2.721	-0.551	4.501
63	-0.308	0.940	-0.542	2.599	-0.775	4.377
64	-0.448	0.880	-0.682	2.539	-0.916	4.318
65			-0.233	1.584	-0.466	3.283
66			-0.233	1.584	-0.466	3.283
67			-0.233	1.584	-0.466	3.283
68			-0.233	1.584	-0.466	3.283
69			-0.233	1.584	-0.466	3.283
70			-0.233	1.584	-0.466	3.283
71			-0.233	1.584	-0.466	3.283
72			-0.233	1.584	-0.466	3.283
73			-0.233	1.584	-0.466	3.283
74			-0.233	1.584	-0.466	3.283
75			-0.233	1.584	-0.466	3.283
76			-0.233	1.584	-0.466	3.283
77			-0.233	1.584	-0.466	3.283
78			-0.233	1.584	-0.466	3.283
79			-0.233	1.584	-0.466	3.283
80			-0.233	1.584	-0.466	3.283
81			-0.233	1.584	-0.466	3.283
82			-0.233	1.584	-0.466	3.283
83			-0.233	1.584	-0.466	3.283
84			-0.233	1.584	-0.466	3.283
85			-0.233	1.584	-0.466	3.283
86			-0.233	1.584	-0.466	3.283
87			-0.233	1.584	-0.466	3.283
88			-0.233	1.584	-0.466	3.283
89			-0.233	1.584	-0.466	3.283

90	-0.233	1.584	-0.466	3.283
91	-0.233	1.584	-0.466	3.283
92	-0.233	1.584	-0.466	3.283
93	-0.415	1.584	-0.649	3.290
94	-0.233	1.584	-0.466	3.283
95	-0.233	1.584	-0.466	3.283
96	-0.233	1.584	-0.466	3.283
97	-0.233	1.584	-0.466	3.283
98	-0.233	1.584	-0.466	3.283
99	-0.233	1.584	-0.466	3.283
100	-0.233	1.584	-0.466	3.283
101	-0.233	1.584	-0.466	3.283
102	-0.233	1.584	-0.466	3.283
103	-0.233	1.584	-0.466	3.283
104	-0.233	1.584	-0.466	3.283
105	-0.233	1.584	-0.466	3.283
106	-0.233	1.584	-0.466	3.283
107	-0.233	1.584	-0.466	3.283
108	-0.233	1.584	-0.466	3.283
109	-0.233	1.584	-0.466	3.283
110	-0.233	1.584	-0.466	3.283
111	-0.233	1.584	-0.466	3.283
112	-0.233	1.584	-0.466	3.283
113	-0.233	1.584	-0.466	3.283
114	-0.233	1.584	-0.466	3.283
115	-0.233	1.584	-0.466	3.283
116	-0.233	1.584	-0.466	3.283
117	-0.233	1.584	-0.466	3.283
118	-0.233	1.584	-0.466	3.283
119	-0.233	1.584	-0.466	3.283
120	-0.233	1.584	-0.466	3.283
121	-0.233	1.584	-0.466	3.283
122	-0.233	1.584	-0.466	3.283
123	-0.233	1.584	-0.466	3.283
124	-0.233	1.584	-0.466	3.283
125	-0.233	1.584	-0.466	3.283
126	-0.233	1.584	-0.466	3.283
127	-0.233	1.584	-0.466	3.283
128	-0.233	1.584	-0.466	3.283
129	-0.233	1.584	-0.466	3.283
130	-0.233	1.584	-0.466	3.283
131	-0.233	1.584	-0.466	3.283
132	-0.233	1.584	-0.466	3.283
133	-0.233	1.584	-0.466	3.283
134	-0.233	1.584	-0.466	3.283
135	-0.233	1.584	-0.466	3.283
136	-0.233	1.584	-0.466	3.283
137	-0.233	1.584	-0.466	3.283

138	-0.233	1.584	-0.466	3.283
139	-0.233	1.584	-0.466	3.283
140	-0.233	1.584	-0.466	3.283
141	-0.233	1.584	-0.466	3.283
142	-0.233	1.584	-0.466	3.283
143	-0.233	1.584	-0.466	3.283
144	-0.233	1.584	-0.466	3.283
145	-0.233	1.584	-0.466	3.283
146	-0.233	1.584	-0.466	3.283
147	-0.233	1.584	-0.466	3.283
148	-0.233	1.584	-0.466	3.283
149	-0.233	1.584	-0.466	3.283
150	-0.233	1.584	-0.466	3.283
151	-0.233	1.584	-0.466	3.283
152	-0.233	1.584	-0.466	3.283
153	-0.233	1.584		
154	-0.233	1.584		
155	-0.233	1.584		
156	-0.233	1.584		
157	-0.233	1.584		
158	-0.233	1.584		
159	-0.233	1.584		
160	-0.233	1.584		
161	-0.233	1.584		
162	-0.233	1.584		
163	-0.233	1.584		
164	-0.233	1.584		
165	-0.233	1.584		
166	-0.233	1.584		
167	-0.233	1.584		
168	-0.233	1.584		
169	-0.233	1.584		
170	-0.233	1.584		
171	-0.233	1.584		
172	-0.233	1.584		
173	-0.233	1.584		
174	-0.233	1.584		
175	-0.233	1.584		
176	-0.233	1.584		
177	-0.233	1.584		
178	-0.233	1.584		
179	-0.233	1.584		
180	-0.233	1.584		
181	-0.233	1.584		
182	-0.233	1.584		
183	-0.233	1.584		
184	-0.233	1.584		

Sediment texture data for the three cores of the Eastern Arabian Sea

	SK129/GC02			SK129/GC08			SK129/CR04		
Section	Sand %	Silt %	Clay %	Sand %	Clay %	Silt %	Sand %	Clay %	Silt %
1	88.5	1.7	9.8	24.4	31.9	43.8	19.4	31.8	48.7
2	83.2	3.1	13.7	23.4	29.7	47.0	19.7	30.0	50.2
3	84.6	3.0	12.4	23.4	34.0	42.6	20.3	30.4	49.2
4	84.1	4.2	11.7	25.3	35.8	38.9	20.4	30.7	48.9
5	83.9	4.9	11.2	22.5	38.8	38.7	23.9	29.4	46.7
6	86.3	2.5	11.2	19.9	38.6	41.4	24.8	29.2	46.1
7	84.6	5.4	10.1	19.2	37.0	43.8	26.9	29.2	43.9
8	84.1	4.1	11.8	20.5	32.8	46.8	27.3	30.9	41.7
9	87.1	1.9	11.0	15.8	34.4	49.9	28.5	29.3	42.2
10	87.9	1.6	10.5	14.5	30.7	54.8	27.6	32.5	39.9
11	85.7	1.5	12.7	13.1	28.7	58.3	28.6	30.8	40.6
12	79.8	7.1	13.2	11.7	24.7	63.6	30.2	29.1	40.8
13	82.5	4.9	12.6	10.9	24.8	64.3	34.1	24.2	41.7
14	84.7	4.6	10.7	11.5	29.8	58.7	35.5	26.1	38.4
15	83.2	4.5	12.3	14.2	27.0	58.7	32.3	27.4	40.3
16	80.9	5.9	13.1	14.0	24.8	61.3	31.6	24.3	44.2
17	82.0	5.6	12.4	15.5	23.7	60.9	37.7	23.0	39.3
18	78.1	7.2	14.7	19.9	21.0	59.2	31.4	24.4	44.2
19	71.0	11.9	17.0	17.1	20.4	62.4	30.1	23.7	46.3
20	64.2	14.7	21.1	12.0	21.6	66.4	32.6	24.3	43.2
21	68.4	12.8	18.8	11.6	25.6	62.8	30.0	24.7	45.3
22	78.8	3.2	18.0	11.1	26.1	62.8	27.2	25.3	47.5
23	73.8	6.5	19.6	12.4	27.4	60.2	28.9	26.1	45.0
24	21.3	38.2	40.5	12.3	31.2	56.5	27.8	22.4	49.8
25	6.6	43.3	50.1	12.4	29.0	58.7	28.3	22.7	49.0
26	8.2	43.3	48.5	9.1	38.0	52.9	25.0	22.9	52.1
27	8.1	46.6	45.3	10.3	39.6	50.1	25.1	19.8	55.2
28	6.6	43.8	49.7	10.5	39.1	50.4	25.5	21.7	52.8
29	3.7	44.8	51.5	12.9	40.1	47.0	27.1	19.4	53.6
30	3.3	45.4	51.3	11.4	40.4	48.3	26.4	21.7	51.9
31	6.5	45.2	48.3	11.2	40.1	48.7	20.3	20.5	59.2
32	23.0	35.4	41.6	13.5	39.6	46.9	17.9	22.3	59.8
33	5.1	45.4	49.5	14.1	42.0	43.8	17.8	22.8	59.4
34	38.3	27.6	34.1	9.0	43.9	47.1	24.1	22.7	53.2
35	3.9	45.0	51.1	7.0	41.1	51.9	25.0	23.4	51.6
36	6.8	44.8	48.4	7.2	44.1	48.7	25.8	22.9	51.3
37	4.5	47.9	47.5	5.2	42.6	52.1	22.6	26.1	51.3
38	3.4	45.7	50.9	5.2	43.1	51.6	21.9	27.2	50.9
39	3.1	43.8	53.1	5.7	44.7	49.6	21.2	27.0	51.8
40	3.0	47.2	49.9	6.1	42.4	51.5	21.0	25.4	53.6
41	3.3	45.5	51.3	6.4	47.1	46.5	24.0	25.8	50.2
42	38.5	28.9	32.6	5.9	50.7	43.4	24.9	23.9	51.2
43	2.9	44.6	52.4	5.1	48.2	46.7	21.7	26.6	51.8
44	2.3	44.7	51.8	3.6	46.9	49.5	21.8	23.7	54.5

45	3.8	44.8	51.3	3.4	50.2	46.4	17.8	26.8	55.4
46	2.7	42.6	54.7	4.0	43.1	52.9	21.0	25.1	53.9
47	3.3	44.9	51.8	4.3	43.1	52.6	18.4	25.8	55.8
48	2.9	44.3	52.8	6.8	44.3	48.9	19.2	27.8	53.1
49	2.9	45.5	51.6	10.4	42.0	47.6	19.1	26.1	54.9
50	3.0	43.9	53.1	12.5	41.3	46.2	21.0	27.2	51.8
51	4.0	46.6	49.4	11.4	44.2	44.4	19.3	26.2	54.5
52	2.3	43.6	54.1	9.9	43.0	47.1	21.4	26.8	51.8
53	3.3	39.8	56.8	9.2	42.8	48.1	18.9	27.4	53.7
54	2.3	42.4	55.3	10.2	42.9	46.8	23.6	25.7	50.7
55	5.1	41.5	53.4	12.4	41.8	45.8	22.8	28.3	48.9
56	3.2	39.3	57.5	10.4	44.4	45.3	27.3	24.9	47.8
57	2.9	44.8	52.3	9.8	44.3	45.9	24.5	25.8	49.7
58	2.1	43.0	54.9	7.0	52.1	40.9	28.8	24.4	46.8
59	3.2	43.2	53.6	5.5	49.1	45.5	23.4	25.6	51.1
60	2.5	42.8	54.6	5.1	47.6	47.3	20.6	26.9	52.5
61	3.4	44.0	52.5	4.5	46.6	48.9	18.0	26.0	56.0
62	4.0	43.1	53.0	4.9	46.2	48.9	17.3	26.3	56.4
63	3.4	42.4	54.2	4.2	50.1	45.7	22.5	27.1	50.4
64	2.5	44.1	53.3	3.3	49.6	47.1	20.5	25.3	54.2
65	4.7	43.0	52.3	3.1	46.3	50.6	21.2	24.7	54.1
66	3.1	41.7	55.2	3.5	48.5	48.0	18.4	26.2	55.4
67	3.1	42.0	54.9	3.0	47.8	49.2	21.2	24.7	54.1
68	2.4	41.2	56.4	2.6	50.9	46.5	22.3	25.6	52.1
69	5.8	41.1	53.1	2.8	49.7	47.5	21.9	25.2	52.9
70	2.9	42.4	54.7	3.0	48.3	48.6	22.1	25.3	52.6
71	3.1	41.8	55.1	3.0	43.5	53.5	24.2	27.2	48.7
72	2.9	42.1	55.0	3.0	40.7	56.3	16.9	27.2	55.9
73	5.3	42.0	52.7	3.1	35.0	61.9	18.9	26.5	54.5
74	2.2	42.8	55.0	3.8	32.6	63.6	16.6	27.8	55.6
75	2.2	43.3	54.5	3.2	34.5	62.2	18.0	28.6	53.3
76	2.5	43.1	54.3	3.2	40.5	56.4	19.5	25.2	55.3
77	2.7	41.0	56.3	3.3	43.0	53.6	19.2	25.4	55.4
78	1.8	41.7	56.5	3.6	47.5	48.9	18.4	26.5	55.0
79	2.4	39.7	57.9	5.0	45.0	50.0	19.0	27.9	53.1
80	3.6	41.8	54.6	6.7	43.1	50.3	20.1	27.2	52.7
81	3.2	44.5	52.3	7.0	44.2	48.7	22.1	28.0	49.9
82	2.6	45.3	52.1	7.6	45.9	46.5	20.2	28.0	51.7
83	3.5	46.1	50.4	7.9	46.3	45.8	21.3	27.5	51.2
84	3.0	44.5	52.4	7.5	46.7	45.9	15.6	29.3	55.1
85	2.8	44.2	52.9	4.5	48.0	47.6	15.6	28.8	55.6
86	2.5	47.0	50.5	3.4	47.5	49.1	16.9	30.7	52.5
87	2.9	45.6	51.5	2.8	47.9	49.3	20.2	29.6	50.2
88	3.4	45.7	50.9	3.5	49.7	46.9	19.5	28.1	52.3
89	2.7	47.6	49.7	4.4	45.1	50.5	21.0	28.7	50.3
90	4.3	47.5	48.2	6.4	42.9	50.7	20.5	31.4	48.1
91	5.2	46.8	47.9	4.9	50.6	44.5	17.5	33.1	49.4
92	4.1	47.6	48.3	4.0	49.4	46.6	15.8	35.0	49.2
93	7.2	49.2	43.6	4.2	49.3	46.5	14.6	34.7	50.7

94	6.9	46.6	46.6	4.8	50.4	44.8	15.6	32.0	52.5
95	9.0	46.2	44.8	5.2	50.1	44.7	12.6	32.0	55.4
96	9.3	47.1	43.6	5.9	48.1	46.0	11.6	33.3	55.1
97	11.3	48.0	40.7	7.1	50.3	42.6	13.4	29.7	56.9
98	10.6	45.9	43.5	7.3	52.2	40.5	10.5	31.3	58.2
99	9.2	42.7	48.1	7.5	52.9	39.6	9.5	30.7	59.9
100	8.7	47.4	43.9	6.5	53.9	39.6	11.0	33.3	55.7
101	5.8	50.0	44.3	5.4	50.7	43.9	12.3	35.7	52.1
102	8.6	49.0	42.5	4.6	51.2	44.2	8.5	31.1	60.3
103	12.2	46.1	41.7				8.6	29.4	62.0
104	8.8	46.5	44.7				8.0	27.7	64.3
105	13.0	45.9	41.1				8.4	26.6	65.0
106	12.6	46.8	40.6				11.8	27.3	60.9
107	11.2	45.7	43.1				10.7	26.4	62.9
108	8.6	47.6	43.7				10.6	26.9	62.5
109	9.5	46.4	44.0				9.5	28.1	62.4
110	10.1	46.4	43.5				9.4	26.6	64.0
111	11.5	45.4	43.2				9.2	21.0	69.8
112	12.2	45.9	41.9				9.6	19.5	71.0
113	13.3	47.3	39.4				10.5	18.9	70.6
114	12.5	47.2	40.3				8.5	20.0	71.6
115	11.8	46.8	41.4				8.3	23.3	68.5
116	22.9	41.9	35.1				7.2	29.1	63.6
117	14.9	45.7	39.3				7.6	29.8	62.7
118	20.8	44.0	35.2				7.9	31.0	61.2
119	17.3	44.8	37.9				9.6	30.6	59.8
120	13.8	46.7	39.5				10.3	30.6	59.2
121	16.4	45.7	37.9				13.9	29.7	56.4
122	14.5	46.3	39.2				11.8	35.4	52.9
123	13.3	46.3	40.3				12.9	34.7	52.4
124	13.4	48.8	37.9				13.1	35.8	51.0
125	19.0	45.8	35.2				17.7	35.8	46.5
126	24.7	41.8	33.4				20.4	35.0	44.6
127	19.0	45.4	35.6				18.3	36.3	45.5
128	25.2	41.1	33.8				16.3	37.4	46.3
129	28.8	39.5	31.7				15.7	38.9	45.5
130	21.5	43.4	35.1				13.2	40.1	46.8
131	27.7	39.9	32.5				16.9	39.0	44.1
132	33.3	35.9	30.8				15.4	40.4	44.2
133	28.8	39.7	31.5				12.5	42.4	45.1
134	31.1	37.7	31.2				11.5	41.0	47.5
135	30.8	37.7	31.5				10.0	42.0	48.0
136	35.5	35.1	29.4				10.1	41.1	48.8
137	36.6	35.2	28.2				8.5	37.8	53.8
138	37.6	34.7	27.7				10.9	33.9	55.2
139	32.0	38.0	29.9				10.6	34.3	55.1
140	44.3	31.2	24.5				14.8	31.1	54.1
141	43.5	31.7	24.8				16.8	29.7	53.5
142	44.6	29.9	25.5				13.1	33.5	53.3
143	55.8	23.9	20.4				14.7	31.5	53.8

144	44.0	29.6	26.3	12.7	33.1	54.2
145	48.6	27.3	24.1	14.6	31.5	53.9
146	56.4	23.3	20.3	12.8	34.2	53.1
147	60.5	21.6	17.9	13.1	32.2	54.8
148	58.1	19.1	22.8	14.2	31.8	54.1
149	60.3	21.4	18.3	14.0	34.3	51.7
150	62.9	19.5	17.7	14.2	34.5	51.3
151	64.8	16.3	18.9	12.1	37.1	50.8
152	66.1	16.4	17.5	12.7	36.6	50.7
153	55.9	23.6	20.5	11.6	37.0	51.4
154	55.3	21.9	22.8	14.9	35.8	49.3
155	66.2	16.2	17.5	15.6	37.6	46.8
156	68.2	16.2	15.6	16.1	35.3	48.6
157	68.6	15.8	15.7	14.8	35.2	50.1
158	71.2	13.8	15.0	14.4	34.4	51.2
159	64.3	17.1	18.6	17.4	33.8	48.8
160	69.9	13.7	16.4	17.0	34.6	48.4
161	65.2	16.3	18.5	19.4	38.0	42.6
162	66.6	15.4	18.0	21.3	35.3	43.4
163	73.0	12.6	14.5	17.9	37.3	44.9
164	69.6	14.2	16.2	15.0	36.9	48.1
165	63.9	16.4	19.7	13.5	34.5	52.0
166	74.5	10.5	15.0	13.2	33.1	53.7
167	73.5	12.0	14.5	16.5	35.3	48.2
168	63.6	17.5	18.9	15.4	35.6	48.9
169	72.9	12.1	15.0	13.3	30.6	56.2
170	71.6	12.5	15.8	13.3	32.5	54.3
171	59.4	19.1	21.5	13.7	32.0	54.3
172	79.6	8.2	12.2	13.2	33.9	52.9
173	71.8	12.0	16.2	12.2	33.3	54.5
174	73.9	10.6	15.5	14.3	31.6	54.1
175	73.7	12.0	14.4	16.3	33.8	49.9
176	38.4	23.4	38.2	21.9	31.5	46.6
177	29.6	30.4	39.9	22.7	33.2	44.1
178	15.6	30.8	53.6	23.5	30.9	45.6
179	72.0	11.4	16.6	25.9	33.8	40.3
180	16.2	31.3	52.5	28.2	31.4	40.4
181	25.6	27.7	46.7	36.6	26.6	36.7
182	40.2	22.2	37.5	33.4	27.0	39.6
183	38.0	23.6	38.4	36.6	25.7	37.7
184	10.2	33.7	56.1	29.3	31.0	39.7
185	75.1	9.2	15.7	29.6	29.8	40.5
186	27.7	28.1	44.1	31.2	26.9	41.9
187	5.3	37.6	57.0	32.8	27.7	39.5
188	7.8	34.9	57.3	30.0	24.1	46.0
189	6.4	36.6	56.9	28.9	26.0	45.1
190	6.6	35.5	57.9	28.8	27.0	44.2
191	5.5	37.1	57.4	28.3	24.8	46.9
192	5.3	37.8	57.0	29.1	25.7	45.2
193	5.5	36.2	58.3	24.9	22.8	52.3

194	8.7	36.4	54.9	25.1	24.2	50.7
195				25.6	22.5	51.9
196				24.7	23.5	51.8
197				26.4	23.0	50.6
198				25.5	23.5	51.0
199				26.6	24.0	49.4
200				25.7	24.4	49.9
201				26.4	24.6	48.9
202				24.6	26.4	49.0
203				23.2	27.8	49.0
204				23.5	27.3	49.2
205				25.2	28.3	46.5
206				24.6	30.6	44.8
207				24.2	30.4	45.5
208				23.8	31.1	45.1
209				28.2	28.1	43.7
210				26.8	28.9	44.3
211				26.4	30.0	43.6
212				26.0	28.9	45.1
213				23.9	31.0	45.1
214				25.5	29.9	44.6
215				21.9	31.3	46.9
216				19.9	32.7	47.4
217				19.4	33.3	47.2
218				19.6	33.0	47.4
219				21.9	31.3	46.8
220				19.7	29.0	51.3
221				21.8	27.1	51.0
222				22.7	25.9	51.4
223				21.3	25.4	53.3
224				20.8	24.9	54.3
225				19.8	26.1	54.1
226				19.0	25.3	55.7
227				18.7	27.4	54.0
228				17.4	28.8	53.8
229				16.1	30.7	53.2
230				13.2	32.6	54.2
231				14.0	31.4	54.7
232				15.6	34.5	49.9
233				16.0	35.3	48.7
234				19.4	31.7	49.0
235				20.5	31.7	47.8
236				22.5	32.7	44.9
237				22.6	32.1	45.3
238				23.1	31.0	45.9
239				21.6	29.9	48.5
240				20.9	30.9	48.2
241				17.8	37.2	45.0
242				19.1	36.9	44.0
243				15.6	34.2	50.2

244	14.4	35.7	49.9
245	12.0	33.4	54.6
246	11.8	31.6	56.5
247	10.1	31.1	58.8
248	19.6	34.2	46.2
249	18.9	33.5	47.6
250	11.6	35.6	52.8
251	10.1	33.1	56.8

Calcium carbonate, scavenged-Al, and particulate-Mn content in the sediment cores

	SK129/GC02			SK129/GC08	SK129/CR04
Section	$CaCO_3$ (%)	Al (%)	Mn (ppm)	$CaCO_3$ (%)	$CaCO_3$ (%)
1	78.7	0.35	49	48.2	56.3
2	74.9	0.46	57	49.4	57.0
3	78.9	0.46	67	47.4	56.2
4	79.7	0.47	61	43.9	57.4
5	81.2	0.53	65	41.9	58.0
6	82.7	0.52	70	38.0	56.9
7	81.2	0.51	73	36.7	57.6
8	97.6	0.52	83	35.7	58.2
9	97.9	0.52	78	37.5	58.0
10	88.9	0.44	67	35.7	57.6
11	91.9	0.47	62	39.2	56.6
12	83.4	0.47	80	36.0	58.5
13	86.9	0.50	85	40.5	58.1
14	88.1	0.53	87	39.7	59.1
15	87.6	0.47	79	45.4	58.7
16	84.6	0.55	80	42.9	59.8
17	83.6	0.58	88	41.9	59.8
18	87.4	0.61	92	40.0	59.8
19	83.4	0.55	111	38.5	60.5
20	86.6	0.58	106	36.0	59.0
21	61.2	0.43	85	35.2	54.9
22	63.9	0.42	78	37.0	54.8
23	62.4	0.42	78	36.4	55.2
24	55.7	0.44	96	35.9	56.5

25	54.2	0.42	93	35.7	57.1
26	56.4	0.38	93	33.9	55.4
27	55.7	0.30	130	33.1	55.9
28	55.2	0.30	96	35.7	55.1
29	54.7	0.31	96	40.0	56.6
30	53.4	0.30	102	40.0	54.7
31	55.2	0.30	98	40.5	51.4
32	56.7	0.32	84	37.0	50.2
33	56.7	0.32	94	37.0	51.0
34	61.4	0.32	91	34.2	53.9
35	67.4	0.34	102	30.7	55.7
36	68.9	0.34	102	32.7	54.5
37	67.7	0.35	127	38.2	53.7
38	65.7	0.35	119	36.2	53.6
39	66.7	0.34	115	34.7	54.0
40	65.7	0.35	107	35.5	51.5
41	66.2	0.35	132	35.2	53.8
42	63.4	0.32	91	35.0	54.7
43	61.2	0.32	138	32.7	54.7
44	59.4	0.31	117	32.2	53.3
45	63.9	0.33	106	32.7	51.2
46	58.4	0.29	93	36.0	52.2
47	56.7	0.39	106	36.0	52.4
48	62.4	0.36	114	38.7	49.7
49	62.7	0.34	111	41.7	52.0
50	76.4	0.39	135	45.2	52.3
51	67.5	0.52	124	42.2	53.0
52	64.5	0.56	112	40.5	51.0
53	61.7	0.55	116	38.7	51.5
54	57.8	0.47	98	39.5	52.6
55	55.0	0.49	101	39.5	55.1
56	56.8	0.48	95	39.7	54.6
57	55.3	0.49	140	38.7	57.4
58	53.3	0.44	92	37.9	55.9
59	53.0	0.41	98	35.0	56.4
60	51.7	0.42	89	32.3	53.4
61	62.9	0.29	109	32.3	55.3
62	62.7	0.29	121	31.7	56.2
63	61.2	0.28	121	29.0	55.7
64	62.9	0.30	119	28.2	55.7
65	63.4	0.30	116	28.5	55.6
66	63.9	0.31	122	29.2	54.8
67	64.2	0.29	115	24.4	55.4
68	61.9	0.29	115	23.8	53.4
69	61.9	0.28	110	22.7	57.2
70	64.2	0.29	113	25.2	56.2
71	62.7	0.30	138	24.2	55.0
72	61.4	0.30	105	23.5	51.1

73	61.7	0.30	115	20.2	54.2
74	62.4	0.31	122	19.0	50.6
75	63.7	0.29	113	22.6	52.1
76	65.4	0.29	95	27.2	52.6
77	64.4	0.28	95	29.1	54.1
78	65.7	0.29	104	27.4	53.7
79	68.2	0.27	90	30.1	53.6
80	68.9	0.24	83	34.4	54.6
81	69.7	0.23	79	35.0	54.8
82	71.4	0.21	72	33.9	53.3
83	73.2	0.19	64	30.9	54.0
84	73.4	0.20	62	29.8	50.9
85	74.2	0.19	61	24.7	48.7
86	74.7	0.18	59	22.6	50.8
87	76.9	0.18	55	19.1	49.8
88	76.2	0.17	52	21.7	51.3
89	77.7	0.20	53	28.8	50.5
90	76.4	0.22	67	37.4	47.3
91	74.2	0.21	54	41.2	46.0
92	79.2	0.18	45	42.5	44.3
93	79.7	0.17	47	43.8	46.1
94	79.9	0.19	44	42.9	41.8
95	79.2	0.19	39	45.7	42.4
96	81.4	0.17	39	45.2	38.8
97	79.7	0.20	43	44.2	37.9
98	78.2	0.23	44	44.9	36.5
99	77.2	0.23	52	42.2	37.0
100	79.4	0.17	37	39.0	36.3
101	77.9	0.22	54	34.7	36.6
102	80.7	0.18	37	37.0	35.5
103	78.9	0.19	38		34.7
104	75.7	0.21	42		33.9
105	79.4	0.19	37		35.6
106	80.9	0.17	35		35.4
107	77.9	0.21	39		35.7
108	78.9	0.20	40		30.6
109	76.9	0.18	36		34.1
110	79.2	0.17	34		30.5
111	76.2	0.18	36		26.3
112	76.7	0.19	36		26.2
113	81.2	0.18	36		22.3
114	82.9	0.18	36		27.7
115	77.2	0.18	32		28.2
116	77.2	0.23	39		34.9
117	75.9	0.19	33		37.4
118	78.4	0.20	33		37.9
119	80.2	0.19	34		40.7
120	77.4	0.18	31		37.8

121	79.7	0.20	32	40.6
122	79.9	0.19	32	44.4
123	79.4	0.19	33	45.2
124	80.7	0.17	30	46.7
125	81.4	0.21	33	48.7
126	78.7	0.24	37	51.4
127	80.7	0.24	39	50.1
128	77.4	0.28	40	45.4
129	79.2	0.25	40	43.4
130	81.4	0.25	37	41.4
131	81.9	0.29	39	41.9
132	79.9	0.31	46	40.3
133	84.6	0.26	47	37.6
134	85.9	0.23	41	33.7
135	84.6	0.21	39	36.5
136	86.6	0.25	44	36.6
137	83.2	0.26	44	36.6
138	76.9	0.25	41	36.3
139	75.2	0.23	40	44.0
140	75.4	0.21	38	49.4
141	76.2	0.30	45	51.2
142	74.7	0.31	48	51.1
143	72.9	0.27	43	52.7
144	79.4	0.24	39	48.8
145	76.7	0.33	50	51.6
146	73.9	0.39	57	51.7
147	74.2	0.39	56	54.8
148	73.2	0.33	48	53.9
149	75.2	0.38	53	55.3
150	76.4	0.47	64	57.9
151	80.2	0.39	57	53.9
152	73.9	0.46	64	55.0
153	74.9	0.44	61	53.9
154	74.2	0.43	61	47.7
155	72.7	0.46	65	53.6
156	72.7	0.52	68	52.0
157	66.2	0.52	71	52.2
158	69.9	0.51	71	51.5
159	70.4	0.58	78	43.6
160	73.4	0.47	71	44.7
161	71.4	0.56	81	46.2
162	72.9	0.51	72	48.3
163	69.9	0.56	75	47.0
164	68.4	0.59	87	53.0
165	70.9	0.50	84	50.1
166	65.9	0.62	90	51.9
167	65.9	0.63	92	52.2
168	67.7	0.51	83	54.6

169	65.9	0.57	87	56.1
170	65.9	0.55	84	59.7
171	65.9	0.40	72	58.5
172	65.2	0.41	69	57.3
173	60.7	0.43	75	56.8
174	60.9	0.44	74	56.0
175	59.4	0.53	100	55.6
176	44.4	0.60	181	55.3
177	41.5	0.58	185	54.6
178	34.2	0.61	238	53.4
179	51.7	0.50	106	50.7
180	38.2	0.54	180	51.9
181	41.9	0.53	153	54.9
182	35.2	0.56	183	56.3
183	21.5	0.56	219	57.3
184	21.3	0.61	248	55.1
185	47.2	0.47	121	59.0
186	21.9	0.61	233	56.1
187	19.2	0.66	253	54.9
188	18.1	0.68	262	61.2
189	18.5	0.66	267	57.9
190	19.7	0.62	240	58.2
191	18.8	0.67	272	57.9
192	19.1	0.68	257	55.7
193	19.1	0.65	253	53.2
194	19.8	0.70	256	52.7
195				52.9
196				61.6
197				59.2
198				58.6
199				59.4
200				58.3
201				52.9
202				53.8
203				51.7
204				48.7
205				51.4
206				48.7
207				49.7
208				49.2
209				50.2
210				51.9
211				50.9
212				54.4
213				52.4
214				53.1
215				53.1
216				49.4

217	48.0
218	49.4
219	48.7
220	50.7
221	51.9
222	54.2
223	53.4
224	53.7
225	53.7
226	53.7
227	50.7
228	54.9
229	52.2
230	48.9
231	48.7
232	55.4
233	54.2
234	55.9
235	58.4
236	49.4
237	49.4
238	50.7
239	51.2
240	45.9
241	47.7
242	47.4
243	47.4
244	44.4
245	41.0
246	40.5
247	42.2
248	49.7
249	46.2
250	46.4
251	46.9

Sedimentary organic components and their isotopes in deep-water core SK117/GC08

Section	C_{org}	Tot-N	C/N	$\delta^{13}C_{org}$	$\delta^{15}N$	ΣAlkenone
	%	%	mol/mol	‰ PDB	‰ Air	ppm
1	0.93	0.15	6.2	-19.4	8.5	0.033
2	0.68	0.13	5.2	-19.3	8.6	0.040
3	1.00	0.16	6.3	-19.2	8.7	0.075
4	0.81	0.13	6.2	-18.8	8.1	0.036
5	0.88	0.13	6.8	-18.9	8.2	0.068
6	0.86	0.13	6.6	-18.8	7.5	0.056
7	0.61	0.09	6.8	-18.1	7.6	0.050
8	0.69	0.09	7.7	-17.7	7.2	0.104
9	0.83	0.10	8.3	-18.0	7.3	0.131
10	0.72	0.09	8.0	-18.4	7.0	0.107
11	0.49	0.08	6.1	-18.7	7.2	0.269
12	0.64	0.09	7.1	-18.6	6.6	0.636
13	0.61	0.09	6.8	-18.6	6.7	0.969
14	0.84	0.11	7.6	-18.7	6.7	1.126
15	0.97	0.13	7.5	-18.6	6.8	1.446
16	0.97	0.13	7.5	-18.6	6.7	1.609
17	1.20	0.15	8.0	-18.6	7.0	1.200
18	1.20	0.16	7.5	-18.7	6.9	0.775
19	1.20	0.16	7.5	-18.6	7.2	1.066
20	1.30	0.17	7.6	-18.6	7.0	0.876
21	1.30	0.17	7.6	-18.7	7.1	0.719
22	0.92	0.12	7.7	-18.6	6.8	0.593
23	0.96	0.13	7.4	-18.5	6.8	0.538
24	0.98	0.13	7.5	-18.4	6.8	0.827
25	0.90	0.12	7.5	-18.4	6.9	1.311
26	1.20	0.15	8.0	-18.4	6.7	1.208
27	1.40	0.18	7.8	-18.6	7.0	0.928
28	1.30	0.16	8.1	-18.7	7.1	2.951
29	1.10	0.15	7.3	-18.4	6.7	0.938
30	1.10	0.14	7.9	-18.4	6.8	0.729
31	0.90	0.12	7.5	-18.4	6.7	0.556
32	0.89	0.12	7.4	-18.3	6.6	0.915
33	1.00	0.13	7.7	-18.2	7.0	0.520
34	1.10	0.14	7.9	-18.4	7.0	0.605
35	1.10	0.13	8.5	-18.2	6.8	
36	1.10	0.14	7.9	-18.5	7.1	
37	1.30	0.15	8.7	-18.6	7.3	
38	1.20	0.15	8.0	-18.9	7.7	
39	1.10	0.14	7.9	-18.5	7.4	
40	1.20	0.16	7.5	-18.7	7.6	
41	1.60	0.19	8.4	-18.9	7.6	

42	1.60	0.20	8.0	-19.0	7.8
43	1.60	0.19	8.4	-19.5	8.6
44	1.10	0.14	7.9	-18.6	7.6
45	1.60	0.19	8.4	-18.6	8.0
46	1.80	0.21	8.6	-18.5	8.3
47	1.80	0.21	8.6	-18.6	8.8
48	1.50	0.18	8.3	-18.4	9.2
49	1.30	0.16	8.1	-18.7	8.3
50	0.86	0.11	7.8	-18.5	8.0
51	0.87	0.12	7.3	-18.6	7.3
52	1.00	0.13	7.7	-18.8	7.7
53	0.99	0.13	7.6	-18.7	7.1
54	0.63	0.09	7.0	-18.8	6.4
55	0.57	0.08	7.1	-18.7	6.0
56	0.64	0.09	7.1	-18.8	6.1
57	0.84	0.11	7.6	-18.8	5.9
58	0.90	0.12	7.5	-19.0	5.6
59	0.85	0.11	7.7	-19.0	6.0
60	1.00	0.13	7.7	-19.1	6.3
61	1.00	0.14	7.1	-19.1	6.1
62	1.20	0.15	8.0	-19.1	7.0
63	1.30	0.16	8.1	-19.3	8.0
64	0.97	0.13	7.5	-18.8	7.0
65	0.87	0.11	7.9	-18.6	6.6
66	0.75	0.11	6.8	-18.8	6.8
67	0.87	0.11	7.9	-18.7	7.4
68	1.20	0.14	8.6	-18.8	7.5
69	1.50	0.18	8.3	-19.0	8.5
70	1.10	0.13	8.5	-18.4	7.0
71	1.10	0.14	7.9	-18.3	7.1
72	0.99	0.12	8.3	-18.5	7.2
73	0.60	0.09	6.7	-18.2	6.8
74	0.49	0.08	6.1	-18.3	6.4
75	0.50	0.07	7.1	-18.1	6.3
76	0.55	0.08	6.9	-18.2	6.4
77	0.76	0.10	7.6	-18.6	6.7
78	1.20	0.16	7.5	-19.2	8.5
79	1.10	0.15	7.3	-19.2	8.7
80	1.10	0.15	7.3	-19.4	8.6
81	0.90	0.12	7.5	-19.2	9.4
82	0.92	0.13	7.1	-19.2	8.6
83	0.82	0.11	7.5	-18.8	7.8
84	0.58	0.09	6.4	-18.6	7.6
85	0.43	0.08	5.4	-18.8	6.2
86	0.60	0.09	6.7	-19.4	7.1

Publication List

1. Banakar, V. K., Galy, A., Sukumaran, N. P., Parthiban, G. and **Volvaiker, A. Y., (Chodankar, A. R.,)** 2003. Himalayan sedimentary pulses recorded by the silicate detritus within a ferromanganese crust from the Central Indian Ocean. ***Earth and Planetary Science Letters***, 205: 337-348.
2. Rajani, R. P., Banakar, V. K., Parthiban, G., Mudholkar, A. V., and **Chodankar, A. R.,** 2005. Compositional variation and genesis of ferromanganese crusts of the Afanasiy-Nikitin Seamount, Equatorial Indian Ocean. ***Journal of Earth System Science,*** 114, 51-61.
3. **Chodankar, A. R**., Banakar, V. K., and Oba, T., (2005, in press). Past 100 ky surface salinity-gradient response in the Eastern Arabian Sea to the summer monsoon variation recorded by $\delta^{18}O$ of *G. sacculifer.* ***Global and Planetary Change.***
4. Banakar, V. K., Oba, T., **Chodankar, A. R**., Kuramoto, T., Yamamoto, M., and Minagawa, M., (2005, in press). Monsoon related changes in sea surface productivity and water column denitrification in the Eastern Arabian Sea during the last glacial cycle. ***Marine Geology.***

Conference papers

1. **Chodankar, A. R.,** Banakar, V. K., and Oba, T., 2003. Past salinity-gradient variations in the Eastern Arabian Sea: Reconstruction from the sedimentary $\delta^{18}O_{G.sacculifer}$ record. International Young Scientist's Global Change Conference, Treiste, Italy, Abstracts, p. 27.
2. Nigam, R., Saraswat, R., Naidu, P. D., Mazumdar, A., Raiker, V., and **Volvaiker, A. Y., (Chodankar, A. R.,)** 2002. Signatures of global and regional climate events during Holocene in the Northern Indian Ocean: Preliminary clues from mean diameter variation in Orbulina universa. 39th Annual Convention and Meeting of Indian Geophysical Union, NEERI, Nagpur, Abstracts, p. 54.